

SOLID STATE NANOCRYSTALLINE TITANIUM OXIDE PHOTOVOLTAIC CELLS

THÈSE N° 1542 (1996)

PRÉSENTÉE AU DÉPARTEMENT DE CHIMIE

ÉCOLE POLYTECHNIQUE FÉDÉRALE DE LAUSANNE

POUR L'OBTENTION DU GRADE DE DOCTEUR ÈS SCIENCES

PAR

Tobias MEYER

Ingénieur chimiste diplômé EPF
originaire de Wohlenschwil (AG)

acceptée sur proposition du jury:

Prof. M. Grätzel, directeur de thèse
Prof. Ch. Comninellis, corapporteur
Dr A. Hagfeldt, corapporteur
Dr A. Ricaud, corapporteur

Lausanne, EPFL
1996

Solid State Nanocrystalline Titanium Oxide Photovoltaic Cells

To my Family

Contents

Abstract	1
Résumé	2
Zusammenfassung	3
1. Introduction	5
1.1. Photovoltaic cells - theory and working principles	5
1.2. p-n Junction	9
1.3. Schottky barrier	15
1.4. Solar energy - why ?	17
2. Novel approaches: The dye solar cell	21
2.1. Working principles	21
2.2. Why use nanocrystalline materials ?	25
2.3. Projected economic data for the dye solar cell	28
3. Strategies towards solid state nanocrystalline solar cells	33
3.1. Materials choice and requirements	33
3.2. Early attempts to make a solid-state sensitized solar cell	35
4. Metal/nanocrystalline-TiO ₂ junctions	43
4.1. Preparation of the nanocrystalline TiO ₂ electrodes	44
4.2. Photovoltaic characterisation	47
4.2.1. Nanocrystalline-TiO ₂ diodes with silver as top contact	47
4.2.2. Gold as top contact metal	54
4.3. Sensitized nanocrystalline-TiO ₂ Schottky junctions	59
4.3.1. Electrode preparation	59
4.3.2. Photovoltaic characterization	61
4.4. Conclusion	67
5. Conductive polymer/nanocrystalline-TiO ₂ junction	71
5.1. Device build-up	74
5.2. Symmetric Au/poly(bithiophene)/Au structure	77
5.3. Gold/p-poly(bithiophene)/aluminium Schottky diode	82
5.4. Flat TiO ₂ /p-poly(bithiophene) heterojunction	85
5.5. Nanostructured TiO ₂ /p-poly(bithiophene) heterojunction	94
5.6. Conclusion	100
6. Inorganic junctions: CuI/nanocrystalline-TiO ₂ cells	103
6.1. Electrode preparation	105
6.2. Flat compact TiO ₂ /CuI heterojunction	108
6.3. Nanocrystalline sensitized TiO ₂ /CuI junction	109
6.4. Conclusion	120
7. Conclusions and outlook	123
List of symbols	128
Acknowledgments	133
Curriculum vitae	134

Abstract

The dye solar cell, is a novel photoelectrochemical solar cell presenting unique advantages, as the use of low cost materials and the potential simplicity of manufacturing. However, a liquid electrolyte is actually required for the transport of the photogenerated positive charges.

A major breakthrough is the replacing of the liquid electrolyte by a solid-state hole conducting material - the aim of this work.

First, the metal/TiO₂ junction was investigated, with either silver or gold as rectifying contact. Sensitization was demonstrated, as action spectra were measured using different dyes. The evaporated metal could not enter the pores of the nanocrystalline TiO₂ to contact all the dye molecules, hence only low photovoltaic performances were obtained. Furthermore, these metal/TiO₂ junctions showed a high sensitivity to humidity and to forward bias polarization.

The use of an electrically conducting polymer, poly(bithiophene), was studied in a metal/polymer junction and in TiO₂/polymer devices with flat and nanocrystalline TiO₂ electrodes. The photoelectric characterizations indicated that electrochemically reduced poly(bithiophene) was able to inject electrons into TiO₂, i.e. sensitizing TiO₂, and it acted as a hole conducting layer. Short-circuit current densities of 2-3 mA/cm² were measured at an irradiation of 1.2 W/cm². The open-circuit voltages were in the 250-350 mV range, depending on the light intensity and temperature.

The use of a transparent hole conducting material, CuI, which is a wide bandgap p-type semiconductor, was demonstrated in a nanocrystalline junction made of highly porous sensitized TiO₂ and solution-cast CuI. A short-circuit current of 1 mA/cm² was achieved under one sun simulated light; the open-circuit voltage was 600 mV and the light-to-power conversion efficiency was 0.3 %. The peak quantum efficiencies of 8 % in the UV, and 3 % in the visible, showed that the nanocrystalline junction was working inefficiently, probably due to the poor electrical contact between the TiO₂ nanocrystallites and the CuI crystals. Furthermore, the sensitizer was not tuned to inject holes into the valence band of CuI.

As conclusion, a controlled-capillary pore based sensitized device is suggested. In this concept, all the internal surface of the TiO₂ electrode coated with sensitizer is contacted with the transparent hole conducting layer, hence improving the photovoltaic properties of the device.

Résumé

La cellule solaire à colorant est une nouvelle cellule photoélectrochimique présentant des avantages uniques, tels que l'utilisation de matériaux de faible coût et la possible simplicité de fabrication. Malheureusement, un électrolyte liquide est actuellement indispensable pour le transport des charges positives au sein de la cellule.

Le remplacement de l'électrolyte liquide, qui est le but de ce travail, par un conducteur de trous solide est une percée technologique.

D'abord la jonction métal/TiO₂ a été étudiée, avec soit de l'or ou de l'argent comme contact bloquant. La sensibilisation de telles jonctions a été démontrée avec les spectres d'action enregistrées avec différents colorants. Les performances photovoltaïques étaient modestes car le métal, déposé par évaporation, ne pouvait pas contacter toutes les molécules de sensibilisateur dans les pores du TiO₂ nanocristallin. En outre, ces jonctions métal/TiO₂ présentaient une sensibilité à l'humidité et à la polarisation électrique.

L'emploi d'un polymère conducteur, le poly(bithiophène), a été étudié avec des jonctions métal/polymère et TiO₂/polymère ayant du TiO₂ lisse et nanocristallin. Les caractérisations photoélectriques indiquaient que le poly(bithiophène) à l'état réduit, était en mesure d'injecter des électrons dans le TiO₂, c'est-à-dire de sensibiliser le TiO₂. De plus il agissait comme conducteur de trous. Des densités de courant de court-circuit de 2-3 mA/cm² ont été mesurés sous une lumière concentrée de 1.2 W/cm². La tension en circuit ouvert était entre 250 et 350 mV, selon la lumière et la température.

L'utilisation d'un conducteur de trous transparent, l'iodure de cuivre (CuI), qui est un semiconducteur type p à large lacune d'énergie, a été démontré avec une jonction nanocristalline composée de TiO₂ poreux imprégné de CuI. Un photocourant de court-circuit de 1 mA/cm² a été mesuré dans une lumière correspondant à un soleil; la tension en circuit ouvert était de 600 mV et le rendement électrique de 0.3 %. Le rendement quantique maximal obtenu a été de 8 % dans l'ultraviolet et de 3 % dans la lumière visible. Ces valeurs indiquaient que la jonction nanocristalline était peu efficace, probablement à cause du mauvais contact entre les nanocristallites de TiO₂ et les cristaux de CuI. En outre, le sensibilisateur n'était pas adapté pour l'injection de trous dans la bande de valence du CuI.

En conclusion, une phot cellule utilisant une électrode à porosité contrôlée est suggérée. Dans ce concept, toute la surface interne du TiO₂, recouverte de sensibilisateur, est mise en contact avec le conducteur de trous transparent pour améliorer les caractéristiques photoélectriques de la cellule.

Zusammenfassung

Die Farbstoffsolarzelle ist eine neue photoelektrochemische Solarzelle mit einzigartigen Vorteilen, wie die Verwendung von kostengünstigen Rohstoffen und eine einfache Herstellung. Jedoch wird ein flüssiger Elektrolyt verwendet, um die positive Ladung in der Zelle zu transportieren.

Das Ziel dieser Arbeit ist es, den flüssigen Elektrolyt durch einen Festkörper-Lochleiter zu ersetzen.

Die Verwendung eines Festkörper-Lochleiter anstelle des flüssigen Elektrolyten ist ein Durchbruch.

Zuerst wurde der Metall/Titanoxid-Uebergang, mit Gold oder Silber als Gleichrichterkontakt untersucht. Die TiO_2 -Sensibilisierung wurde anhand von Aktionsspektren mit verschiedenen Farbstoffe nachgewiesen. Allerdings waren die photoelektrischen Eigenschaften bescheiden, da das aufgedampfte Metall nicht alle Farbstoffmoleküle im Inneren der porösen TiO_2 -Elektrode kontaktieren kann. Zudem waren die Metall/ TiO_2 -Uebergänge feuchtigkeits- und polarisationsempfindlich.

Die Verwendung eines elektrisch leitenden Kunststoffes, Poly(bithiophen) wurde anhand von Metall/Polymer- und TiO_2 /Polymer-Uebergänge, mit glattem und nanokristallinem TiO_2 untersucht. Die photoelektrischen Eigenschaften zeigten, dass Poly(bithiophen) im reduzierten Zustand fähig ist, Elektronen in das Leitungsband des Titanoxids zu injizieren (Sensibilisierung). Kurzschlussströme von ca. 2 bis 3 mA/cm^2 wurden bei 1.2 W/cm^2 Einstrahlung gemessen. Die Leerlaufspannung war zwischen 250 und 350 mV, je nach Lichtstärke und Temperatur.

CuI , ein p-Halbleiter mit grosser Bandlücke, wurde als transparenter Lochleiter in einem nanokristallinen Uebergang, der aus CuI -beschichtetem porösen TiO_2 besteht, eingesetzt. Ein Kurzschlussstrom von 1 mA/cm^2 wurde bei einer Lichtstärke von einer Sonne gemessen; die Leerlaufspannung war 600 mV, und der Wirkungsgrad lag bei 0.3 %. Maximale Quantenwirkungsgrade von 8 % in UV-Licht und von 3 % in sichtbarem Licht wurden erreicht. Diese Werte zeigten, dass der nanokristalline Uebergang nicht optimal war, vermutlich aufgrund des schlechten Kontakts zwischen den TiO_2 -Nanokristalliten und den CuI -Kristallen. Zudem war der Farbstoff nicht abgestimmt, Löcher in das Valenzband des Kupferiodids zu übertragen.

Zum Abschluss wird eine Elektrode mit kontrollierter Porosität vorgestellt. Dabei wird die ganze, mit Farbstoff belegte innere Oberfläche der Titanoxidelektrode mit dem durchsichtigen Lochleiter kontaktiert, um die photovoltaischen Eigenschaften der Zelle zu verbessern.

1. Introduction

1.1. Photovoltaic cells - theory and working principles

A photovoltaic cell converts incident light into electrical energy and heat.

The basic steps required for the transformation of the incoming electromagnetic waves or photons into electrical energy are:

1. Absorption of the incoming photons
2. Charge separation
3. Charge collection

These three functions have to be integrated into the solar cell and they must be perfectly matched in order to achieve best light to electricity conversion.

1. Absorption of the incoming photons:

The incident photons carrying the energy $E = h\nu$, where h is Planck's constant and ν is the frequency of the electromagnetic wave (in Hz), must be absorbed, otherwise their energy cannot be used. A necessary condition for absorption is the presence of at least two energy levels: the ground state level, which is filled with electrons and the excited state level, which is empty. The excited level can accept electrons, lying above the ground state level by the amount $\Delta E = E_g$, where E_g is the energy required to promote an electron from the ground state to the excited state level. In the case where a solid continuous material like a crystal or a glass is used as absorber, E_g is also called the bandgap energy.

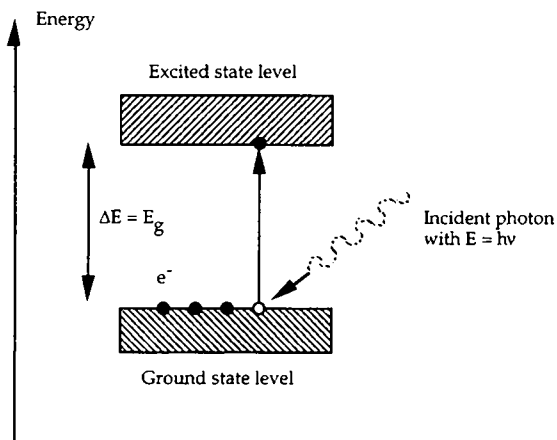


Figure 1: Schematic diagram of the photon absorption in the solid.

The absorption process consists of a "displacement" of an electron from the ground state level into a higher energy level, thus transforming the photon's energy into internal energy of the sensitizer. Only photons with an energy $h\nu > E_g$ are absorbed. The displacement of the electron (black dots in fig.1) leaves a positive charged "hole" in the ground state level (open circles in fig.1). So, the absorption of a photon by the material creates an electron-hole pair (also called a charge pair) separated by the energy E_g . In the case of a solid, the ground state level is called the valence band (VB) and the excited state level is called the conduction band (CB).

2. Charge separation:

The electron-hole pair, created by the photon absorption, is unstable, as the so created high-energy electron (or hole) tends to get rid of the excess energy either by recombining under emission of a photon (fluorescence), or by reacting with the surrounding atoms (principle of photochemistry). The electron-hole pair has a given lifetime. The charge separation, consisting of a physical separation, over a given distance, of the electron and the hole must be done in a time shorter than the charge pair lifetime. Several principles are used to make a successful charge-pair separation.

3. Charge collection

The separated charges must be efficiently collected by the "current collectors" and transported to the external electrical circuit where the potential energy of the charges is used in the load.

The quantum efficiency, or Incident Photon to Current Efficiency (IPCE) is the number of electron-hole pairs created per incident photon and is given by

$$\text{IPCE} = \frac{J/q}{\Phi_{\text{phot}}} \quad [1] \quad (1)$$

where J is the photogenerated current density, q the charge of the electron and Φ_{phot} is the photon flux.

The IPCE can be decomposed into a product of the efficiency of each step, i.e. absorption efficiency η_A , charge separation efficiency η_{sep} and collection efficiency η_{coll} :

$$\text{IPCE} = \eta_A \eta_{\text{sep}} \eta_{\text{coll}} \quad (2)$$

The absorption efficiency η_A will depend on the absorption coefficient $\alpha(\lambda)$ of the absorber material (which itself is wavelength dependent) and the absorber layer thickness. The optical path length in the absorber is crucial, which can be several times longer than the path given by the absorber thickness if a proper light management is used, e.g. by texturing the surface and using anti-reflective coatings.

In the case where light management is used, the layer thickness L to absorb a given amount of light is given by [1]

$$L = \frac{a}{\alpha(1-a) 4 n^2} \quad (3)$$

where n is the refraction index and a is the wanted absorption (percentage of photons absorbed), assuming that the light is scattered. If pyrite (FeS_2 , $n = 4.5$, $\alpha = 6 \times 10^5 \text{ cm}^{-1}$ [1]) is used as absorber, a layer thickness L of only 1.8 nm would be required according to expression (3) when 90 % of the incoming photons should be absorbed.

The absorption characteristics of the solar cell material must be matched to the solar spectrum in order to obtain best conversion efficiencies. The graph in fig. 2 shows the currently achieved light to electricity efficiencies with different solar cell materials. Exact calculations [2 p. 796] of the limiting efficiency showed that a material with a bandgap E_g around 1.35 eV gives the highest efficiency of ca. 33 % (for the AM1.5 spectral distribution, at one sun concentration) as there is the compromise between the amount of absorbed photons (with the energy $h\nu \geq E_g$) and the available open-circuit voltage V_{oc} which is E_g at best. In practical devices a V_{oc} of around 80 % of E_g is reached. A 25 % efficiency is possible with the direct bandgap (1.42 eV) III-V material GaAs.

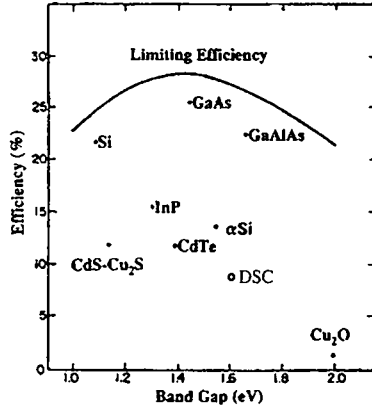


Figure 2: Conversion efficiency dependence on bandgap of different semiconductors

The absorption characteristics of the material is also depending on whether the bandgap is of direct or indirect nature [11]:

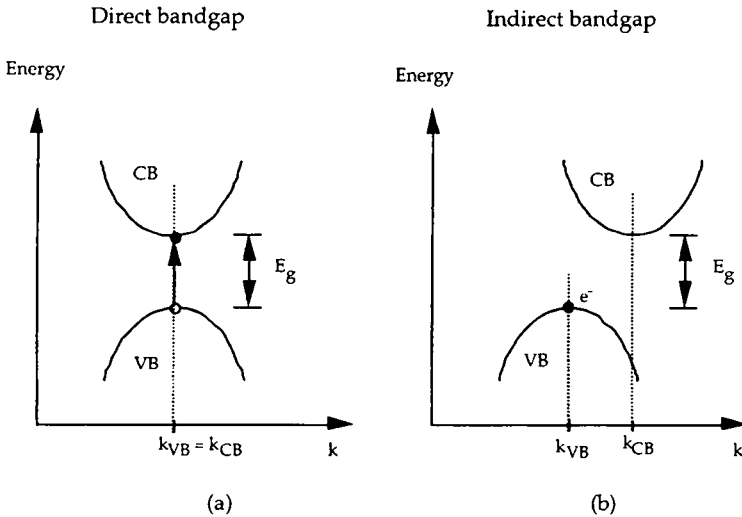


Figure 3: Energy vs. wave vector diagram illustrating the band structure for a semiconductor with direct (a) and indirect (b) bandgap.

The k denotes the wave vector in the "momentum space", also called the "reciprocal lattice space" [3]. The optical transitions are ruled by the "k-selection rule" which states that the transition is only possible when $k_{VB} = k_{CB}$.

In a direct bandgap material, like GaAs, the top of the valence band (VB) coincides with the bottom of the conduction band (CB) as shown in fig. 3 (a). Hence $k_{VB} = k_{CB}$, and the optical transition is easily possible, meaning that the absorption coefficient α of the direct bandgap material is high. In fact GaAs has a absorption coefficient of $\alpha = 4 \times 10^5 \text{ cm}^{-1}$ at 600 nm [2 p. 750]. In the case of an indirect bandgap material like silicon, the top of the VB does not coincide with the bottom of the CB as shown in fig. 3 (b), and $k_{VB} \neq k_{CB}$. In order to absorb a photon with the energy $h\nu = E_g$, a momentum change $\Delta k = k_{CB} - k_{VB}$ must happen prior to the VB to CB electron transition. This momentum change is produced by a lattice vibration, or a phonon, meaning that the light absorption can only occur simultaneously when the reciprocal lattice moves by an amount that $k_{CB} = k_{VB}$. The coincidence of a photon and the appropriate lattice vibration is statistically rare. Most of the incoming light is not absorbed by silicon. Subsequently the absorption coefficient α of Si is ca. $5 \times 10^4 \text{ cm}^{-1}$ at 600 nm [2 p. 750], or roughly 10 times lower than that of GaAs. The practical consequence of this is that indirect bandgap materials must be thick, several 100 μm , to be good absorbers. Such thick layers of silicon cannot be deposited by evaporation without loosing the electronic properties required for solar cell operation, so silicon solar cells are cut out of massive single crystals or polycrystalline Si ingots.

1.2. p-n Junction

The charge separation is assured by the build-in electrical field. This electrical field E , given by $E = V_{bi}/W$, where W is the depletion layer thickness and V_{bi} the build-in voltage, is created when the Fermi-levels of the n-type and p-type junction materials align as they are contacted. This corresponds to the situation of the unbiased junction, i.e. the externally applied voltage is zero.

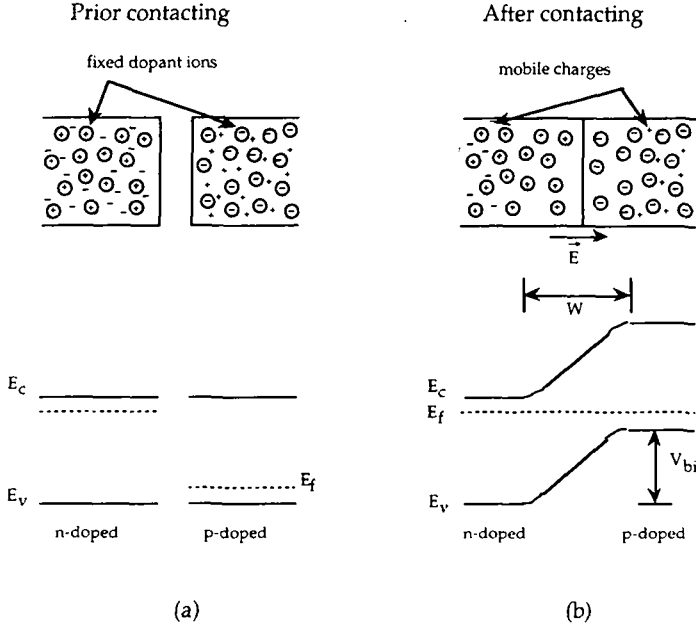


Figure 4: Fermi-level alignment and p-n junction formation upon contact, E_c and E_v denote the conduction band lower edge and the valence band upper edge energies respectively. W is the depletion layer thickness.

The Fermi-level E_f is the energy where the probability to find an electron is $1/2$ at 0°K . The depletion layer is the region where the free carriers of the n-type and p-type material have been neutralized by the holes and electrons that diffused across the junction when the contact of both materials is made (case (b) of fig. 4). The neutralized free carriers in the n-type material are leaving the positively charged dopant ions, respectively the negatively charged dopant ions in the p-type side of the junction. The depletion layer width W can be calculated by integrating Poisson's equation in one dimension [2, p 74]:

$$\frac{d^2\psi}{dx^2} = -\frac{q_v}{\epsilon} \quad (4)$$

where ψ is the electrostatic potential, ϵ the dielectric constant of the material, q_v is the charge density of the fixed dopant ions ($q_n = qN_D$ in the n-type side and $q_v = -qN_A$ in p-type side) and x is the distance from the junction interface. N_D is the doping atoms concentration in the n-type side, N_A the concentration of dopants in the p-type material. The integration of (4) for the n and p sides, and knowing that the charges are equal on both sides, yields the expression of the depletion layer width W

$$W = \sqrt{\frac{2\epsilon V_{bi}}{q} \left(\frac{N_A + N_D}{N_A N_D} \right)} \quad (5)$$

where V_{bi} is the build-in voltage given by the work-function difference of the two junction materials. The work-function is the minimal potential to extract an electron from its Fermi-level to the vacuum.

The electrical field in the depletion zone is responsible for the charge separation as the electrons and holes will drift apart due to their opposed charge. The collection of the charge carriers, i.e. the electrons on the negative terminal and the holes on the positive terminal, is done by appropriate ohmic contacts on both junction sides. The difficulty is that on the one hand the light has to pass through at least one of the current collector with minimal loss, and on the other hand, the electrical resistance should be minimized to avoid ohmic losses. This requires large collector sections and/or highly conductive materials which are (unfortunately) mostly opaque. A solution used in the silicon solar cell technology is to print a patterned collector with narrow metal lines shadowing only a few percent of the incoming light or even to bury the metal lines into deeply etched grooves.

The silicon solar cell uses a homojunction made out of a p-doped silicon wafer, which is n-doped, e.g. by diffusion of phosphorus, on the front surface. The back surface is covered with a palladium-silver layer as contact and the front (illuminated side) is covered a finger-shaped Ag-Pd metal grid as current collector. Its overall energy diagram is shown in figure 5 [3]:

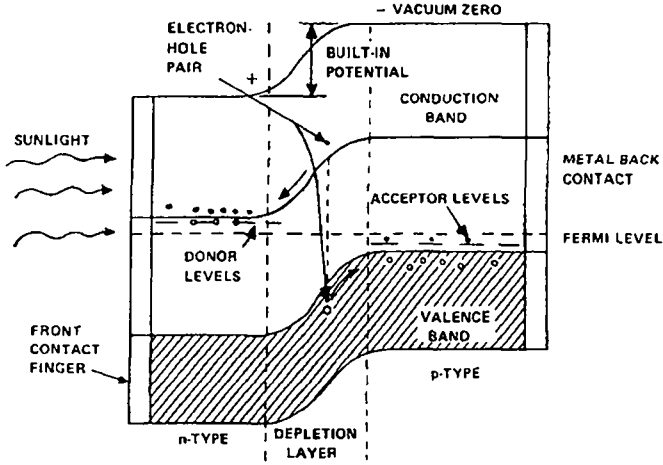


Figure 5: Schematic cross-section of the Si solar cell with the p-n junction energy diagram shown in the short-circuit situation.

The built-in potential is given by the difference in the Fermi-level positions in the n-type and p-type doped sides, whereas the Fermi-level position relative to the band edge energy is given by:

$$E_c - E_f = kT \ln\left(\frac{N_C}{N_D}\right) \quad (6)$$

$$E_f - E_V = kT \ln\left(\frac{N_V}{N_A}\right) \quad (7)$$

Eq. (6) applies for the n-type material and (7) for the p-type material. N_C and N_V are the effective densities of states (for a given temperature) in the conduction band of the n-type doped semiconductor, respective in the valence band of the p-type material. As shown in the figure 5, the light will be absorbed in the n-layer, the depletion layer and the p-layer.

The bulk recombination and the surface recombination of the photogenerated electron-hole pairs will reduce the charge separation efficiency. In the region out of the depletion zone, where no electrical field is present, the charge carriers are just moving by diffusion and their diffusion length is given by [2, p. 53]

$$L = \sqrt{D\tau} \quad (8)$$

where D is the diffusion coefficient and τ the minority carrier lifetime. The minority carriers are electrons in the p-doped region and vice-versa for the holes. The lifetime τ is dependent on the recombination center density (also called the trap density) N_T , as

$$\tau = \frac{1}{\sigma_t V_{th} N_t} \quad (9)$$

where V_{th} is the thermal velocity of the minority carriers given by $V_{th} = \sqrt{3kT/m^*}$ (m^* = effective mass of carrier), N_t the trap density and σ_t the capture cross-section of the trap for the given minority carrier.

If the thickness of the field-free area is larger than the diffusion length L , the minority carriers will be lost by bulk recombination. Thus, for maximal efficiency, it is essential either to lower the impurity and defects level N_t to have a large lifetime, or to reduce the absorber thickness below the charge carrier diffusion length L .

The surface recombination is characterized by a surface recombination velocity $S = \sigma_f V_{th} N_{sc}$, where σ_{sc} is the surface trap capture cross-section and N_{sc} the surface trapping center density per area. The surface recombination is increasing with an increasing S value [2 p. 56]. Surface recombination losses can be either minimized by using defect free surfaces, e.g. by passivating the "dangling" bonds of the Si surface by SiO_2 , or by using a back surface field [4] preventing the minority carriers to reach the back surface (by the electrical field), as shown in fig. 6.

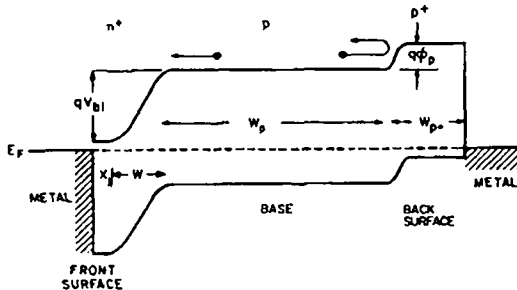


Figure 6: p-n Junction energy diagram with back surface field made by strong p doping (denoted p^+), taken from [4].

The back surface field is made by strongly doping the region (marked p^+) close to the back metal current collector. The Fermi-level is lowered in the highly doped zone by increasing the acceptor concentration, thus an additional built-in field is

created that will push away the electrons (minority carriers) from the surface. The gain of such a design is twofold, first the apparent surface recombination velocity is reduced, second the open-circuit voltage is increased by the additional term ϕ_p .

The ideal J-V characteristics of a solar cell under illumination are given by [2 p. 793, 5]

$$J = J_s \left[\exp\left(\frac{qV}{nkT}\right) - 1 \right] - J_L \quad (10)$$

where J_L is the photocurrent density, V the applied bias, n is the ideality factor and J_s the diode saturation current density given by

$$J_s = qN_C N_V \left(\frac{1}{N_A} \sqrt{\frac{D_n}{\tau_n}} + \frac{1}{N_D} \sqrt{\frac{D_p}{\tau_p}} \right) e^{-E_g/kT} \quad (11)$$

where D_n (D_p) is the diffusion coefficient for the electrons (holes) and τ_n (τ_p) the electron (hole) lifetime.

From (10), the open-circuit voltage is deduced knowing that $J = 0$ at $V = V_{oc}$.

$$V_{oc} = \frac{nkT}{q} \ln\left(\frac{J_L}{J_s} + 1\right) \approx \frac{nkT}{q} \ln\left(\frac{J_L}{J_s}\right) \quad (12)$$

The open-circuit voltage is sensitive to the saturation current density J_s , which itself depends on the inverse of lifetime τ . Hence large minority carrier lifetimes i.e. meaning low recombination rates, are increasing the output voltage.

The solar cell is characterized by its J-V diagram, where the photocurrent density is plotted against the applied voltage in a given light intensity, fig. 7 shows a typical J-V curve.

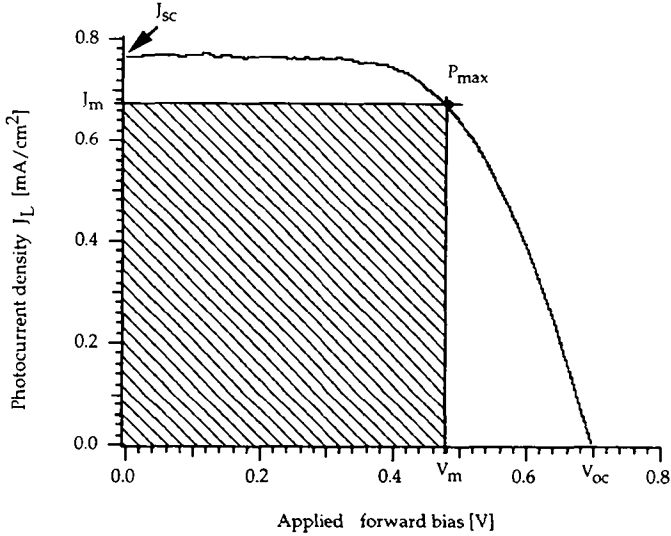


Figure 7: J-V plot of a solar cell with the hatched square showing the maximal power output, $J_{sc} = J_L$ is the short-circuit current density and V_{oc} is the open-circuit voltage.

The maximal electrical output power P_{max} is given by the point where the hatched rectangle $J \times V$ has the largest surface.

The non-dimensional fill-factor FF is defined as

$$FF = \frac{J_m V_m}{J_{sc} V_{oc}} \tag{13}$$

and the efficiency η is given by

$$\eta = \frac{P_{max}}{P_{light}} = \frac{J_{sc} V_{oc} FF}{P_{light}} \tag{14}$$

1.3. Schottky barrier

Another way of charge separation is to use a metal-semiconductor junction, also called Schottky junction or Schottky barrier.

Such a Schottky junction or diode is made by contacting a low work-function metal like Al or In with a p-type semiconductor. Or doing the same with a n-type semiconductor and a high work-function metal like Au or Pt. In a similar way as

described for the p-n junction formation, a built-in voltage appears across the junction due to the Fermi-level alignment. A Schottky barrier based solar cell has the advantage that the junction lies very close to the metal current collector, thus ensuring optimal charge collection. Figure 8 shows the energy diagram of a p-type semiconductor based Schottky diode under illumination.

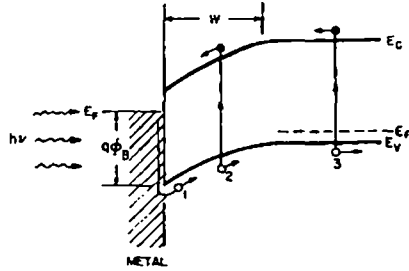


Figure 8: Energy diagram of a Schottky barrier based metal/p-type semiconductor junction showing the electron (filled circles) and hole (open circles) flows. ϕ_B denotes the built-in voltage or the barrier height (taken from [2 p. 821]).

When the device is made in a way that the depletion layer stretches throughout the whole device thickness, it will work as a majority carrier device where, in the example above, only holes are moving in the p-type material, thus avoiding bulk recombination. The drawbacks of the Schottky-diode solar cell are that the light must penetrate through the low work function front contact, which is usually a metal, and that surface recombination is rather high since the metal-semiconductor interface is far from perfect.

The J-V characteristics of the Schottky barrier under illumination are given by [2 p.822]

$$J = J_s \left[\exp\left(\frac{qV}{nkT}\right) - 1 \right] - J_L \quad (10)$$

and

$$J_s = A_R T^2 \exp\left(\frac{-q\phi_b}{kT}\right) \quad (15)$$

where J_L is the photocurrent density, V the applied bias, n is the ideality factor, A_R the effective Richardson constant ($\approx 120 \text{ Acm}^{-2}/\text{K}^2$ for the free electron) and ϕ_B the barrier height given by $\phi_B = \phi_M - \chi$, with χ being the semiconductor electron affinity and ϕ_M the metal work function.

Eq. (10) may be simplified to

$$J = J_s \left[\exp \left(\frac{qV}{nkT} \right) \right] - J_L \quad (16)$$

when the applied bias $V \gg kT/q$ ($= 26 \text{ mV}$ at $300 \text{ }^\circ\text{K}$).

The open-circuit voltage V_{oc} can be deduced from the expressions (15) and (16) by knowing that $J = 0$ when $V = V_{oc}$, thus giving

$$v_{oc} = \frac{nkT}{q} \left[\ln \left(\frac{J_L}{A_R T^2} \right) + \frac{q\phi_B}{kT} \right] \quad (17)$$

1.4. Solar energy - why ?

The first practical solar cell made of a silicon p-n junction was built in 1954 by Chapin, Fuller and Pearson [6] working at the Bell Telephone laboratories in the USA. Their "Bell Solar Battery" with an efficiency of 6 % was driving a transistor radio [7]. A commercial version of this solar power pack was 185 US \$, and compared with the cost of dry batteries of less than 1 US \$ per 100 hours of operation (1957 \$) [8] Furnas stated: "So you can see we have a long way to go before this can be an economical source of power for all except the most special purposes. Here again we, as experimenters, should not be too easily discouraged, and the work should continue". In the same year, the watchmakers Patek Philippe in Geneva, improved their "self-winding photo-electric clock" [9]. Today, 39 years after Furnas' statement, the photovoltaic (PV) energy is still not economically viable if conventional sources like oil or nuclear power have to be replaced, as the PV KWh costs ca. 60 to 120 cents which is ≈ 5 to 10 higher than the conventional non-regenerative sources. The economic difficulty resides in the fact that always a large surface has to be used to collect the solar light, since the averaged (continuous) PV output power per m^2 is ≈ 100 -120 W as calculated in reference [10]. An additional fact is that the solar cells themselves (e.g. the Si-diodes) make only ca 1/3 to 1/4 of the total PV installation costs, as the Si-diodes must be connected and packaged into modules and the modules must be mounted on the roofs or facades. The inverter transforming the DC PV-power into the grid-power of the utility adds to the total costs, too.

These facts leave three ways open to lower total costs and to make PV power more attractive, compared to conventional energy sources.

1. Lower the cost of the photovoltaic generator (solar cell) itself by using novel junction designs or new junction materials.

2. Avoid the expensive cell-to-module manufacturing step by directly making an "internally connected" module out of the new junction design/materials.
3. Integrate the PV modules in double functional elements like tiles on a roof, facade elements on the building walls or even windows if a semi-transparent solar cell would be available.

Way 1. and 2. are directly linked to the technology and the materials choice.

The topics treated in the following chapters might indicate a possible way towards an economically interesting PV based energy supply.

References for chapter 1.

1. A. Ennaoui, S. Fiechter, Ch. Pettenkofer, N. Alonso-Vante, K. Bükler, M. Bronold, Ch. Höpfner and H. Tributsch, *Solar Energy Materials and Solar Cells*, 29 (1993) 294
2. S. Sze in "Physics of Semiconductor Devices" 2nd. Edition, John Wiley & Sons, New York, 1981.
3. R. Komp in "Practical Photovoltaics", 2nd. Edition, Aatec Publications, Ann Arbor, Michigan USA, 1989, pp. 99.
4. J. Mandelkorn and J. Lamneck, *Conf. Rec. 9th IEEE Photovoltaic Spec. Conf.*, IEEE, New-York (1972) 83.
5. M. Prince, *Journal of Applied Physics*, 26 (1955) 534.
6. D. Chapin, C. Fuller and G. Pearson, *Journal of Applied Physics.*, 25 (1954) 676.
7. G. Person "Electricity from the sun" *Proceeding of the World Solar Symposium on Applied Solar Energy*, (1957) 281-288.
8. C. Ferns, *Journal of Solar Energy Science and Engineering*, 1, (1957) 71.
9. C. Ferns, *Journal of Solar Energy Science and Engineering*, 1 (1957) 55.
10. Recommendation pour l'utilisation de l'énergie solaire 1/94, §3.7.1. "Dimensions-caractéristiques" PROMES /SOFAS/OFEN.
11. A. Hagfeldt and M. Graetzel, *Chemical Reviews*, 95 (1995) 51.

2. Novel approaches: The dye solar cell

2.1. Working principles

The so-called "dye solar cell" (DSC) is based on the principles of a regenerative photoelectrochemical photovoltaic cell [1-7,9,10]. Regenerative means that no chemicals are accumulated or depleted during the operation of the device. The dye solar cell's active layer is made of a highly porous, or "nanocrystalline" wide bandgap semiconductor layer, such as TiO_2 (preferably in the anatase crystalline phase), which is covered with a monomolecular layer of a "sensitizing" dyestuff to absorb the incoming visible light. The sensitizing effect of the dyestuff consists of an electron transfer from the excited state of the dye into the conduction band of the TiO_2 . In order to achieve this electron transfer, which is also called electron "injection", three conditions must be fulfilled:

1. The energy level of the excited state of the dyestuff, which in the case of the ruthenium based complexes, is a triplet state, must lie above the conduction band edge of the TiO_2 , i.e. above - 4 V vs. the vacuum level.
2. The excited state of the dye must have a minimal lifetime of around 100 ps [4, 9 p. 100].
3. The dyestuff molecules must be chemically bound to the TiO_2 surface by using attaching groups that ensure a maximal electronic coupling between the excited molecular orbital of the dye and the conduction band d-orbitals of the TiO_2 [2, 5, 8].

The device is completed by a counter-electrode and an electrolyte containing a redox couple having an electrochemical potential which lies above that of the sensitizer in its ground state [1, 9 p. 100].

In practice, the sensitizing dye, also called the sensitizer, is an organometallic compound using the noble d-metal ruthenium as an octahedrally coordinated central atom. The best sensitizer so far is *cis*-bis(isothiocyanato)bis(2,2'-bipyridyl-4,4'-dicarboxylato)-ruthenium(II), abbreviated $\text{RuL}_2(\text{NCS})_2$, where the attaching groups consists of the carboxy moieties which are well adsorbed on the TiO_2 surface [5,7]. The electrolyte used is an organic solvent such as acetonitrile or glutarodinitrile, or a molten salt containing iodide (I^-) and tri-iodide (I_3^- , made by mixing iodine and iodide) as the redox couple. A schematic energy diagram (fig. 9) of the dye solar cell shows the electron flow in the device [13].

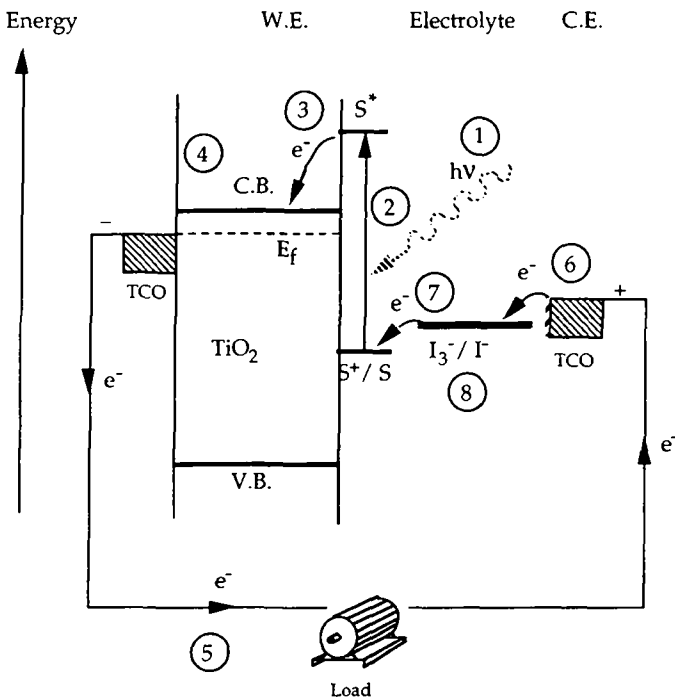


Figure 9: Schematic energy diagram of the dye solar cell showing the steps in the electron flow. TCO stands for Transparent Conducting Oxide used to render the inner glass surface electrically conductive, W.E. for the working electrode and C.E. for the counter-electrode.

The electrical cycle starts when a photon (1) with an energy above 1.65 eV (= 750 nm) hits a dye molecule in its ground state, thus initiating a metal-to-ligand charge transfer (2) where the electron is in an excited orbital (π^* orbital) of the dicarboxy-bipy ligand. From that π^* orbital and after a probable singlet-to-triplet transition (not shown in fig. 9), the electron is injected (3) into the Ti(IV) orbitals forming the conduction band. The electron injection is an extremely rapid process, as it takes only ca. 180 fs [11]. The electron percolates [12] through the nanocrystalline material (4), till it reaches the SnO_2 -coated (or any other transparent conducting oxide) glass electrode which is the *negative terminal*. The electron loses its potential by passing through the external load (5) and reaches the SnO_2 -coated glass plate of the counter-electrode (6). There, the low-potential electron is picked-up by the oxidized form of the redox-couple, the tri-iodide I_3^- , which is thus reduced into iodide (I^-). The I^- in the electrolyte diffuses towards the nanocrystalline TiO_2 surface and gives away the electron (7) to the previously photo-oxidized sensitizer molecule. During this dye reduction step, the iodide is

oxidized to tri-iodide (8), which is again ready to pickup an electron at the counter-electrode. The overpotential of the tri-iodide to iodide reduction reaction at the counter-electrode is minimized by using a catalyst like carbon or platinum which is deposited at the counter-electrode in tiny amounts like 5 to 10 $\mu\text{g}/\text{cm}^2$ either by electrodeposition or by pyrolysis of an alcoholic H_2PtCl_6 solution at 450 $^\circ\text{C}$ [14]. A large concentration of I^- in the electrolyte, typically 0.5 M, ensures a rapid reduction (takes ca. 10 ns) of the labile oxidized form of the Ru-sensitizer [13].

In fig. 10, is the schematic build-up of such a nanocrystalline dye solar cell, showing the cross-section of the device and a TiO_2 crystallite with a Ru-based sensitizer molecule attached on its surface.

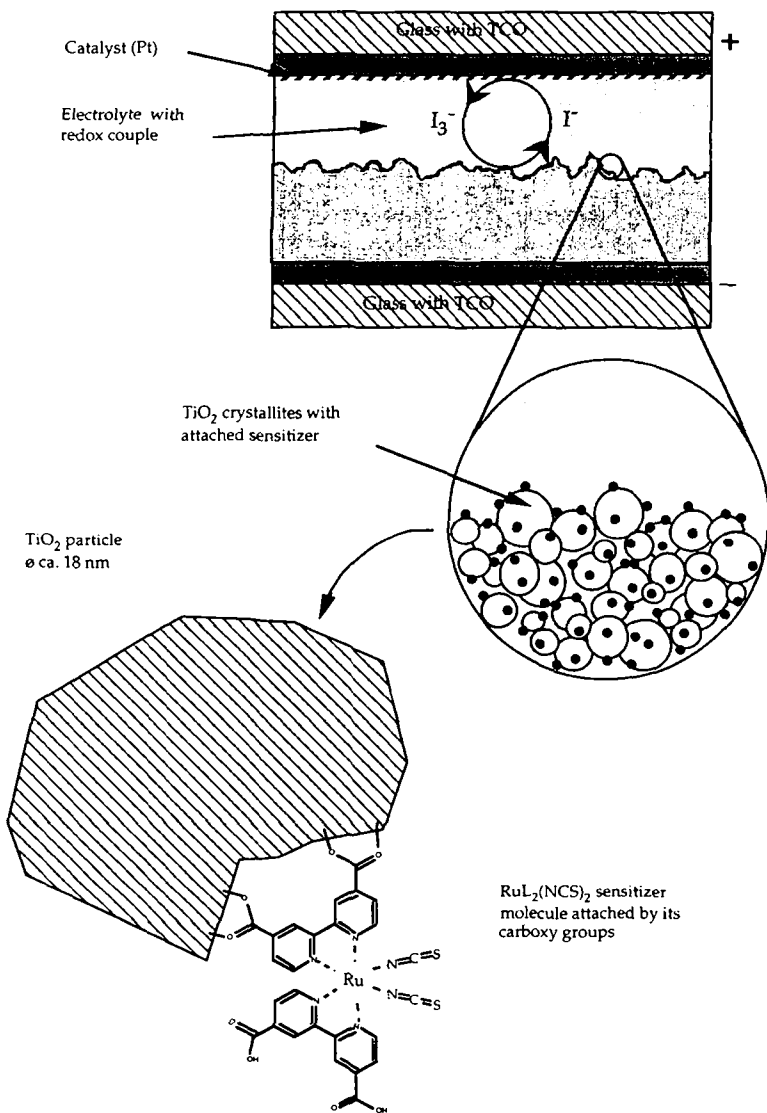


Figure 10: Cross-section of the dye solar cell with the blow-up of the nanocrystalline TiO₂ electrode showing the dye molecules attached on the TiO₂ crystallites (not to scale).

2.2. Why use nanocrystalline materials ?

The photon-to-electron conversion efficiency or IPCE term shown in chapter 1 (eq. 2) can be rewritten into the following expression when dealing with the dye solar cell [4]:

$$\text{IPCE}(\lambda) = \text{LHE}(\lambda) \phi_{\text{inj}} \eta_{\text{coll}} \quad (18)$$

where LHE stands for the wavelength dependent light harvesting efficiency, corresponding to the light absorption, ϕ_{inj} is the quantum yield of charge injection of the sensitizing dye and η_{coll} the efficiency of collecting the injected charges at the back contact. In order to have an efficient photovoltaic cell, the IPCE must be close to 100 % throughout the biggest part of the absorption spectrum of the dye. To achieve this, LHE, ϕ_{inj} and η_{coll} must be maximized. The injection efficiency ϕ_{inj} is only dependent on the energy levels of the dye and the semiconductor, and is strongly dependent on the electronic structure of the excited state of the dye and its excited state lifetime [4]. If the nanocrystalline particles were in the 2-10 nm range, however the bandgap and the conduction band edge position will be affected by particle size due to quantization effects as shown by Hoyer et al. in the case of nm sized nanocrystalline ZnO [15].

Hence, the nanocrystalline nature of the oxide semiconductor electrode plays an essential role in the maximization of the LHE and the η_{coll} values:

1. Improve the light harvesting efficiency (LHE) by optical serial connection of absorbing dye molecules.

The Ru-sensitizer must be adsorbed on the TiO_2 surface in a molecular monolayer to enable rapid electron injection since the dye itself is not an electron conductor. Knowing that the Ru-sensitizer has a maximal absorption cross section of $\sigma = 1.42 \times 10^7 \text{ cm}^2/\text{mol}$ for $\text{RuL}_2(\text{NCS})_2$ (value deduced from the extinction coefficient of $\epsilon = 14'200 \text{ M}^{-1} \text{ cm}^{-2}$) [4 p. 6385] and that a molecule of $\text{RuL}_2(\text{NCS})_2$ occupies an area of ca. 1 nm^2 [9 p. 75], one can calculate that a monomolecular layer (thickness $< 1 \text{ nm}$) of dye, will only catch less than one percent of the incoming radiation if put on a flat surface [3, 10, 12]. The only way to overcome this problem is to put the absorber molecules optically in series: For a given solar cell area, the incoming photons that will see a lot of dye molecules put one behind the other and being separated by transparent TiO_2 (and electrolyte). In other words, if the dye accessible surface is increased by several orders of magnitude, there will be more sensitizer molecules per projected area, thus the light harvesting will be dramatically improved.

Currently an internal surface increase of ca. 1000:1 is achieved with $10 \mu\text{m}$ thick colloidal nanocrystalline anatase electrodes [3], thus multiplying the apparent absorption cross-section of the sensitizer by a factor of 1000. The result is an absorption of $> 99 \%$ of the light by the dye [4]. This accessible surface increase is measured by desorbing the dye from the TiO_2 and by checking the resulting

absorbance in solution with a calibrated optical path or by measuring the absorption isotherms [2 p. 1795].

2. The charge transport characteristics of the nanocrystalline materials:

Two operating modes must be distinguished:

- a) Direct band-gap excitation of the semiconductor with creation of electron-hole pairs.
- b) Schottky diode or majority carrier device operating mode, where only electrons (majority carriers in the case of n-type TiO₂) are injected and travelling in the semiconductor, while the holes are carried away by the redox couple in the electrolyte, which is wetting the nanocrystalline semiconductor sponge.

Mode a)

The direct recombination of charge carrier pairs (electrons and holes) during their migration in the bulk of the semiconductor towards the contacts, is a very critical issue in the silicon and GaAs semiconductor technology, as only ultra-high purity materials can be used to avoid recombination due to the impurities of either chemical nature (heteroatoms, unwanted crystalline phases) or physical nature like lattice defects or grain joints. This problem is overcome in the case of the nanocrystalline film, as the particle size (10-20 nm) is smaller than the diffusion length of the minority carriers (holes) $L = \sqrt{D\tau} = 100 \text{ nm}$ [13]. Although in practice, the nanocrystalline TiO₂ cell is not operating in the intrinsic excitation mode, as only 1-2 mA/cm² of current are produced this way in full sun. Furthermore, the incoming UV ($h\nu < 3.2 \text{ eV}$) radiation is creating holes in the anatase particles that are acting as a very strongly oxidizing species, able to attack the electrolyte and the sensitizer. This intrinsic excitation mode is only interesting for nanocrystalline semiconductors with a bandgap in the visible range, e.g. around 1.5 eV.

Mode b)

The conduction band of the TiO₂ accepts the electrons from the electronically excited sensitizer, hence only the electrons are carried in the n-type semiconductor and the holes are carried by the chemical species (donor) acting as a redox-couple in the electrolyte, as shown in fig. 11. The device works as a majority carrier device, similar to a metal-semiconductor junction, or a Schottky diode. In this case, direct hole-electron recombination within the bulk of the semiconductor electrode is avoided as only one type of charge is present in the solid.

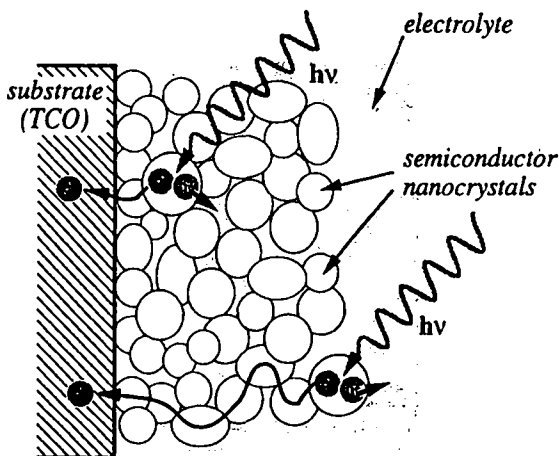


Figure 11: Light induced charge separation in a nanocrystalline semiconductor film where holes are scavenged more rapidly than electrons at the particle-electrolyte interface. As a consequence, the film exhibits n-type behavior (adapted from [16]).

The transport of the electron from the outer surface to the TCO current collector occurs via diffusion of the carriers throughout the nanocrystalline particle network [13,16]. The transit time of the electrons has been calculated by O'Regan et al. [12], and a typical value in the fraction of μs range was found for 2.7 μm thick nanocrystalline TiO_2 membranes. But as the observed photocurrent transient times are in the ms range [12], the transit time increase is due to the successive trapping and thermal detrapping (or tunneling) of the electrons when they hop from one TiO_2 particle to the other [12 p. 8735]. Hence the charge transport behavior of the nanocrystalline TiO_2 electrodes is essentially a trap governed behavior as there are ca. 10^{14} surface states per cm^2 of electrode acting as a trap. In other words, ca. 1% of the Ti atoms are traps [5], as the 3d-Ti(III) centers are located ca. 0.3 eV below the conduction band edge [17 p. 251]. This high trap concentration is not critical, apart from conduction band lowering which decreases the photovoltage, since the device acts as a majority carrier device, and there are no holes in the valence band of the TiO_2 with which the electron could recombine. The only two remaining recombination paths are:

1. when a conduction band electron is reducing the tri-iodide in the electrolyte, or
2. the recapture of the conduction band electrons by the still oxidized sensitizer molecules.

Case 1. is minimized by the fact that the electron must be at the surface of the crystallites in order to be in contact with the surrounding I_3^- in the electrolyte.

Case 2. is minimized since the steady state concentration of oxidized sensitizer is very low as the I⁻ in the electrolyte acts as the electron donor which will regenerate the oxidized dye very efficiently [13]. Furthermore, the Ru 3d-orbital contraction upon oxidation of the sensitizer lowers the overlap integral between the Ru(III) d-orbitals and the d-orbitals of the Ti(IV) forming the conduction band [16]. Another favorable argument is the entropy increase when the localized electron of the excited state of the sensitizer is "diluted" over several thousand Ti(IV) atoms of the nanocrystallite [16 p.58]. As a result, overall IPCE values close to 85 % (without correction for reflection and absorption losses in the glass) [4,18] are observed in (well made) dye solar cells. This means that the light harvesting efficiency, the injection, and the charge collection are close to 100 % of efficiency, despite the many possible photoelectron loss paths mentioned above [4].

Recently, at the NREL in Golden, Colorado (USA), a light-to-electrical energy conversion efficiency of 8.5 % under 1000 W/m² AM1.5 normalized simulated light was achieved for a 0.315 cm² cell [13]. The short-circuit current density was 18.37 mA/cm², the open-circuit voltage was 762 mV and the fill-factor was 0.6. Efficiencies between 9 and 10 % were reached for lower light intensities, where the serial resistance of the conducting glass did not affect too badly the fill-factor [4, 13, 19].

As a conclusion, the interplay between the Ru-sensitizer, the nanocrystalline TiO₂ electrode and the electrolyte can be considered as perfect, and any improvement of this well-tuned system will be extraordinarily difficult !

2.3. Projected economic data for the dye solar cell

The prospect of a truly affordable solar energy source for the power market is justified by the fact that the dye solar cell uses mainly low cost materials and it is manufactured using well-known thick film deposition techniques like spraying and screen-printing. Several industrial groups and research labs are currently working on the industrialization of the dye solar cell [20]. Smestad et al. [21] estimated the cost of the nanocrystalline solar cell modules to be around 60-70 US \$/m², which is probably a too low figure. Solaronix [22] has estimated the costs for a 20 x 30 cm sized 3 Wp dye solar cell module to be in the 4-5 US \$ range, when assuming a production output of 4 MWp p.a., a module efficiency of 5 % and a security factor of 1.5, i.e. meaning that the overall reject rate throughout the 20 step production process is 33%. The detailed cost breakdown is listed in table 1.

Item/process	US cents per module
Anatase screenprint paste	30
Ru dye	60
SnO ₂ :F glass (10 Ω/square)	180
Pt at counter electrode	10
Electrolyte and iodide salt	3
Sealant (primary + plug)	18
Interconnects + contacts	30
Subtotal materials	331
Labor (12 people)	79
Depreciation (20 %) of investment	48
Rent floorspace (6% mortgage)	5.5
Total module cost	463.5 US cents
Cost per peak watt (3W/module)	154.5 US cents per Wp

Table 1: Cost repartition of the different constituents needed to make 20 x 30 cm sized dye solar cell modules. The peak watt (Wp) is the maximal electrical power that the module will give when illuminated with a standardized light intensity of 1000 W/m² with the AM 1.5 solar spectrum.

The cost breakdown in table 1 shows that the total costs of such a 20 x 30 cm sized modules are mostly due to the materials used. The most expensive parts seems to be the TCO glass (tempered glass) and the Ru-dyestuff. If such 20 x 30 cm modules would be used for the energy supply, e.g. as tiles on a roof, an additional cost factor due to improved connectings and weatherproofing overcoats, similar to the ones used with crystalline silicon, should be taken into account. Maybe, this adds 2 US \$ more to the modules, so a watt-peak cost of ca. 220 US cents/Wp comes up. Assuming a future conversion efficiency of 7 % instead of the used 5 %, a figure of 160 US cents/Wp can be estimated.

To this cost, the "balance of system (BOS)" costs should be added, i.e. the cost of the module supporting structures, electrical wiring, mounting and converters. Depending on the PV-power plant layout, e.g. in a 3 KWp rooftop PV installation, the BOS related costs can be as much as the module costs itselfs [23]. Despite this fact, the nanocrystalline solar cells appears as to be a possible contender for an acceptably priced renewable energy source, which should lie around 3 US \$ per installed watt or at ca. 20 cents/KWh [24]. This fact justifies the intense research made in this field in several labs and industries throughout the world [25]. To compare these US \$/Wp cost figures, today in Switzerland, a 3 KWp photovoltaic installation using monocrystalline silicon cells costs ca. 45'000 US \$, where the

solar cells alone are ca. 22'000 to 28'000 US \$, so the total Wp costs are 15 US \$ and the contribution of the solar generator to this cost figure is ca. 7 to 9 US \$ per peak watt.

References for chapter 2.

1. N. Vlachopoulos, P.Liska, A.J. McEvoy and M. Graetzel, *Surface Science*, 189/190 (1987) 823.
2. M.K. Nazeeruddin, P. Liska, J. Moser, N. Vlachopoulos and M. Graetzel, *Helvetica Chimica Acta*, 73 (1990) 1788.
3. B. O'Regan and M. Graetzel, *Nature*, 353 (1991) 737.
4. M.K. Nazeeruddin, A. Kay, I. Rodicio, R. Humphry-Baker, E. Müller, P.Liska, N. Vlachopoulos and M. Graetzel, *Journal of the American Chemical Society*, 115 (1993) 6382.
5. A. Kay, R. Humphry-Baker and M. Graetzel, *Journal of Physical Chemistry*, 98 (1994) 952.
6. A. Hagfeldt, B. Didriksson, T. Palmquist, H. Lindström, S. Södergren, H. Rensmo and S.-E. Lindquist, *Solar Energy Materials and Solar Cells*, 31 (1994) 481.
7. A. Coghlan, *New Scientist*, January ed. (1995) 22.
8. J. Moser, S. Punchihewa, P. Infelta and M. Graetzel, *Langmuir*, 7 (1991) 3013.
9. A. Kay, "Solar Cells Based on Dye-Sensitized Nanocrystalline TiO₂ Electrodes" Ph.D thesis work N° 1214 (1994) EPFL.
10. P. Liska, "Praktische Aspekte der Licht-Energieumwandlung am Beispiel einer TiO₂-Farbstoffzelle" Ph.D thesis work N° 1269 (1994) EPFL.
11. J. Moser, M. Graetzel, J. Durrant, D. Klug, *Proceedings Lausanne Conference on Femtochemistry*, 1995.
12. B. O'Regan, J. Moser, M. Anderson and M. Graetzel, *Journal of Physical Chemistry*, 94 (1990) 8725.
13. M. Graetzel in "Nanocrystalline Semiconductor Materials", P.V Kamat and D. Maisel, Ed., Elsevier Science, Amsterdam, The Netherlands, 1996, pp. 14.
14. N. Papageorgiou, W.F. Maier and M. Graetzel, *Journal of the Electrochemical Society*, to be published.
15. P. Hoyer, R. Eichberger and H. Weller, *Berliner Bunsen-gesellschaft Physikalische Chemie*, 97 (1993) 634.
16. A. Hagfeldt and M. Graetzel, *Chemical Reviews*, 95 (1995) 51.
17. A. Hagfeldt, S.-E. Lindquist and M. Graetzel, *Solar Energy Materials and Solar Cells*, 32 (1994) 245.

18. O.Kohle, S. Ruile and M. Graetzel, *Inorganic Chemistry*, to be published.
19. T. Meyer, O. Kohle, S. Ruile, P. Comte, N. Vlachopoulos and M. Graetzel, Optimization works to get highest efficiency possible made 1994 leading to measurements done at the ISE in Freiburg i.Br. (Germany).
20. Flachglas AG, Gelsenkirchen (Germany), GlasTrösch, Bützberg (Switzerland), STA, Canberra (Australia), Solterra SA, Manno (Switzerland), Leclanché SA, Yverdon (Switzerland), Asulab SA, Bienne, Switzerland, Solaronix SA, Aubonne (Switzerland).
21. G. Smestad, C. Bignozzi and R. Argazzi, *Solar Energy Materials and Solar Cells*, 32 (1994) 259.
22. Solaronix SA, L'Ouriettaz 140, CH-1170 Aubonne/VD, Switzerland, e-mail: solaronix@ibm.net, fax +41 21 808 82 31.
23. S. Novak, Forschungsprogramm Photovoltaik 1995, Swiss Federal Office for Energy, 1995, N° 10.
24. L. Shinnar, *Chemtech*, January issue (1993) 50.

3. Strategies towards solid state nanocrystalline solar cells

3.1. Materials choice and requirements

When working on dye solar cells, immediately the idea comes to mind to replace the liquid electrolyte carrying the redox-couple with a solid agent being able to either carry the ions or, better, only the electrical charges (holes). This solid hole conducting material must fulfill the following physical and chemical conditions, as listed order of priority:

- Have an adequate energy level position in respect to the redox potential of the dye, i.e. below 0.85 V vs. SCE (Standard Calomel Electrode) for the $\text{RuL}_2(\text{NCS})_2$ dye [1 p. 6385].
- Be transparent or only weakly absorbing in the visible range (400 - 700 nm) i.e. have a bandgap around or above 3 eV.
- Processable in way to be brought into the nano-sized pores, e.g. by electrodeposition, chemical bath deposition, melting and solution casting, and this without exceeding 150 °C.
- Reasonably stable towards air and humidity.
- Low toxicity.

A rough estimation of the required hole mobilities can be made, assuming that the light is completely absorbed in the 5 μm thick sensitized nanocrystalline TiO_2 layer and that the total hole transporting layer thickness is ca. 30 μm , which is a usual thickness value found in practical liquid-electrolyte based devices.

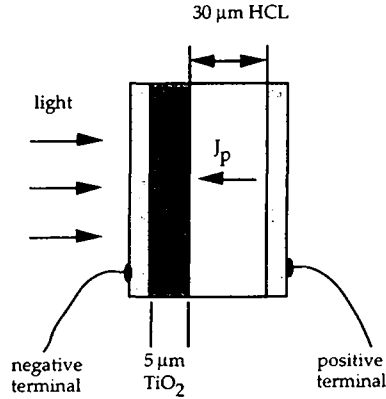


Figure 8: simplified solid state dye solar cell model with hole conducting layer (HCL). J_p denotes the hole flux in the HCL.

Fick's law expresses the current flow J in charges/s cm^2 as

$$J = -D \frac{dc}{dx} \quad (20)$$

where D is the diffusion coefficient in cm^2/s , dc the charge concentration (cm^{-3}) difference within the distance dx (in cm).

The practically observed photocurrents for the dye solar cells are in the range between 15 to 20 mA/cm^2 at full sunlight illumination. The hole conducting layer should be able to carry currents like that without too high an ohmic voltage drop. So, $J = 0.02 [\text{C}/\text{s cm}^2] / 1.6 \times 10^{-19} [\text{charges}/\text{A}] = 1.25 \times 10^{17} \text{ charges}/\text{s cm}^3$. In the example shown in fig. 8, the hole conducting layer thickness is $dx = 30 \mu\text{m} = 3 \times 10^{-3} \text{ cm}$, and the photogenerated charge concentration is given by the number of incoming photons converted into electrons and holes in the TiO_2 layer, as the IPCE can be assumed to be 100 % (see chapter 2). At full sun ($100 \text{ mW}/\text{cm}^2$), ca. $\phi_{\text{phot}} = 1.25 \times 10^{17}$ photons/s are converted into the same amount of holes in the TiO_2 electrode having a volume of $V = 5 \times 10^{-4} \text{ cm}^3$, for a 1 cm^2 sized cell. Thus $dc = \phi/V = 2.5 \times 10^{20} \text{ charges}/\text{s cm}^3$, as at the positive terminal all the charges are collected. Extracting D from eq. 20 and replacing J , dc and dx by their values, yields a diffusion coefficient $D = 1.5 \times 10^{-6} \text{ cm}^2/\text{s}$, which is the lower limit for the hole diffusion coefficient that the hole conductor should have. Otherwise, cell performances would be too much decreased.

From the Einstein relation [2]

$$D_p = \left(\frac{kT}{q} \right) \mu_p \quad (21)$$

linking the hole diffusion coefficient D_p to the hole mobility μ_p , the minimal hole mobility value can be estimated from the above found diffusion coefficient. So, we have $\mu_p = 5.8 \times 10^{-5} \text{ cm}^2/\text{Vs}$. These hole mobility and diffusion values have to be compared with the electron diffusion coefficient and the electron mobility in the nanocrystalline TiO_2 electrode, which are $D_n = 0.02 \text{ cm}^2/\text{s}$ [3] and $\mu_n = 0.77 \text{ cm}^2/\text{Vs}$. In the liquid based dye solar cell case, where the iodide/tri-iodide redox couple is used as the hole conducting agent, a diffusion coefficient of $D = 8.5 \times 10^{-6} \text{ cm}^2/\text{s}$ is measured for the tri-iodide when acetonitrile is taken as a solvent [4]. A high liquid phase diffusion coefficient is required to achieve good light-to-electricity efficiency values around 8-9 % in strong illumination (full sun), and any solvent used in the dye solar cell with a higher viscosity than acetonitrile, will show bad fill-factors affecting seriously the conversion efficiency [5], as the diffusion coefficient is lowered in viscous solvents.

In conclusion, the hole conducting layer should have a minimal hole mobility around $5 \times 10^{-5} \text{ cm}^2/\text{Vs}$, knowing that higher values would give more margin to account for non-ideal hole transport processes in the hole conducting layer.

3.2. Early attempts to make a solid-state sensitized solar cell

In the thesis work of Skotheim [6], sensitized TiO_2 junctions are described using a merocyanine dye as sensitizer and a flat n-doped TiO_2 single crystal. A IPCE value of 12 %, at a wavelength of 520 nm, have been found using a iodine doped 50 nm thick merocyanine layer acting as the sensitizer and the hole conduction layer. This IPCE value was increased to 21 % when a 75 nm thick perylene layer was put on top of the sensitizing layer, acting as a spacer between the merocyanine dye and the gold electrode, as shown in the schematic diagram below (fig. 9).

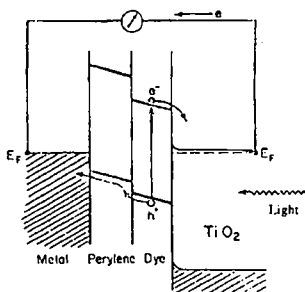


Figure 9: Schematic energy levels diagram of the metal/perylene/merocyanine/ TiO_2 sandwich structure, showing the excitation of the merocyanine dye and the charge separation (adapted from [6]).

With such a device, an open-circuit voltage of ca. 310 mV and a short-circuit current density around $1.8 \mu\text{A}/\text{cm}^2$ at 520 nm with a light intensity of $70 \mu\text{W}/\text{cm}^2$ was achieved. Morel et al. [7] are reporting on a 1% efficiency solar cell using a merocyanine sensitized Al/Al₂O₃ electrode. The observed open-circuit voltage (V_{oc}) was around 1.2 V at ca. $100 \text{ mW}/\text{cm}^2$ irradiation. Extensive studies of the merocyanine optimization were done by Piechowski et al. [8]. Stable cadmium sulfide (CdS) photovoltaic devices using 2,9-dimethyl quinacridone as a sensitizer were reported by K. Manabe et al., and a V_{oc} of 0.61 V was found in 2/3 sun irradiation [9]. A copper phthalocyanine based heterojunction using a sprayed cadmium zinc sulfide electrode was described by M. Ben-Said, where a short-circuit current of around $1 \text{ mA}/\text{cm}^2$ was observed at $100 \text{ mW}/\text{cm}^2$ irradiation [10]. This work demonstrated the possibility of sensitizing a wide band-gap material like CdZnS with a phthalocyanine based dye. Youm et al. were using doped poly(3-methyl thiophene) as a sensitizer and hole conductor deposited electrochemically onto the CdZnS electrode [11].

A novel approach is used by A. Ennaoui et al. [12] where pyrite (FeS₂), a p-type semiconductor, is used as a sensitizer. This material has the advantage of having an extremely high absorption coefficient in the visible light, as $\alpha = 6 \times 10^5 \text{ cm}^{-1}$, meaning that 90% of the incoming light would be absorbed in a less than 10 nm thick FeS₂ layer. Impressive photocurrents in the range of $30 \text{ mA}/\text{cm}^2$ have been measured with a flat Pt/FeS₂ Schottky diode based photocell [12]. This experiment demonstrated the possibility of using a very strongly absorbing material as a light collector that also acts as the hole conducting layer.

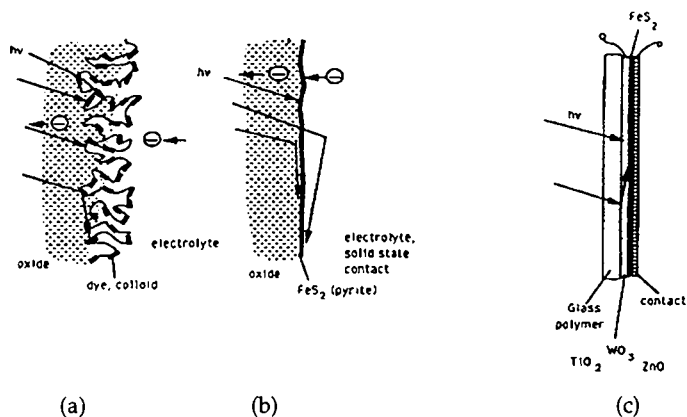


Figure 10: (a) Scheme of a dye sensitized fractal oxide solar cell; (b) scheme of a pyrite sensitized smooth oxide solar cell; (c) design of a pyrite sensitized oxide solar cell [Taken from ref. 12].

A close approximation of a p-semiconductor sensitized device was achieved with certain types of n-type cadmium sulfide/p-type copper sulfide (CdS/Cu₂S)

heterojunction based photovoltaic devices [13-17]. As shown in the fig. 11, a certain active surface increase was possible during the manufacturing of the CdS/Cu₂S cell, the CdS grows with columnar grains and the chemically deposited "Clevite process" Cu₂S was able to penetrate into the CdS grain joints. Efficiencies close to 10 % were achieved which such thin layer cells. Again, the Cu₂S acted as the sensitizer and on the same time as the hole conducting layer.

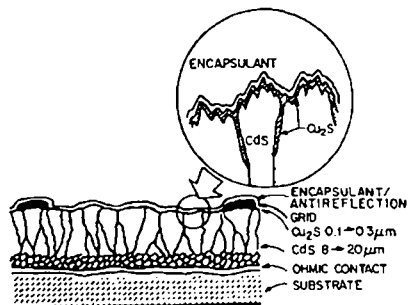


Figure 11: Schematic thin-film CdS solar cell. (After Barnett et al., [13])

The energy diagram applying for this heterojunction based photovoltaic cell is shown in fig. 12.

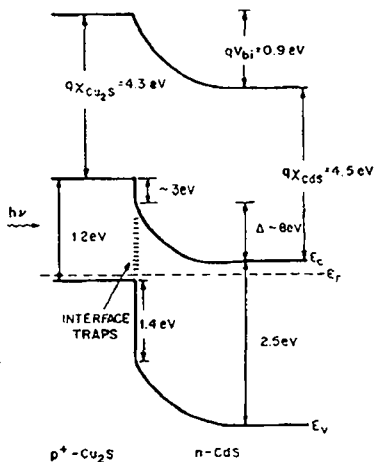


Figure 12: Energy-band diagram of a Cu₂S/CdS solar cell (taken from [14]).

The interface between the CdS and the Cu₂S is far from perfect as their crystalline lattices are not properly matched, thus creating surface traps at the junction itself.

An other possible way of making a "folded" junction is to have thin active layers of n and p silicon, as shown in fig 13. The bulk recombination is minimized for given lifetime as $L = \sqrt{D\tau}$ and again the cell thickness is much lower than the diffusion length L of the charge pairs, hence bulk recombination is avoided. The junction thickness reduction must be balanced by a minimal optical path length of ca. 250 μm [18], as silicon is an indirect band-gap material. Fig. 13 shows a possible way to make a structured interconnected high surface area junction, where obviously the Si-bulk is replaced by transparent window material like CdS or TiO₂, and the strongly doped Si (denoted n⁺ and p⁺ in fig. 13) is replaced by a sensitizer, either of organic or mineral nature like Cu₂S or pyrite.

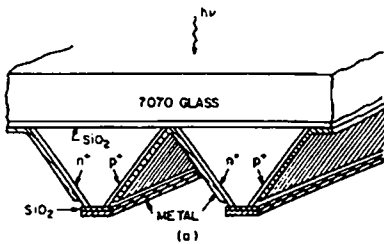


Figure 13: Vertical-groove multijunction solar cell.

Recently Tennakone et al. described "A dye-sensitized nano-porous solid-state photovoltaic cell" [19], where a nano-porous TiO₂ electrode is sensitized by a naturally extracted cyanidine dye, and copper iodide (CuI) is used as the hole conducting layer. Effectively CuI is a p-type semiconductor which is transparent in the visible as its bandgap is 2.95 eV [20].

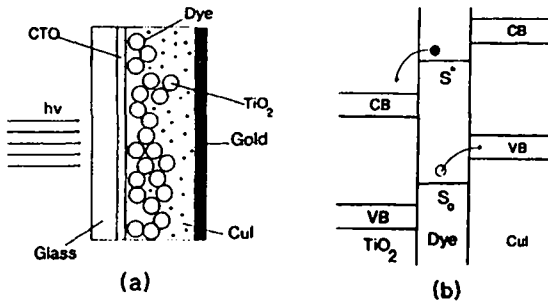


Figure 14: (a) The construction of the nano-porous n-TiO₂/cyanidine/p-CuI photovoltaic cell. (b) A schematic energy level diagram illustrating the relative band positions of TiO₂ and CuI and the energy levels of the dye (taken from [19]).

An impressive short-circuit current of 2.5 mA/cm² and an open-circuit voltage of ca. 370 mV were observed when the above described device is put into direct sunlight (800 W/m²). Apparently the used cyanidine dye has the ability to inject holes into the valence band of p-CuI, as the sensitized CuI electrode worked well in a photoelectrochemical cell. In another article of Tennakone et al. [21], the sensitization of a CuI electrode by chlorophyll is reported, which also seems to be able to inject the photogenerated holes into the valence band of the CuI layer. Another p-type wide bandgap semiconductor, copper thiocyanate, CuSCN, is also a candidate as a transparent hole conducting layer. O'Regan [22] and Tennakone [23] are reporting on photovoltaic properties of CuSCN when sensitized with 3,3'-diethyl-4,5,4',5'-dibenzo-thiocarbocyanine or with methyl violet, respectively.

From the above mentioned examples of different types of "sensitized" junctions, there are essentially two ways of making solid state dye solar cells:

1. Use a highly absorbing material as sensitizer, as only a thin layer is required. An essentially flat junction has the advantage that the intimate contact between sensitizer and p-type material (or the hole conducting layer) is guaranteed and only minimal thicknesses of hole transporting material are needed. The best example of such a device is the TiO₂/pyrite cell described by Ennaoui.
2. Use a transparent hole conducting material like CuI or CuSCN to replace the electrolyte in the dye solar cell described in chapter 2. In this case, the hole conducting material must be in intimate contact with every dye molecule, i.e. the TiO₂ sponge must be soaked up by the hole conductor. Furthermore, the hole injection from the oxidized dye into the valence band of the hole conductor must be as efficient as possible, maybe by using some sort of attaching groups linked to the dye molecule, similar to the carboxyl groups used for the "electron side" of the dye solar cell.

In this work, the first experiments described are Schottky TiO₂/metal diodes, where Ag or Au is directly evaporated on the porous TiO₂ layer. Then, poly(bithiophene) was used as hole conductor and as a sensitizer in an other set of experiments, and finally a mineral transparent hole conductor, copper iodide, was tested in the nanocrystalline TiO₂ junction.

References for chapter 3.

1. M.K. Nazeeruddin, A. Kay, I. Rodicio, R. Humphry-Baker, E. Müller, P.Liska, N. Vlachopoulos and M. Graetzel, *Journal of the American Chemical Society*, 115 (1993) 6382.
2. S. M. Sze "Physics of Semiconductor Devices" 2nd. Edition, John Wiley & Sons, New York, pp. 30.
3. A. Hagfeldt and M. Graetzel, *Chemical Reviews*, 95 (1995) 49.
4. N. Papageorgiou, M. Graetzel and P. Infelta in "On the Relevance of Mass Transport in Thin Layer Nanocrystalline Photoelectro-chemical Solar Cells", *Solar Energy Materials and Solar Cells*, to be published.
5. T. Meyer, O. Kohle, S. Ruile, P. Comte, N. Vlachopoulos and M. Graetzel, Optimization works to get highest efficiency possible made 1994, leading to measurements done at the ISE in Freiburg i.Br. (Germany).
6. T.A. Skotheim "Photovoltaic Properties of Metal-Merocyanine-TiO₂ Sandwich Cells", Ph.D thesis made at the Lawrence Berkeley Laboratory, Univ. of California, 1979.
7. D. Morel, A. Ghosh, T. Feng, E. Stogryn, P. Purwin, R. Shaw and C. Fishman, *Applied Physics Letters*, 32 (1978) 495.
8. A. Piechowski, G. Bird, D. Morel and E. Stogryn, *Journal of Physical Chemistry*, 88 (1984) 934.
9. K. Manabe, S. Kusubayashi and M. Yokohama, *Chemistry Letters*, (1987) 609.
10. M. Ben-Said, S. Belgacem, M. Dachraoui, R. Bennaceur and H. Bouchriha, *Revue de Physique Appliquée*, 21 (1986) 407.
11. I. Youm, M. Cadène and D. Laplaze, *Journal de Chimie Physique*, 89 (1992) 1111.
12. A. Ennaoui, S. Fiechter, Ch. Pettenkofer, N. Alonso-Vante, K. Büker, M. Bronold, Ch. Höpfner and H. Tributsch, *Solar Energy Materials and Solar Cells*, 29 (1993) 289.
13. A. Barnett, J. Bradagnolo, R. Hall, J. Phillips and J. Meakin, *Conference Records of the 13th IEEE Photovoltaic Specialists Conference*, IEEE, New York (1978) 419.
14. L. Burton, B. Baron, W. Devaney, T. Hench, S. Lorenz and J. Meakin, *Conference Records of the 12th IEEE Photovoltaic Specialists Conference*, IEEE, New York (1977) 526.

15. E. Aperathitis, F Bryant and C. Scott, *Solar Energy Materials*, 20 (1990) 15.
16. L. Partain, *Journal of Applied Physics*, 63 (1988) 1762.
17. J. Thornton and W. Anderson, *Applied Physics Letters*, 40 (1982) 622.
18. T. Chapall, "The V-groove Mutijunction Solar Cell" *IEEE Transport in Electronic Devices*, ED-26 (1979) 1091.
19. K. Tennakone, G. Kumara, A. Kumarasinghe, K. Wijayantha and P. Sirimanne, *Semiconductor Science and Technology*, 10 (1995) 1689.
20. O. Magdelung in *Landolt-Börnstein*, New Series III/22a "Cuprous iodide (g-CuI)", Springer-Verlag, Berlin, 1987, pp. 250.
21. K. Tennakone, A. Kumarasinghe, P. Sirimanne and G. Kumara, *Journal of Photochemistry and Photobiology A: Chemistry*, 91 (1995) 59.
22. K. Tennakone, K. Hewaprakkarama, M. Dewasurenra, A. Jayatissa and L. Weerasana, *Semiconductor Science and Technology*, 3 (1988) 382.
23. B. O'Regan and D. Schwartz, *Chemistry Materials*, 7 (1995) 1349.

4. Metal/nanocrystalline-TiO₂ junctions

Skotheim presented the photovoltaic properties of gold contacted dye coated single-crystals of n-type TiO₂ (rutile) in his Ph.D. thesis [1]. Short-circuit current densities around 1.8 $\mu\text{A}/\text{cm}^2$ and an open circuit voltage of 310 mV were observed using monochromatic 520 nm irradiation with an intensity of 70 $\mu\text{W}/\text{cm}^2$. Quantum efficiencies around 12 % at 520 nm irradiation were achieved with these flat single-crystal TiO₂/merocyanine/Au junctions. The used merocyanine layer was 10 to 100 nm thick, and was acting as a hole conductor to transport the carriers towards the metal contact [2,3].

The idea of the following experiments was to extend the concept of dye sensitized TiO₂/metal junctions using a highly porous nanocrystalline (nc-) TiO₂ as n-type semiconductor and a metal like silver or gold to achieve the rectifying contact. The problem of this concept is that on one side the metal should enter into all the pores of the nanocrystalline material in order to make a good contact with all the sensitizer molecules, on the other hand, the metal would act as an absorber that might prevent the incoming light to be caught by the sensitizer. Furthermore, the experiments made by T.A. Skotheim showed that the metallic contact might quench the sensitizer, a phenomenon which is known in literature [1 p.114]. This quenching effect is limited to ca. 200 nm distance from the metal acting as "antenna" to absorb the electromagnetic energy emitted from the dye's electronic oscillator.

Despite this contradiction, preliminary tests using nanocrystalline titanium oxide layers with a silver pad deposited by evaporation showed a current density of 45 $\mu\text{A}/\text{cm}^2$ and an open-circuit voltage of 310 mV when lit through the conducting glass side by an unfiltered Xe-lamp with an intensity of ca. 86 mW/cm^2 . The general cross-section of the TCO/nc-TiO₂/metal junctions is shown in fig. 15.

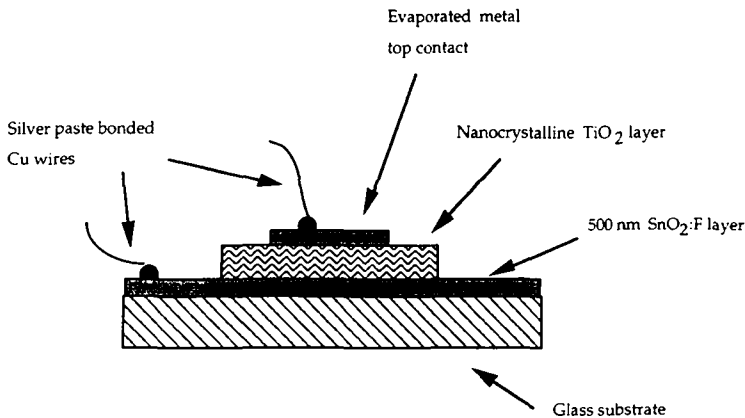


Figure 15: Schematic build-up of the nanocrystalline TiO₂/metal junctions. TCO stands for Transparent Conducting Oxide coated glass.

The top contact, which is the positive terminal of the device, is made by evaporation of a 40 to 200 nm thick layer of either gold or silver in a thin film coater (Auto 306 Edwards). Sometimes, the top contact wire was replaced by a Ni-coated metal tip touching the metal pad as contact.

All the devices made were stored in the dark and in ambient atmosphere.

4.1. Preparation of the nanocrystalline TiO₂ electrodes

Two kind of nanocrystalline TiO₂ layers were used for the build-up of the devices:

- a) "Fractal" nc-TiO₂.
- b) "Colloidal" nc-TiO₂.

Both kinds of nanocrystalline titanium oxides are always n-type semiconductors, with the n-type doping given by oxygen vacancies in the TiO₂ lattice [4 p. 33]. The doping density in the colloidal nc-TiO₂ film was estimated by B. O'Regan et al. to be around 10¹⁷ cm⁻³ [5].

- a) Fractal nc-TiO₂ electrodes:

The fractal nc-TiO₂ electrodes were prepared by a method developed by P. Liska [6,7], where several layers of TiO₂ are deposited on the SnO₂ coated glass by controlled hydrolysis of a TiCl₄ solution prior firing at 450 °C. This method gave ca. 10-15 μm thick nc-TiO₂ layers with a surface morphology resembling that of a dried and crackled soil, as shown in the SEM photographs in figs. 16 and 17.



Figure 16: SEM photograph with magnified view (x 20'000) of "fractal" TiO₂ ceramic electrode made by controlled hydrolysis of a TiCl₄ solution.



Figure 17: SEM photograph with the magnified view ($\times 60'000$) of the fractal TiO_2 ceramic material.

In fig. 16 showing the fracture of a fractal-type titanium oxide electrode, the chaotic and very rough inner surface of the TiO_2 ceramic layer is clearly visible, and in fig. 17, the smallest crack visible, e.g. close to the middle of the picture in fig. 17, is ca. 10 nm or less in width.

These fractal TiO_2 electrodes showed an inner surface of ca. 20 times the geometric area per μm of thickness [7 p. 1217].

b) Colloidal nc- TiO_2 electrodes:

The colloidal nc- TiO_2 electrodes were prepared as following: $\text{SnO}_2\text{:F}$ coated glass, having a surface resistance of $10 \Omega/\text{square}$, kindly given by GlasTrösch (Bützberg, Switzerland) is cut out in strips of 10×2 cm and washed first with absolute ethanol (Fluka, Buchs, Switzerland) then with distilled water and again with absolute ethanol. After drying with a hair dryer, two stripes of Scotch adhesive tape (Scotch Magic 3M), having a thickness of $50 \mu\text{m}$, are put one on the other, this on each edge of the $\text{SnO}_2\text{:F}$ coated glass sheets. About $100 \mu\text{L}$ of titanium TiO_2 colloid paste prepared according to O'Regan et al. [5, 8 p. 738] are spread out by using a glass rod as a squeegee gliding on the $100 \mu\text{m}$ thick spacer formed by the Scotch tapes. The so prepared electrodes are first dried with a hair dryer (air temperature ca. 100°C), then sintered with a hot air blower ("Hotwind S" model 9C2 from Leister in Kägiswil, Switzerland) for about 20 min. at 450°C . The above described nc- TiO_2 deposition technique is also called the "Scotch tape printing" method. After cooling to room temperature, the electrodes are cut in stripes 1×1 cm in size. The average thickness of the sintered nanocrystalline TiO_2 film is ca.

10-11 μm as measured with a stylus profilometer (Tencor, USA). The SEM picture in fig. 18, with a magnification of 100'000 times, shows the nanocrystalline morphology of such a colloidal TiO_2 layer, with its ca. 18 nm sized anatase nanocrystallites partially sintered together to form a highly porous, three dimensional network of TiO_2 with a porosity of ca. 50 %, meaning that half of the total volume is empty space [9 p. 59].

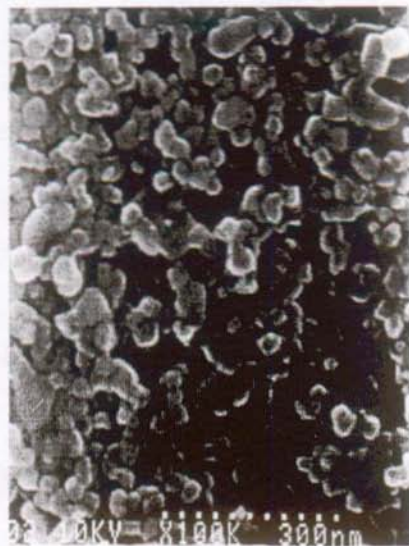


Figure 18: SEM photograph with the magnified view (x 100'000) of the colloidal TiO_2 ceramic material.

Clearly, the nanocrystalline character of the titanium oxide material is visible, as the mostly spherically shaped crystallites are ca. 15 to 20 nm in size. Since these SEM pictures have been taken after baking the TiO_2 electrode at 450 °C for ca. 20 min, a sintering of the TiO_2 particles is visible. It is this sintering process that gives the mechanical stiffness of the electrode, and it is allowing the current conduction from one particle to the other.

4.2. Photovoltaic characterisation

4.2.1. Nanocrystalline- TiO_2 diodes with silver as top contact

The current density-voltage (J-V) characteristics of a particular UV-sensitive nc- TiO_2/Ag junction using a 10 μm thick fractal nc- TiO_2 electrode is shown in fig. 19. The top contact silver pad was 0.27 cm^2 in size and 900 nm thick. The

irradiation source used is an unfiltered Xe-arc lamp having a light intensity of ca. 86 mW/cm² (measured with a calibrated Si-photodiode) at the sample position.

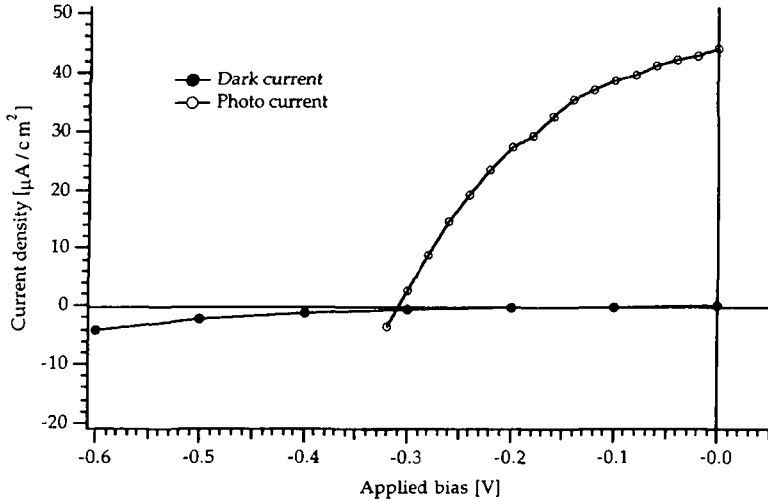


Figure 19: J-V plot of a fractal nc-TiO₂/Ag diode showing the dark current density (black dots) and the photocurrent density (open circles) made at an irradiation intensity of 86 mW/cm².

Clearly a photovoltaic effect is shown as there is a sharp increase of the current for a given forward polarization when the nc-TiO₂/Ag junction is irradiated with UV-light. At a forward bias of 100 mV, a current density of 45 μA/cm² was observed when lit, whereas the dark current density at the same bias is close to zero (not measurable). Intriguing is the fact that the photocurrent curve crosses the dark current curve at a bias of ca. 310 mV. From the J-V expression (eq. 10 p. 14), no crossing of the photocurrent plot with the dark current plot should occur as both are just parallel. Such a behavior may be due to the "photodoping" of the TiO₂, where the photo-induced electrons are rendering the TiO₂ more conductive, thus enabling a shunting of the cell. The doping level of the nc-TiO₂ material has been estimated from photocurrent onset experiments by B. O'Regan et al. [5] to be ca. $N_D = 10^{17}$ cm⁻³. In the UV range between 300 and 400 nm, the unfiltered Xe-lamp delivered ca. 1.5×10^{16} photons/cm² [10], and assuming total absorption by the 10 μm thick fractal TiO₂ layer, the upper value of the photocurrent density can be estimated to be ca. 1.5×10^{19} electrons/cm², assuming 100 % IPCE in this wavelength range. Hence, irradiation increases the carrier density n by a factor of ca. 1000, thus the conductivity σ increases by the same factor as $\sigma = q\mu_n n$, where μ_n is the electron mobility [11]. The dark conductivity can be estimated by knowing the dark resistance and the geometry of the TiO₂ electrode: the upper resistance value is roughly given by the slope of the J-V curve (fig.19) at large bias, a value of $R = 5.5$ MΩ can be calculated at -0.6 V bias, the electrode surface is $S = 0.27$ cm² and its thickness is $L = 10$ μm. From the

relation $R = \rho L/S$ and $\sigma = 1/\rho$, a dark conductivity of the nc-TiO₂ layer of $\sigma = 6.6 \times 10^{-10} \Omega^{-1}\text{cm}^{-1}$ can be calculated. A conductivity value of less than $10^{-7} \Omega^{-1}\text{cm}^{-1}$ was measured by O'Regan et al. [5].

The short-term stability of the nc-TiO₂/Ag junction was checked by monitoring the short-circuit current density while irradiating with an intensity of 86 mW/cm² of unfiltered Xe-light. No change of the short-circuit current density of ca. 45 $\mu\text{A}/\text{cm}^2$ was observed after 40 minutes of irradiation. In order to accelerate the possible light-induced aging of the junction, the same experiment as described above was done under a strong irradiation of 660 mW/cm² with the unfiltered Xe-lamp. During this experiment, the sample temperature increased from room temperature to ca. 45 °C under the intense light. The short-circuit current density behavior in time is shown in fig. 20.

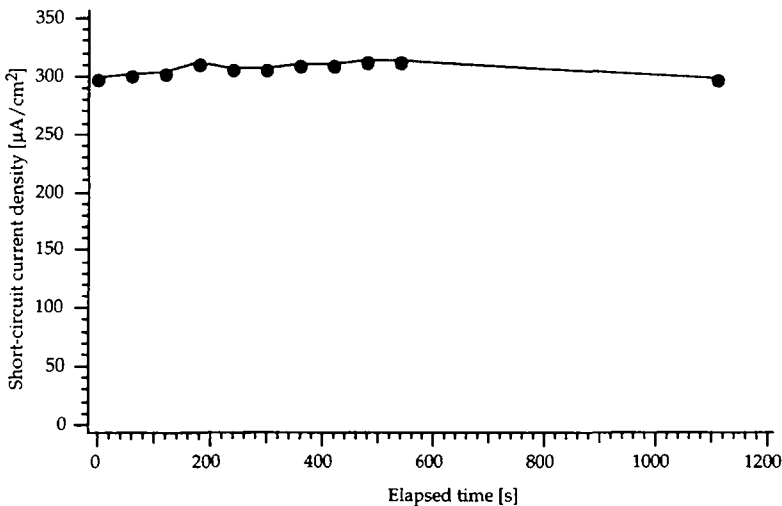


Figure 20: Short-circuit current density measured during 1200 s of irradiation with a unfiltered Xe-lamp at an intensity of 660 mW/cm².

The stability plot shows that the photocurrent density was constant over 20 minutes of irradiation, only a small increase of the current was observed after ca. 9 min. of irradiation, followed by a slight decay after a total of 19 min. of strong irradiation. The initial increase is probably due to the temperature increase of the sample, thus allowing a better current transport in the nc-TiO₂ layer.

Photocurrent transient experiments were done by chopping the incident Xe-lamp light beam. For this experiment, a nc-TiO₂/Ag sample made like the one used for the experiments described above, with a Ag top contact having 0.357 cm² in size, was used. Fig. 21 shows the current transient characteristics of the nc-TiO₂/Ag junction under an intense irradiation of ca. 760 mW/cm² of unfiltered Xe-light.

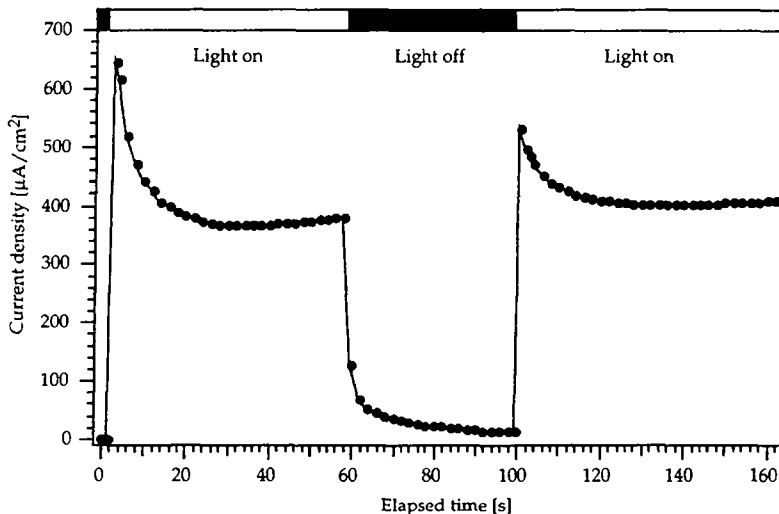


Figure 21: Short-circuit current density transients made by chopping the incoming Xe-light having a intensity of 760 mW/cm^2 . The diode was exposed to the ambient air.

There is a slow response of the photo current towards changes of the light intensity. Apparently, two phenomena are superposed: First the junction shows a current transient peak when the light goes on, followed by a non-linearly decreasing part where the photocurrent seems to stabilize to a steady-state value. Second, just after light interruption, the photo current goes rapidly to ca. a $1/4$ of its steady-state value, then it takes ca. 40 s. to decline towards zero. Furthermore, at the second time when the light switches on, the transient peak is less pronounced than at the first time. Such a photocurrent behavior may be explained by the electron and hole transport characteristics of the rather compact fractal type of TiO_2 electrodes. The problem is that the metallic contact is only on top of the porous layer, so the holes generated in the inner part of the $10 \mu\text{m}$ thick TiO_2 electrode must travel a few μm before being collected by the positive metal electrode. From the photocurrent decay, it seems that a very slow hole transport occurs, or that the transport is limited by a space charge layer created by the fast removal of the electrons, since the electrons cross the TiO_2 layer rapidly [12]. The current decay observed after switching off the light is due to the release of charge carriers from the traps [16].

The action spectrum of a colloidal $\text{nc-TiO}_2/\text{Ag}$ diode shown in fig. 22 was made by recording the photocurrent as a function of the wavelength of the incident light.

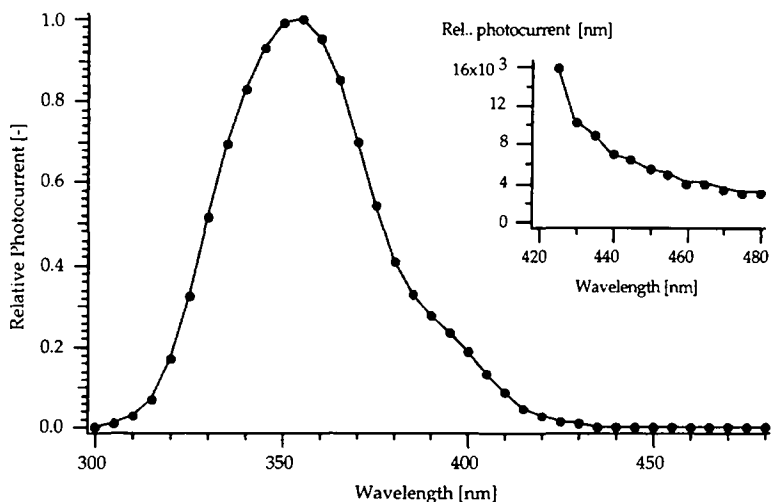


Figure 22: Action spectrum of a colloidal nc-TiO₂/Ag diode. The inset shows the photoresponse in the blue part of the visible light spectrum.

The photocurrent onset at the high energy end is at ca. 310 nm (4 eV) which corresponds to the SnO₂ cutoff of the conducting glass. The photocurrent onset on the lower energy side starts at 420 nm (2.95 eV), indicating the presence of rutile ($E_g = 3$ eV), which is not surprising since the used TiO₂ colloid was autoclaved at 250 °C resulting in the formation of some rutile [9 p. 59]. A photoresponse up to wavelengths of 480 nm (2.58 eV) is observed, as shown in the inset graph of fig. 22, where the signal is amplified 100 times compared with the main action spectrum plot in fig. 22. A similar observation was made by A. Hagfeldt et al. [13] with a colloidal TiO₂ electrode immersed in a SCN⁻ containing electrolyte. Such a photoresponse tail into the visible part of the spectrum may be explained by the presence of surface states and bulk traps having an energy position located below the conduction band edge of the TiO₂ [13]. The existence of surface states was proven by Kay et al. using cyclic voltammetry [14], surface state energy positions are reported to be 0.3 eV to 0.8 eV below the conduction band edge [15]. The observed sub-band gap onset at ca. 480 nm would mean that the trap energy distribution starts at ca. 0.6 eV below the conduction band edge of the anatase ($E_g = 3.2$ eV). The peak photocurrent of ca. 50 $\mu\text{A}/\text{cm}^2$ is obtained at a wavelength of 355 nm (3.5 eV), this maximum is given by the overlap of the photocurrent onset of the TiO₂ with the Xe-lamp spectrum in the 300 to 400 nm range.

During the electrical characterization experiments with the nc-TiO₂/Ag junctions, a quite dramatic change in the J-V characteristics was observed when the diode was forward polarized to -1 V (i.e. the TiO₂ was negative with respect to the Ag top electrode) for up to one minute. Higher forward biases caused the destruction of the device. Reverse polarization did not affect the diodes, except for large reverse biases > 1 V, which also caused destruction of the devices. The J-

V plots before and after a forward polarization at -1 V are shown in fig. 23, the characteristics were taken under Xe-lamp irradiation without UV-filters at an intensity of ca. 100 mW/cm².

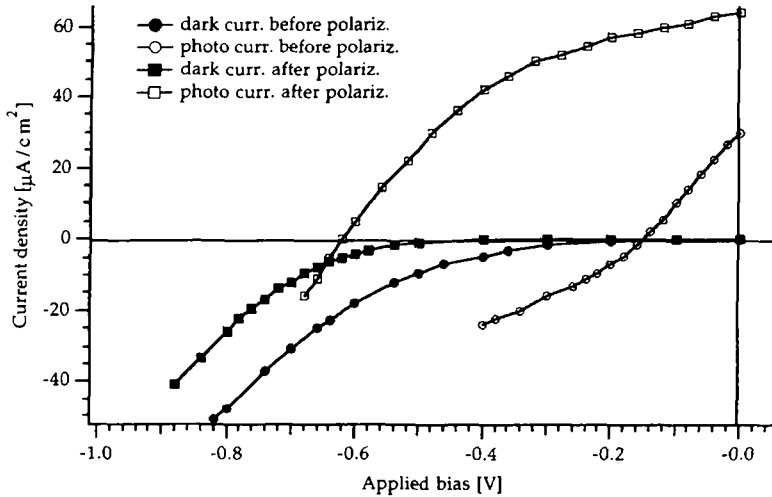


Figure 23: J-V plots of a colloidal nc-TiO₂/Ag junction, before (circles) and after (squares) the forward polarization at -1 V for 30 s. Irradiated at 100 mW/cm² with an unfiltered Xe-lamp.

The dark currents (black marks in fig. 23) and the photocurrents (open marks in fig. 23) were modified by forward polarization, especially the photocurrent increased nearly by a factor of 2, and the open circuit voltage went from initial 150 mV to 620 mV after the polarization. Also the shape of the J-V plot is strongly affected, as with the initial photocurrent curve, a fill-factor of ca. FF = 0.2 is estimated, which increases to ca. 0.42 for the photocurrent plot after the forward bias treatment.

A similar forward biasing experiment was done using only a low level monochromatic irradiation at 390 nm. The J-V plot before and after a forward polarization at -1 V is shown in fig. 24.

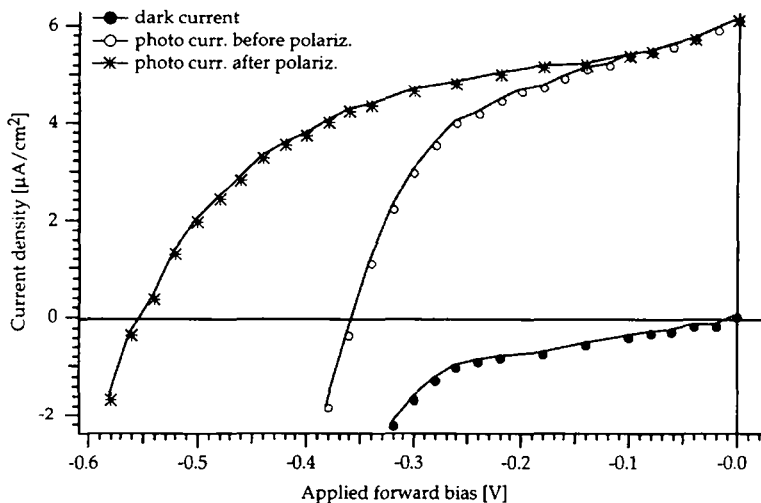


Figure 24: Forward polarization effect on the J-V characteristics of a colloidal nc-TiO₂/Ag junction, the dark current (black dots) and the photocurrent (open circles) are shown prior polarization, and the photocurrent after polarizing to -1 V for 20 s (stars). Monochromatic illumination was made at 390 nm with an intensity of ca. 140 μW/cm².

Apparently, the open-circuit voltage changed from 350 mV to 550 mV upon a forward polarization of -1 V for 20 s. In the low level light case, the photocurrent seemed not to be affected by this treatment. According to the open-circuit expression (eq. 12, chapter 1), a change of 200 mV in the open-circuit voltage corresponds to a saturation current density decrease of ca. 50 times, and the saturation current density J_s is inverse proportional to the minority carrier lifetime τ , as shown in eq. 11 in chapter 1. Apparently, the recombination rate was reduced after the forward polarization. The polarization effect is also clearly demonstrated on the incident photon-to-current conversion efficiency (IPCE) action spectra before and after the forward polarization, as shown in fig. 25.

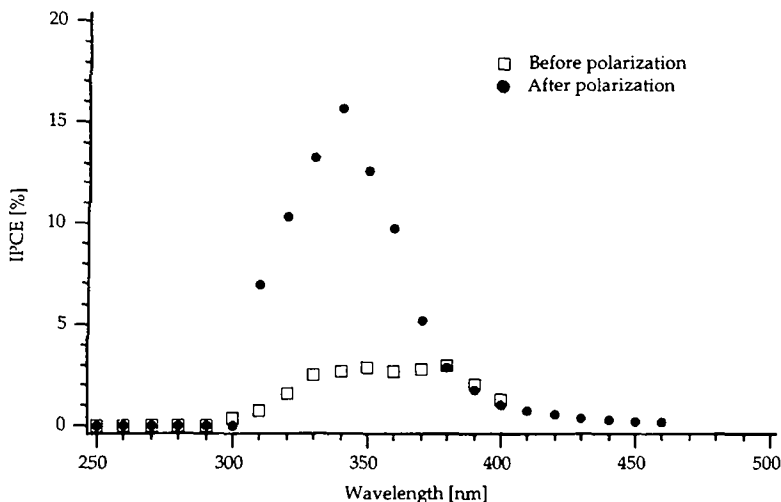


Figure 25: IPCE action spectra of a colloidal nc-TiO₂/Ag diode before (open squares) and after (black dots) a forward polarization of 1 V for 30 s.

The peak IPCE improved from ca. 3 % prior the forward polarization to ca. 16 % after. Prior polarization, the IPCE peak is broad and featurless around 350 to 370 nm. After polarization, in contrast, the IPCE maximum is located at 340 nm. In this experiment, the sub-band gap response is clearly visible, as there is a photoresponse up to 460 nm (2.7 eV), probably due to the photoexcitation of surface states or bulk traps within the nanocrystalline TiO₂ electrode. Furthermore, a color change of the silver pad was observed after the forward polarization, as the color went from shiny metallic to dark gray or even black. If the silver pad was scratched in two electrically disconnected parts, only the part that was connected to the electrical circuit turned to black upon forward polarization. This might be explained by a change in chemical nature of the silver, e.g. an irreversible oxidation, probably due to the forward polarization as the silver pad goes positive in voltage. The black material formed is probably a silver oxide, and AgO₂ or AgO are indeed dark brown to charcoal-gray oxides [17]. Maybe the sub-bandgap photoresponse observed in the action spectrum in fig. 25 (for the case after polarization) is due to the silver oxide injecting photoelectrons into the TiO₂, i.e. acting as a sensitizer, contributing to the photoresponse for wavelengths over 400 nm.

4.2.2. Gold as top contact metal

Gold was chosen as a rectifying top contact layer because it forms no oxides that could modify the nc-TiO₂/Au junction in ambient atmosphere. From the work function of gold, $\phi_{Au} = 5.1$ eV, and the work function of TiO₂ (anatase) at $\phi_{TiO_2} =$

4.3 eV, a theoretical open-circuit voltage of $5.1-4.3 = 0.8$ V can be estimated, assuming that the Fermi-level of the TiO_2 is close to the conduction band edge, which is the case for a doped material. The diodes build-up is the same as that used for the nc- TiO_2/Ag junctions.

The Schottky diode were prepared as following: On a $\text{SnO}_2:\text{F}$ coated glass (Asahi Glass, Japan) a $9 \mu\text{m}$ thick nanocrystalline TiO_2 layer is deposited by the Scotch tape technique described above (§ 4.1). On top of this TiO_2 layer, a 0.44 cm^2 size, 40 nm thick gold pad was evaporated as the positive terminal. The diode was stored at room temperature in the ambient.

The J-V characteristics in the dark of the nc- TiO_2/Au junction are shown in fig. 26.

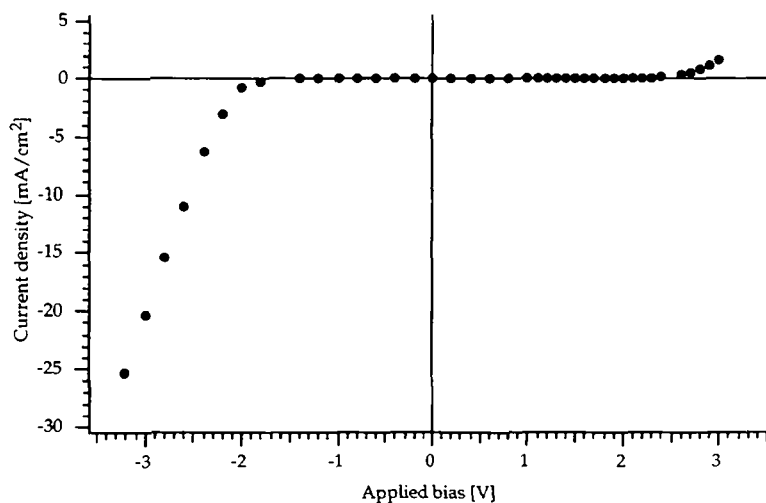


Figure 26: Dark current density plot as a function of the applied bias of a colloid nc- TiO_2/Au diode. Positive bias is the reverse bias direction where the TiO_2 electrode is going positive in voltage.

Clearly a rectifying behavior of the colloidal nc- TiO_2/Au junction is observed as the current plot is dissymmetrical upon forward or reverse polarization. At a bias of ± 3 V, a rectifying ratio of 10 is deduced from fig. 26. The plot of the natural logarithm of the current density vs. applied bias in fig. 27 allows to estimate the nc- TiO_2/Au diode parameters, like the barrier height ϕ_b and the ideality factor n .

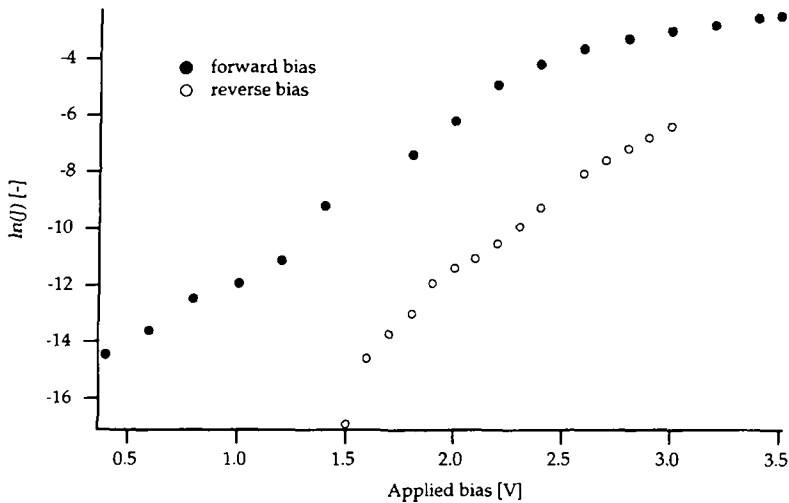


Figure 27: $\ln(J)$ versus the applied bias for the forward bias direction (black dots) and the reverse bias (open circles).

The $\ln(J)$ plot in the forward polarization shows a deviation from linearity probably due to the ohmic resistance in the junction, so the exponential behavior of the current in function of the applied bias does not hold anymore. Hence, only the $\ln(J)$ plot in the voltage range from 0.5 to 2.5 V has been fitted with a line. From the simplified diode equation (see chapter 2)

$$J = J_s \left[\exp\left(\frac{qV}{nkT}\right) \right] - J_L \quad (16)$$

where J is the current density (in A/cm^2), J_s is the saturation current density (in A/cm^2), J_L the photocurrent density ($J_L = 0$ in the dark current situation), q is the charge of the electron (1.602×10^{-19} C), V is the applied potential, n is the diode ideality factor (or diode quality factor), k is the Boltzmann constant (1.3806×10^{-23} J/K) and T is the absolute temperature in $^{\circ}K$, and by plotting the natural logarithm of the current density under different applied potentials in the forward bias, the saturation current J_s and the diode quality factor n can be found. The intercept value (-16.74) corresponds to $\ln(J_s)$ and the slope (5.18) stands for the term q/nkT . The J-V plot in fig. 26 was measured in ambient air at room temperature $T = 295$ $^{\circ}K$. This yields a saturation current density of $J_s = 0.05$ $\mu A/cm^2$ and a diode quality factor $n = 7.5$, and by using eq. 15, a barrier height of $\Phi_b = 0.84$ eV can be estimated. This barrier height value is close to the theoretical value of 0.8 eV given by the difference of the work functions of gold (5.1 eV) and TiO_2 (4.3). These values can be compared with a Au/Si diode, which shows a saturation current density of ca. $J_s = 1$ $\mu A/cm^2$, and a diode quality factor of $n = 1.1$, depending on the doping level [11 p. 266].

With the nc-TiO₂/Au diodes, similar polarization experiments were performed to investigate if this effect appears also with gold as contact metal. Despite gold is expected not to be "oxidized" by the forward polarization action, a strong effect on the J-V photoelectrical behavior has also been found with the gold contacted nc-TiO₂ layers. A colloidal nc-TiO₂/Au diode was electrically characterized before and after applying a forward polarization of -3 V during 170 s, the used irradiation intensity was 5.5 mW/cm² and 55 mW/cm² from a unfiltered Xe-light, the J-V plots are given in fig. 28.

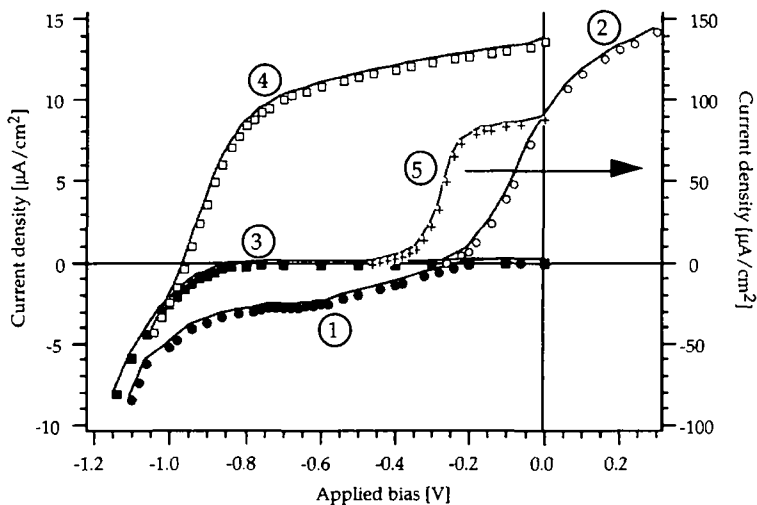


Figure 28: J-V plots of a colloidal nc-TiO₂/Au diode prior and after a forward polarization of 3 V during 170 s. Plot (1) is the dark current made prior polarization (black circles), plot (2) is the corresponding prior polarization photocurrent made at 5.5 mW/cm² irradiation, plot (3) is the dark current after polarization (black squares), and plot (4) represents the photocurrent after polarization (open squares) measured at 5.5 mW/cm² light intensity. For plot (1) to (4), the currents are reported on the left hand axis. Plot (5) is the photocurrent measured after the polarization (crosses), but at an intensity of 55 mW/cm² (current reported on the right hand axis).

The effect of the forward polarization is to increase the open-circuit voltage from 250 mV (see plot (2) in fig. 28) to 955 mV after the polarization (see plot (4) in fig. 28). The photocurrent increased also by ca. 40 % after the forward polarization. The initial dark current plot made with the "virgin" diode (curve (1) in fig. 28) shows rather large increase after ca. 250 mV forward bias with a "hump" at 600 mV. After the polarization treatment, the dark current plot is "smooth" and the current onset is at ca. 800 mV only (plot (3) in fig. 28). It seems, in the case of the nc-TiO₂/Au junction, that a similar junction quality improvement occurs during forward polarization like the one seen with the nc-TiO₂/Ag devices. Surprisingly,

the photocurrent plot made at 55 mW/cm^2 light intensity (plot (5) in fig. 28) shows an open-circuit voltage of only 450 mV after the polarization and the J-V curve itself is "S" shaped. Furthermore, the short-circuit photocurrent was not proportional with the tenfold light intensity increase, as in strong light (55 mW/cm^2) only $96 \text{ }\mu\text{A/cm}^2$ were measured, instead of the $136 \text{ }\mu\text{A/cm}^2$ expected from the tenfold multiple of the short-circuit current measured at 5.5 mW/cm^2 (plot (4) fig. 28). Also prior to the forward polarization, the colloidal nc-TiO₂/Au diodes showed a sub-linear response, and an open-circuit voltage decrease upon light intensity increase. A similar open-circuit voltage reduction and sub-linearity in current upon light intensity increase was found by Skotheim [1, p.59], and was explained by the fact that in the high illumination regime, the Fermi-level is shifted towards the conduction band edge of the TiO₂, thus more traps are available to act as recombination centers lowering the output voltage and shunting the current.

From the plot (2) of fig. 28, the photocurrent increased upon reverse bias. Such a phenomenon was also observed with other nc-TiO₂/Au devices, where the photocurrent levelled off at a reverse bias of ca. 400 mV. This indicates that the charge separation process is not fully effective when only the photogenerated electrical field is available, but the additional 400 mV of reverse bias are strengthening the electrical field within the TiO₂ layer, thus increasing the photocurrents by ca. 60 %. From the polarization experiments performed with the nc-TiO₂/Au diodes, it appeared that the high open-circuit potentials were not stable in time. Figure 29 shows the current dependence in time, after forward polarization for 6 minutes at -3 V.

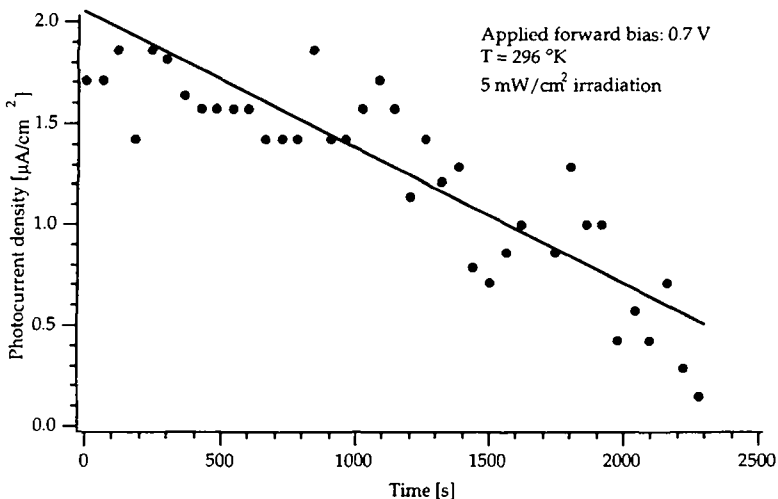


Figure 29: Time dependence of the photocurrent of a colloidal nc-TiO₂/Au diode, measured at a forward bias of 0.7 V in a light intensity of 5 mW/cm^2 of unfiltered Xe-light, after being forward polarized at 3 V for 6 min.

A slow degradation of the photocurrent is visible, and after 1000 s, the degradation accelerated. Using the same diode, and repolarizing again in the forward direction at 3 V for 17 minutes, produces again an open-circuit voltage of 0.9 V at 5 mW/cm² light intensity, and the photocurrent, measured in the same light intensity, decreased from 1.7 μA/cm² to 0.8 μA/cm² after 3840 s. All the experiments were performed in ambient air at room temperature (296 °K). The polarization effect seems to vanish with time, but it can be "refreshed" by just redoing a forward polarization for a few minutes at 3 V, at least for the TiO₂/Au devices. From the above described results, it seems that the forward polarization of the nc-TiO₂/Au junction affects strongly the junction interface itself as the photocurrent and open-circuit voltages are increased after the polarizing treatment. A similar behavior was observed with the nc-TiO₂/Ag diodes, even with a color change from metallic to black of the silver pad after the forward polarization.

In an other experiment, the following structure was made:

- TCO glass/nc-TiO₂/Ag/Au +

i.e. a silver pad protected with a gold top layer.

Polarizing such a diode in forward direction also produced the characteristic color change of the silver pad, despite the gold protection layer. It seems that the chemical change came from inside, i.e. the nc-TiO₂ side of the electrode. A possible explanation might be the presence of tiny amounts of water taken up by the highly porous and hydrophilic TiO₂ through a process called "capillary condensation" [18 p. 70]. The presence of some adsorbed water would explain the oxidation effect of the silver, as this electrode goes positive in voltage and the water may act as electrolyte tarnishing the silver to form colored oxides.

Finally, an intriguing observation was made: the photocurrent increased by a factor of 2, when humid air from expiration is blown directly on an illuminated nc-TiO₂/Au, and the photocurrent decreased again to its initial value after ending the humid air exposure. In other words, the highly porous nc-TiO₂/metal device behaved as a good humidity sensor.

4.3. Sensitized nanocrystalline-TiO₂ Schottky junctions

4.3.1. Electrode preparation

All dyestuff solutions were made of absolute ethanol (Fluka, Buchs, Switzerland) and a sample series is put in a 0.3 mM ethanolic solution of *cis*-bis(isothiocyanato)bis(2,2'-bipyridyl-4,4'-dicarboxylato)-ruthenium(II), abbreviated RuL₂(NCS)₂, [19 p. 6383] (kindly given by Solaronix, Aubonne, Switzerland), an other sample series was put in a 0.3 mM solution at pH = 3.5 to 4 of tris(2,2'-

bipyridyl-4,4'-dicarboxylato)-ruthenium(II), abbreviated RuL₃ [20], a third series was put in a 10 mg /10 ml ethanolic solution of Cu-chlorophyllin "E6" (Porphyrin Product) [18 p. 111]. After 24 hours at room temperature, all the electrodes were removed from the dye solutions and dried with a hair dryer, and stored under argon. A fourth series without dye adsorbed was used as a "blank" in the experiments. All dye UV-VIS spectra were taken in absolute ethanol using a diode array spectrophotometer (Hewlett-Packard Model 8452A).

A 50 nm gold film (Fluka) or a 200 nm silver film (Fluka) is deposited at ca. 5×10^{-6} mbar in a bell jar evaporation apparatus (Auto 306 Edwards) on the titanium oxide electrodes coated with the different dyes. The so deposited metal patch had a diameter of ca. 7 mm (surface = 0.5 cm²). The diodes are contacted by a tin stripe (Merck) glued on the metal patch by silver paint (Ag 200 Demetron). The current-voltage characteristics of the diodes were taken by irradiating with a xenon lamp (Oriel Model 450 W) provided with optional filters for UV (polycarbonate Maagtechnik, Crissier CH), solar simulation (Schott Nr 113) and attenuation for 1/10 and 1/100 of the nominal intensity (in-house made filters with metal grid). The voltage scan was made manually by steps of 10 mV and a settle time of ca. 10 sec between every point with a potentiostat (Wenking) and recorded on a X-Y writer (ABB Goertz). The SEM picture (fig 30) shows the device build-up, which is the same as for the non-sensitized colloidal nc-TiO₂/metal diodes described previously, except for different metal top electrode thicknesses.

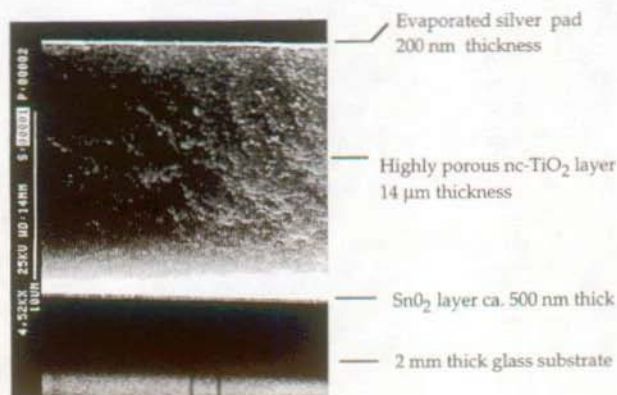


Figure 30: SEM photograph (magnification of 4250 x) showing the cross-section through the TCO/nc-TiO₂/Ag sandwich structure.

The top metal electrode (positive terminal) made of 200 nm thick silver layer deposited by evaporation, is shown in the SEM picture in fig. 31.

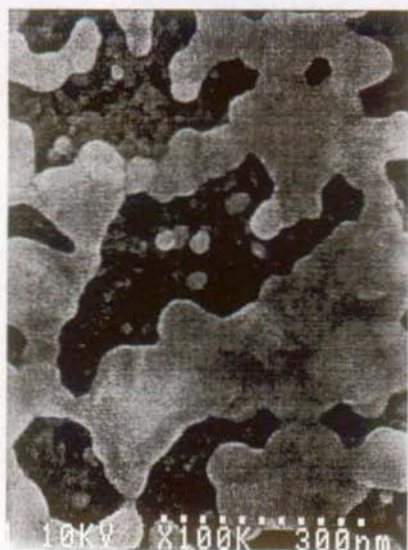


Figure 31: SEM photograph (magnification 100'000 x) of the top 200 nm thick silver electrode of the nc-TiO₂/Ag diode.

It is interesting to notice that even with a 200 nm thick evaporated silver layer, which looks shiny metallic, not all the surface of the very rough nanocrystalline TiO₂ is covered, as the ca. 20 nm sized colloidal TiO₂ particles are clearly visible through the "holes" in the silver layer.

4.3.2. Photovoltaic characterization

The J-V characteristics of a sensitized fractal type nc-TiO₂/Ag junction using the dye RuL₂(NCS)₂ are given in fig. 32. The used Xe lamp was filtered with a Schott 113 filter, cutting all the wavelengths below 380 nm, and the light intensity was varied from 1 to 100 mW/cm².

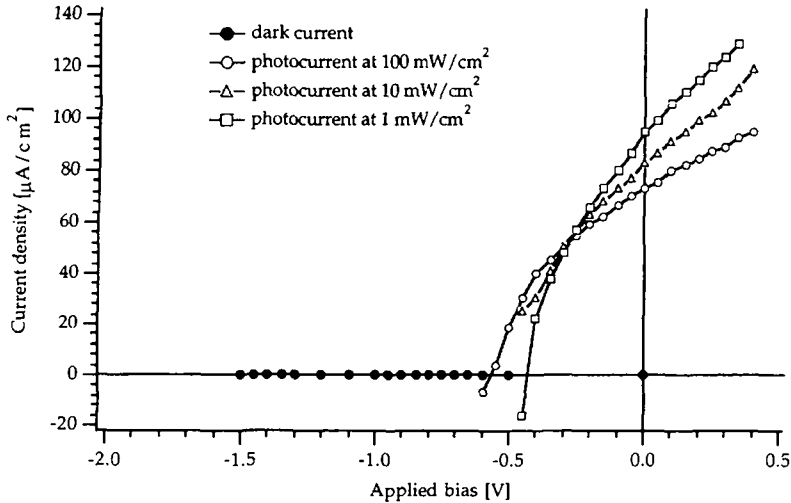


Figure 32: J-V characteristics of a sensitized fractal nc-TiO₂/Ag diode in the dark (black dots) and under different illuminations, 1 mW/cm² (open squares, current scale on left axis divided by 100), 10 mW/cm² (open triangles, current scale on left axis divided by 10) and 100 mW/cm² (open circles).

In fig. 32, the dark current is practically zero, even at 1.5 V forward bias, and a crossing of the photocurrent plot (open circles in fig. 32) with the dark current plot is again observable like in the non-sensitized TiO₂/metal junctions. The short-circuit currents are sub-linear, as shown in fig 32, where all the currents have been "normalized" to the full bright plot. By plotting the open-circuit voltage against the logarithm of the light intensity (fig. 33), the diode quality factor n can be estimated, knowing that for an ideal junction with $n=1$, the open-circuit voltage increases by $\ln(10) kT/q = 59$ mV per decadic increase of the light intensity.

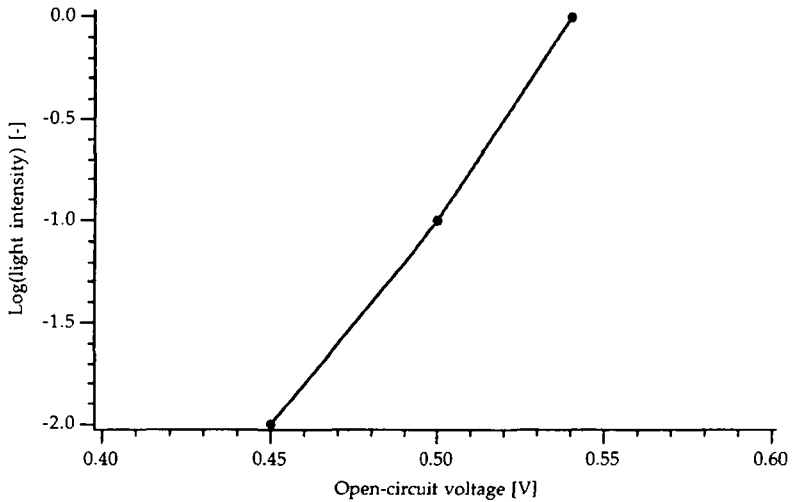


Figure 33: Plot of the open-circuit voltage vs. the logarithm of the light intensity of a sensitized fractal nc-TiO₂/Ag junction.

The slope in fig. 33 is ca 50 mV/decade, indicating a apparent diode quality factor of $n = 50/59 = 0.84$. This diode quality factor close to unity indicates that the device behaves as a ideal junction where the open-circuit voltage increases by 59 mV for a 10 times increase in irradiation intensity.

The action spectrum of a RuL₂(NCS)₂ sensitized fractal nc-TiO₂/Ag junction is depicted in fig. 34.

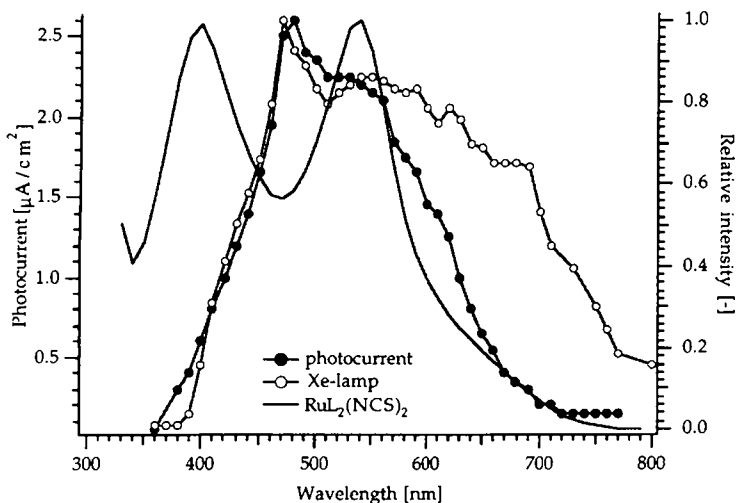


Figure 34: Photocurrent action spectrum of a fractal $\text{nc-TiO}_2/\text{Ag}$ diode (black dots, current indicated on left hand axis), with the Xe-lamp intensity distribution (open circles, relative intensity reported on right hand axis) and $\text{RuL}_2(\text{NCS})_2$ relative absorption spectrum made in ethanol (continuous line, relative intensity reported on right hand axis).

A strong photoresponse is observed up to wavelengths of 700 nm, indicating that the adsorbed dye $\text{RuL}_2(\text{NCS})_2$ acts as a sensitizer, improving the spectral response into the visible wavelength range of the highly porous wide band gap semiconductor. In order to verify this sensitization effect of the dye in the colloidal $\text{nc-TiO}_2/\text{Ag}$ diodes, the action spectrum was taken with $\text{RuL}_2(\text{NCS})_2$ and other known sensitizers like RuL_3 [20] and a copper chlorophyllin "E6" investigated by A. Kay et al. [14, 18]. A "blank" was also measured, with no sensitizer adsorbed on the nc-TiO_2 (fig. 35).

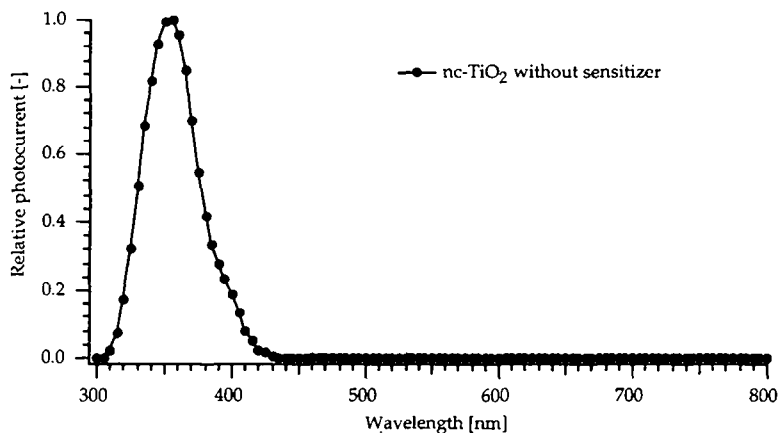


Figure 35: Photocurrent action spectrum of a non-sensitized $\text{nc-TiO}_2/\text{Ag}$ junction.

In fig. 35, the already mentioned sub-bandgap response is observable as the photocurrent onset starts at already 440 nm (2.8 eV). The action spectrum using the yellow-orange RuL_3 dye is given in fig. 36.

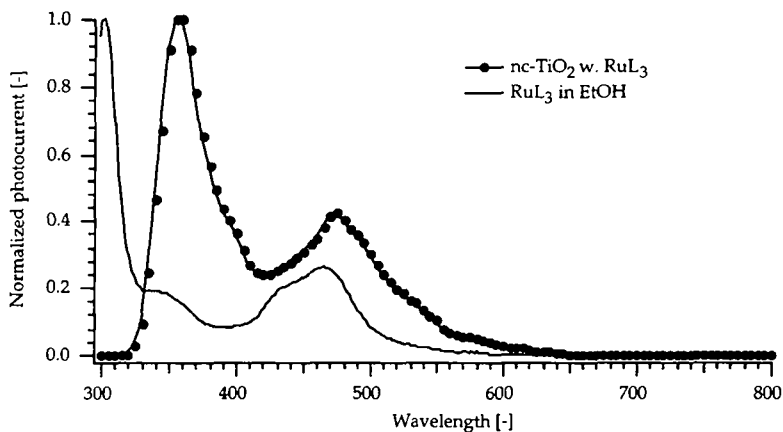


Figure 36: Photocurrent action spectrum of a RuL_3 sensitized $\text{nc-TiO}_2/\text{Ag}$ junction (black dots) compared with the absorption spectrum of an ethanolic RuL_3 dye solution (continuous line).

Clearly, a sensitization effect is visible as the photoresponse is perceptible up to 650 nm. The peak at 470 nm is probably due to the Xe-lamp emission, as shown in fig. 34. The action spectrum measured with the wine red sensitizer $\text{RuL}_2(\text{NCS})_2$ is shown in fig. 37.

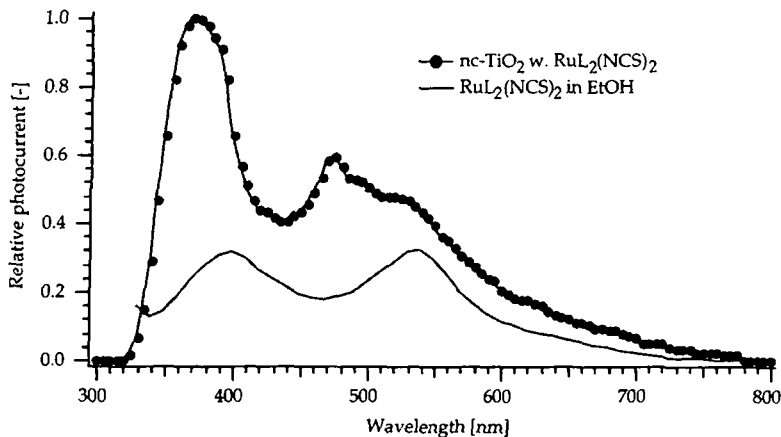


Figure 37: Photocurrent action spectrum of a $\text{RuL}_2(\text{NCS})_2$ sensitized $\text{nc-TiO}_2/\text{Ag}$ junction (black dots) compared with the absorption spectrum of an ethanolic $\text{RuL}_2(\text{NCS})_2$ dye solution (continuous line).

In this case, the photoresponse in the visible was even more extended towards the longer wavelengths, as the $\text{RuL}_2(\text{NCS})_2$ dye itself has also a stronger absorption in the red part of the visible spectrum with an onset at ca. 750 nm when compared with the RuL_3 dye. Finally, the action spectrum in fig. 38 was made with the green Cu-chlorophyllin "E6" as sensitizer. The so treated nc-TiO_2 electrodes looked dark green.

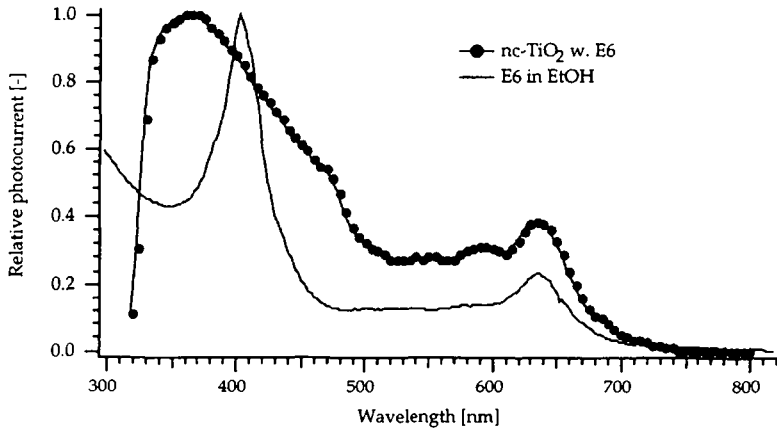


Figure 38: Photocurrent action spectrum of a Cu-chlorophyllin "E6" sensitized nc-TiO₂/Ag junction (black dots) compared with the absorption spectrum of an ethanolic Cu-chlorophyllin "E6" dye solution (continuous line).

Here again, a clear sensitization effect is visible, especially the absorption peak of the E6 dye centered around 640 nm [18 p. 116] is very well reflected in an increase of the photocurrent in the same wavelength region. This shows that the photogenerated holes, which are on the dye molecule, are carried away by the silver pad.

In all the sensitized nc-TiO₂/Ag junction photocurrent action spectra plots, the UV response, created by the direct excitation of the TiO₂ bandgap by the UV photons, is always stronger compared with the sensitized current output. This is a sign that generally there is probably a significant amount of losses in the holes transfer from the oxidized dye to the metal top electrode. This is not surprising since the metal is only poorly contacting the TiO₂ nanocrystallites.

4.4 Conclusion

A photovoltaic effect in UV light was measured with junctions made of nanocrystalline TiO₂, either of the fractal or colloidal type, with silver or gold as contact metal. Surprisingly a polarization effect was observed with both kinds of contact metals: The short-circuit currents, open-circuit voltages and fill-factors were improved after a forward polarization of the TiO₂/metal junctions at 3 V for a few seconds, often a color change from metallic to black was observed when silver was used as contact metal. In the case of a TiO₂/Ag diode, the quantum efficiency increased from 3 to 16 % in UV irradiation at 350 nm, and with a TiO₂/Au junction, an open-circuit voltage improvement from 250 mV to 955 mV was observed, together with a current short-circuit enhancement from 8 to 12

$\mu\text{A}/\text{cm}^2$ at $5.5 \text{ mW}/\text{cm}^2$ simulated sunlight. No color change was seen with the TiO_2/gold devices. The forward polarization effect was time dependend, as the improved photovoltaic performances faded after a few minutes, especially upon heating of the diodes.

The exact nature of the change happening in the $\text{TiO}_2/\text{metal}$ junctions is not known. The ambient atmosphere might play a role in the observed phenomena, as the photoelectric and dark current properties were affected by the humidity of the surrounding atmosphere. This effect may be used in a sensor application of the nanocrystalline $\text{TiO}_2/\text{metal}$ junctions.

The sensitization of the nanocrystalline $\text{TiO}_2/\text{metal}$ junctions with two ruthenium dyes and chlorophylline was proven as photocurrents in the visible part of the spectrum were observed, especially where the used dyes had their absorption maximum. This sensitization effect means that the dye was able to inject the holes into the gold or silver contact metal. Obviously poor photovoltaic characteristics, ca. $70 \mu\text{A}/\text{cm}^2$ short-circuit current density and 450 mV of open-circuit voltage at $100 \text{ mW}/\text{cm}^2$ simulated sunlight, were measured with the sensitized systems, compared to the photocurrents of ca. $10 \text{ mA}/\text{cm}^2$ which are measured with the liquid electrolyte based sensitized dye solar cells. These poor photocurrents are probably caused by improper contacting of all the dye molecules of the photoelectrode, as the evaporated metal was only contacting the top layer of the sensitized TiO_2 layer, thus only a small part of the junction was really photoelectrically active.

References for chapter 4

1. T.A. Skotheim "Photovoltaic Properties of Metal-Merocyanine-TiO₂ Sandwich Cells", Ph.D thesis made at the Lawrence Berkeley Laboratory, Univ. of California, 1979.
2. T. Skotheim, J.-M. Yang, J. Otvos and M. Klein, *Journal of Chemical Physics*, 77 (1982) 6144.
3. T. Skotheim, J.-M. Yang, J. Otvos and M. Klein, *ibid.*, 6151.
4. H. Tang, "Electronic Properties of Anatase TiO₂ Investigated by Electrical and Optical Measurements on Single Crystals and Thin Films, Ph.D thesis work N° 1311 (1994) EPFL.
5. B. O'Regan, J. Moser, M. Anderson and M. Graetzel, *Journal of Physical Chemistry*, 94 (1990) 8720.
6. P.Liska, "Praktische Aspekte der Licht-Energieumwandlung am Beispiel einer TiO₂-Farbstoffzelle" Ph.D thesis work N° 1269 (1994) EPFL.
7. N. Vlachopoulos, P.Liska, J. Augustynski and M. Graetzel, *Journal of the American Chemical Society*, 110 (1988) 1216.
8. B. O'Regan and M. Graetzel, *Nature*, 353 (1991) 737.
9. A. Hagfeldt and M. Graetzel, *Chemical Reviews*, 95 (1995) 49.
10. Calculated from the action spectrum of the Xe-lamp published in the catalogue "Solar Simulation", (1993), Oriel Corp., Stratford, CT, (USA), pp. 24.
11. S.M. Sze in "Physics of Semiconductor Devices", 2nd Edition, John Wiley & Sons, New-York, 1981, pp. 31.
12. M. Graetzel in "Nanocrystalline Semiconductor Materials", P.V Kamat and D. Maisel, Ed., Elsevier Science, Amsterdam, The Netherlands, 1996, pp. 11.
13. A. Hagfeldt, U. Björkstén and S.-E. Lindquist, *Solar Energy Materials and Solar Cells*, 27 (1992) 293.
14. A. Kay, R. Humphry-Baker and M. Graetzel, *Journal of Physical Chemistry*, 98 (1994) 952.
15. J. Moser, S. Punchihewa, P. Infelta and M. Graetzel, *Langmuir*, 7 (1991) 3012.
16. F. Willig, R. Kietzmann and K. Schwarzburg, *Proceedings of the Ninth International Conference on Photochemical Conversion and Storage of*

Solar Energy; IPS-9, August 23-28, 1992, Beijing China; International Academic Publishers: Beijing China, 1992; pp 129-139.

17. The Merck Index, Ninth Ed., Merck & Co., Rahway, New-Jersey USA, 1976, pp 8262.
18. A. Kay, "Solar Cells Based on Dye-Sensitized Nanocrystalline TiO₂ Electrodes" Ph.D thesis work N° 1214 (1994) EPFL.
19. M.K. Nazeeruddin, A. Kay, I. Rodicio, R. Humphry-Baker, E. Müller, P.Liska, N. Vlachopoulos and M. Graetzel, *Journal of the American Chemical Society*, 115 (1993) 6382.
20. N. Vlachopoulos, P.Liska, A.J. McEvoy and M. Graetzel, *Surface Science*, 189/190 (1987) 823.
21. P. Liska, N. Vlachopoulos, M. Nazeeruddin, P. Comte and M. Graetzel, *Journal of the American Chemical Society*, 110 (1988) 3686.

5. Conductive polymer/nanocrystalline-TiO₂ junction

Several research groups [1-6] are working on metal/polymer or semiconductor/polymer interfaces to investigate the electronic properties or the photovoltaic behavior of the so formed junctions.

H. Nguyen Cong et al. [7] found a photovoltaic conversion efficiency around 0.8 % at 56 mW/cm² irradiation intensity using a doped poly(3-methylthiophene)/CdS:Al junction. But so far no attempt was made to use a highly porous, or even nanostructured, semiconductor/polymer junction.

The energy diagram in fig. 39 shows the relative positions of the valence band and conduction band edges of different organic and inorganic materials compared to the band positions of TiO₂:

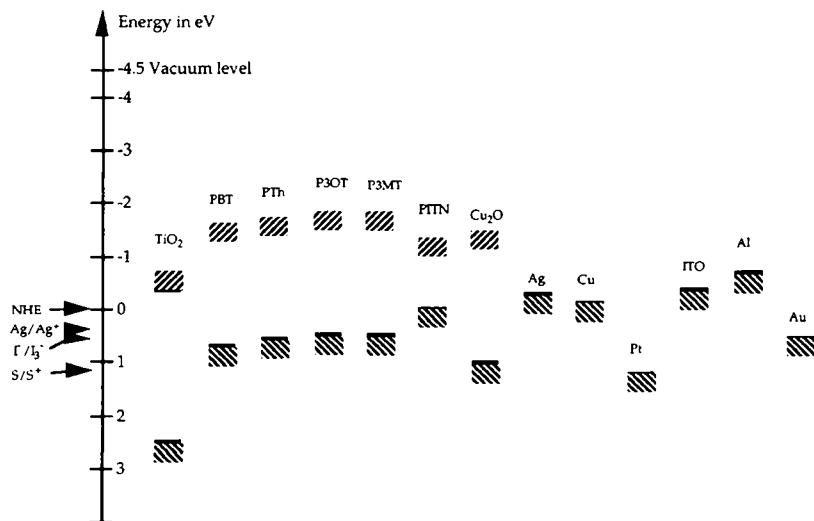


Figure 39: Conduction and valence band edge energy positions of different organic and inorganic semiconductors with respect to the vacuum energy scale. The energies are reported in eV, with the vacuum energy level being at -4.5 eV vs. the Normal Hydrogen Electrode (NHE) having a standard electrochemical potential of 0 V vs. the vacuum level. TiO₂ denotes anatase with band gap of 3.2 eV and the energy level position taken at pH = 7, PBT is poly(bithiophene), PTh is

polythiophene, P3OT is poly(3-octylthiophene), P3MT is poly(3-methylthiophene), PITN is poly(isothianaphthene), also called poly(benzo[c]thiophene), and ITO stands for indium tin oxide (90% In_2O_3 10% SnO_2). On the left side of the arrow indicating the energies, Ag/Ag^+ denotes the electrochemical potential position of the standard silver/silver chloride electrodes used as reference in the electrochemical experiments. ($E^\circ \text{Ag}/\text{Ag}^+ = 0.24\text{V}$ vs. NHE), S/S^+ denotes the electrochemical potential of the sensitizing dye *cis*-bis(isothiocyanato)bis(2,2'-bipyridyl-4,4'-dicarboxylato)-ruthenium (II) and I^-/I_3^- indicates the electrochemical potential of the iodide/tri-iodide redox couple which is used in the photoelectrochemical dye solar cells operating with an TiO_2 /electrolyte junction.

From the energy level diagram, several conducting polymers like P3MT, PBT, P3OT and PTh could be used directly as a sensitizer of the nanocrystalline TiO_2 since the valence band edge of these polymers are lying below the conduction band-edge of TiO_2 , and their conduction band-edges are lying above the conduction band of TiO_2 . The same polymers could also replace the I^-/I_3^- redox couple used in liquid systems as their valence band edge lies above the electrochemical potential of the sensitizer ($\text{S}/\text{S}^+ = 1.12\text{V}$ vs. NHE). Inorganic materials like Cu_2O could also serve either as a sensitizer or as hole conductor. Torsi et al. described a n- TiO_2 /p-poly(bithiophene) (p-PBT) heterojunction [8]. They are using titanium oxide made by anodic treatment of a titanium sheet. From the J-V characteristics of their diode, using a 50 nm thick electrodeposited PBT layer in the oxidized form, a barrier height of $\phi_b = 0.8\text{V}$ can be deduced. Raman experiences performed on such n- TiO_2 /p-PBT junctions indicated a possible photovoltaic effect [8]. According to the above mentioned publication, the following energy diagram can be drawn (fig 40).

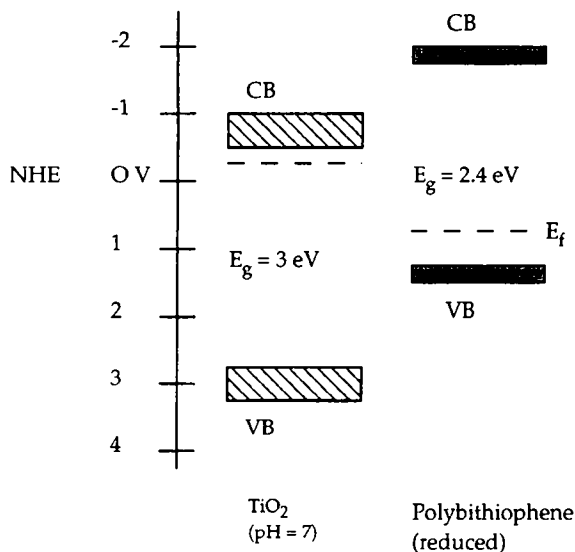
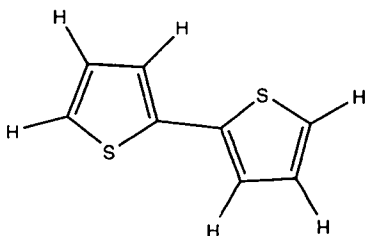


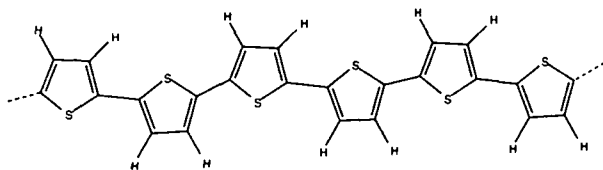
Figure 40: Energy band diagram of the TiO_2 /poly(bithiophene) diode (adapted from [8]).

Preliminary electrodeposition experiments done with polyaniline, PITN [9], P3MT and poly(bithiophene), PBT, showed that PBT was easy to electrodeposit and it showed to be stable in ambient air in the reduced (orange colored) state. In contrast the oxidized state of poly(bithiophene) (blue colored) seemed to be unstable in ambient air as it turned brownish within a few days of atmospheric exposure. The monomer bithiophene has the following chemical structure:



The electropolymerization occurs at the reactive α -position, i.e. the carbon (with a attached hydrogen) just next the sulfur atom of the thiophene moiety, where the next monomer will attach to form the dimer. Then again the α -position in the newly joint monomer will be oxidized and an other monomer will be attached there by nucleophilic reaction. The polymerization reaction propagates by further oxidation of the α -position at the ends of the molecular string, till termination occurs either by the attack of a nucleophilic agent other than the monomer, or

the oxidation potential of the, already several monomer units distant, α -position has a too high electrochemical potential to be still oxidized by the applied voltage at the electrode. Ramification of the polymeric chain may also occur when a γ - and a α -position are oxidized and a monomer binds on each position. The structure of the neutral (undoped) poly(bithiophene) is:



The dotted lines on each side of this hexamer indicated where the polymeric chain continues. In the neutral (undoped) form, the polymer is practically an electrical insulator with a bandgap given by the energy difference between the highly delocalized aromatic π -orbital that stretches over all carbon and sulfur atoms and its corresponding π^* antibonding orbital. Electrical conductivity is achieved by oxidation, or doping of the aromatic chain. Like that, either polarons (radical cations) at low doping levels or bipolarons (dications) at high doping levels are formed [10]. In practice, doping is either made by exposing the polymer to an oxidizing agent like iodine vapors or FeCl_3 , or by applying a positive potential to the polymer electrode in a solution containing a salt, e.g. LiClO_4 or NOPF_6 , that will act as a counterion to balance the positive charges (polarons or bipolarons) in the polymeric chain.

5.1. Device build-up

In all the following experiments, PBT was electropolymerized from a 10 mM solution of bithiophene (Fluka, Buchs, Switzerland) in pure acetonitrile (Fluka) with 0.1 M LiClO_4 as supporting salt, using a Metrohm three electrode cell. The working electrode was either a metal like gold, or a piece of so-called conducting glass, i.e. a glass coated with a conducting layer of $\text{SnO}_2\cdot\text{F}$ (LOF TEC 3 mm $10 \text{ } \Omega/\text{sq}$, or Asahi Glass 1 mm $10 \text{ } \Omega/\text{sq}$), or different sorts of titanium oxides deposited on conducting glass. The counter-electrode was a small sheet of Pt, ca 0.5 cm^2 in size attached to a Ti rod. The reference electrode was a silver wire coated with AgCl (made by dipping a silver wire into a HCl solution). Sometimes the reference electrode was omitted, and only a two electrode system was used for the electrodeposition or the subsequent electroreduction of the PBT film. Deposition was made either galvanostatically at ca. 0.1 to $0.5 \text{ mA}/\text{cm}^2$ or potentiostatically when using a rather insulating working electrode like sputtered titanium oxide (sample from Flachglas AG, Gelsenkirchen, Germany).

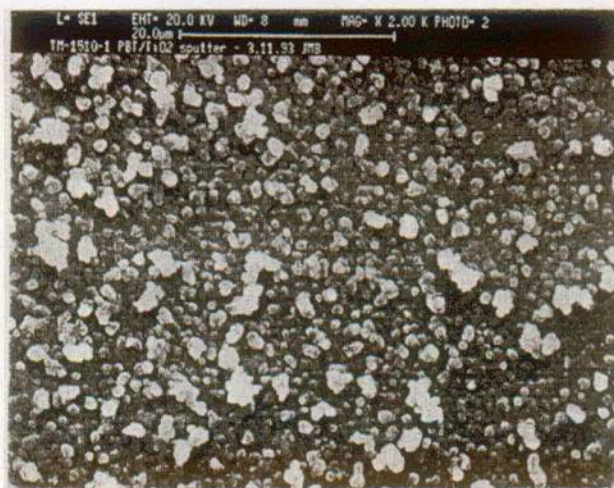


Figure 41: SEM photograph (magnification of 2'000 x) of a reduced poly(bithiophene) layer electrochemically deposited onto a sputtered TiO_2/ITO electrode.

The polymer forms 1 to 3 μm sized spherically shaped nodules as shown in fig 41.

Preliminary experiments using PBT in the oxidized or doped form (dark blue material) as p-type hole conductor showed no photoresponse when deposited on titanium oxide. Hence, the PBT was reduced electrochemically by biasing the working electrode negatively to ca. 1.0 V vs. the Ag/AgCl reference, till the color change from dark blue to orange-red was complete and the current was in the μA range (starting from ca 1 mA/cm^2 initially). This process took ca. 3 min. for a ca. 1 μm thick PBT electrode. Furthermore, oxidized PBT electrodes, i.e. as taken after the electropolymerization, showed a color change upon storage in the ambient going from dark blue to brownish within a few days. This probably indicated a partial reduction of the PBT film. Electrochemically reduced PBT films did not show any color change, even after over two years of storage in ambient conditions.

In order to check possible effects of the supporting salt, which was acting as counterion to balance the positive charges in the oxidized (or doped) PBT film, two PBT electrodes with the same amount of passed charges during electrodeposition, were prepared with two different supporting salts, and the absorption spectra of the reduced solid PBT layers (fig. 42) were measured.

	Sample 1	Sample 2
Supporting salt	LiClO ₄	TPATBF
Deposition potential	1.2 V vs. Ag/AgCl	1.25 vs. Ag/AgCl
Passed depos. charge	70 mC/cm ²	70 mC/cm ²
Reduction potential	-0.5 V vs. Ag/AgCl	-0.5 V vs. Ag/AgCl
Passed red. charge	8 mC/cm ²	8 mC/cm ²
Absorption max.	460 nm	474 nm

TPATBF denotes tetrapropylammonium tetrafluoroborate (Fluka)

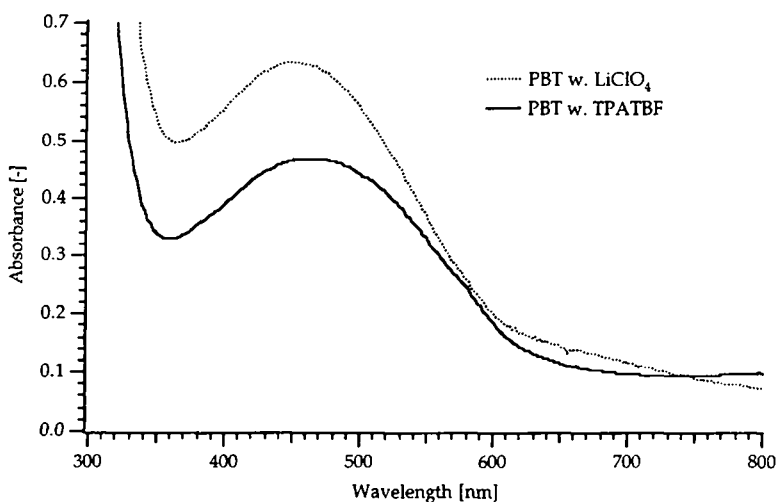


Figure 42: Absorption spectrum (corrected for the ITO-glass absorption) of the solid PBT layers electrodeposited with LiClO₄ (dotted line) or TPATBF (solid line) used as supporting salt during the electrodeposition.

The absorption onsets of the PBT solid layers are located at ca. 610-620 nm, which corresponds to a bandgap of ca. 2 eV, the tails beyond 650 nm are due to light interferences of the thin films. The absorption maxima are not the same for both PBT solid film, which is probably due to the deposition process, where the precise amount of deposited PBT is not controlled. A small shift of ca. 14 nm of the absorption maximum is observed, with the LiClO₄ giving a blue-shifted PBT film. Only a small change of the UV-VIS absorption properties is expected, since in the reduced form of PBT, essentially all the counterions are expelled from the PBT film. Probably, the very few counterions left in the film are influencing either on the conformation, or on the conjugation length of the molecular chains of the PBT film, hence some change in the absorption characteristics.

5.2 Symmetric Au/poly(bithiophene)/Au structure

The temperature dependence of the resistivity, shown in fig. 44, of the reduced form (also called the 'dedoped' form) of p-PBT was investigated by using a 320 nm thick galvanostatically electrodeposited PBT layer sandwiched between two 100 nm thick gold electrodes deposited by vacuum evaporation (Auto 306 Edwards). The active area of the device was 0.07 cm^2 , given by the size of the top gold electrode. Fig. 43 shows the device build-up. The temperature of the device was changed between 23°C and 82°C by using a thermostated heating plate.

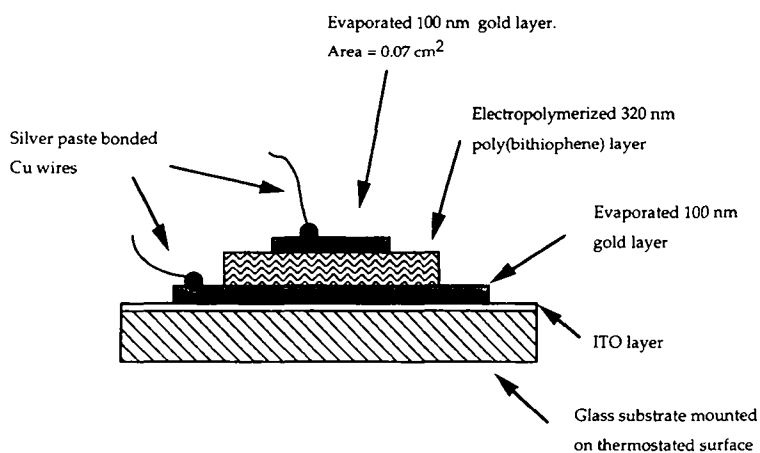


Figure 43: Schematic build-up of the Au/PBT/Au device intended to probe the Au/PBT contact.

The nature of the Au/PBT interface was studied by plotting the current passing through the junction while applying a voltage ranging from 4 V to - 4 V. Fig. 45 shows the current density dependence on small bias of the Au/PBT/Au sandwich device.

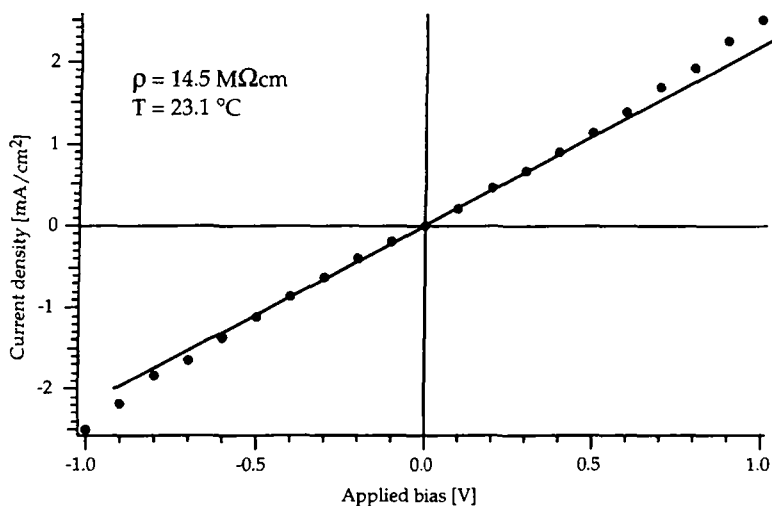
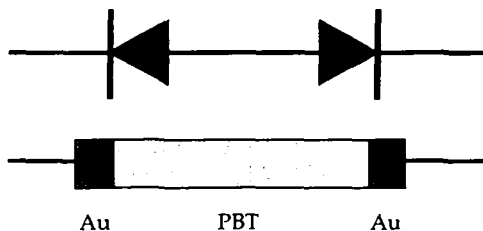


Figure 45: Current density plot in dependence of the applied bias for the Au/PBT/Au device.

The current density plot is linear and symmetric in the $\pm 500 \text{ mV}$ bias range, indicating an ohmic behavior of the Au/PBT interface, where the current is proportional to the applied bias and the proportionality is independent of the bias direction. From the slope taken between $\pm 500 \text{ mV}$, a resistivity of ca. $\rho = 14.5 \text{ M}\Omega\text{cm}$ can be estimated at room temperature ($23 \text{ }^\circ\text{C}$).

In fact, an ohmic behavior could be also explained by that the Au/PBT junction forms a rectifying junction and that the used symmetric Au/PBT/Au structure could be seen as the serial connection of a Au/PBT diode e.g. connected in the forward direction and an opposite connected PBT/Au diode. In this case, the equivalent electrical diagram would be:



and this equivalent electrical circuit behaves as a pseudo-ohmic contact with the overall resistance given by the reverse bias behavior of each, maybe poorly rectifying, diodes.

Actually, the electrical behavior of the Au/PBT junction is not truly ohmic, as shown the J-V plot in fig. 46, where the linearity holds only in a bias range of +/- 500 mV. Above this range, ohmic law is not anymore valid as the current (resp. the conductivity) increases in an exponential manner at large biases (+/- 4 V). This phenomenon has been reported by Fichou et al. to occur in other thiophene-oligomers/Au junctions [11].

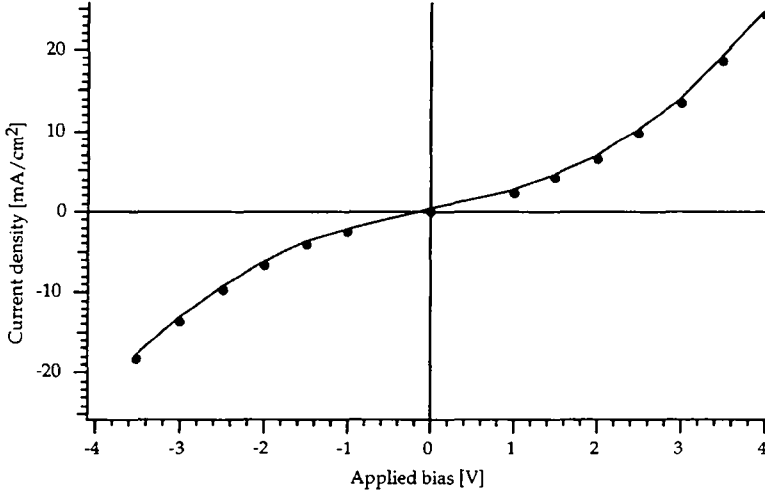


Figure 46: Current density dependence on large bias (+/- 4V) for the Au/PBT/Au device.

The non-linearity shows that the current does not follow Ohm's law in the high bias (>500 mV) regime, but is a space charge limited current [11 p. C725]. The voltage dependence of the current density J is then given by [12] :

$$J = \frac{V}{R} + k_{sc} V^2 \quad (22)$$

where

$$k_{sc} = \frac{\epsilon \epsilon_0 \mu}{d^3} \quad (23)$$

Here, R represents the surface resistance in Ωcm^2 observed in the linear range of the J-V plot (fig. 46), μ is the mobility in cm^2/Vs and d the thickness of the

polymer layer ($d = 3.2 \times 10^{-4}$ cm for this device). Using a quadratic fit of the positive (or the negative branch) of the J vs. V plot in fig. 46 (e.g. from 0 to 4 V bias), it is possible to estimate the mobility in the reduced PBT layer. Quadratic fitting of the positive branch from 0 to 4 V (negative branch from 0 to -3.5 V) yields a R value of 2500 (1100) Ω/cm^2 and a $K_{sc} = 1.38 \times 10^{-3}$ (1.2×10^{-3}) $\text{A}/\text{V}^2\text{cm}^2$. From the K_{sc} values and assuming a relative dielectric constant of $\epsilon = 20$ [1 p. 383] for reduced PBT, the carrier mobility was estimated to be around $\mu = 2.5 \times 10^{-5}$ (2.2×10^{-5}) cm^2/Vs at room temperature (23°C). In the literature [1] a carrier mobility of 3.5×10^{-9} cm^2/Vs was reported for chemically deposited undoped poly(3-octyl thiophene), and a other reference [13] indicates a mobility of ca. 10^{-5} cm^2/Vs for electrochemically deposited and doped poly(3-hexyl thiophene). Hence, the found mobility value for undoped polybithiophene lies in between the order of magnitudes of the reported mobility of undoped and doped poly(3-alkyl thiophenes). From the J-V slope around 0 V in fig. 45, an experimental value of $R = 220 \Omega/\text{cm}^2$ was measured.

The space charge limited current model gives an indication of the order of magnitude of the R value. The difference found between the actually measured R value (220 Ω/cm^2) and that estimated from the quadratic fit of the J-V plot (2500 and 1100 Ω/cm^2) is probably due to the high sensitivity of the intercept of the quadratic fitting, as there is already a difference of a factor 2 in the R value between the quadratic fit for the positive branch and that made for the negative branch. But for the same two quadratic fits, the K_{sc} values and thus the mobility values μ are close together with a difference of ca. 10 %, indicating a low sensitivity towards measurement errors and slightly changing measurement conditions.

From the expression of conductivity, $\sigma = 1/\rho = N_A q \mu$, where N_A is the ionized carrier density (cm^{-3}) and q the electrical charge of the electron (1.602×10^{-19} C), the carrier density in the reduced PBT can be estimated, with the assumption that all the ionized carriers take part in the conductivity. From the resistivity $\rho = 14.5 \text{ M}\Omega\text{cm}$ we have $\sigma = 6.9 \times 10^{-8} \Omega^{-1}\text{cm}^{-1}$ and $\mu = 2.5 \times 10^{-5} \text{ cm}^2/\text{Vs}$, we have a ionized carrier density of $N_A = 1.7 \times 10^{16} \text{ cm}^{-3}$. For the p-PBT semiconductor, the ionized carriers are the holes.

The temperature dependence of the resistivity of the undoped (reduced) PBT layer is shown in fig. 47.

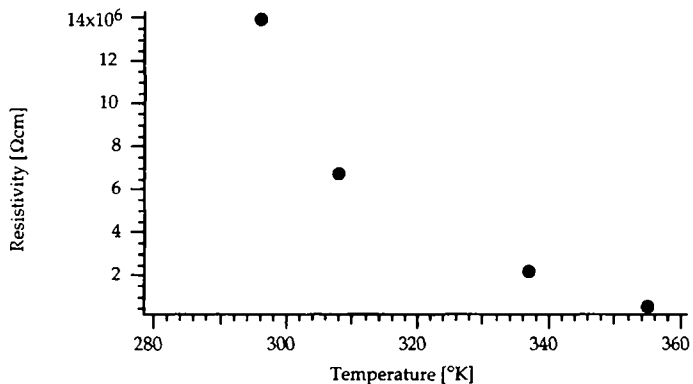


Figure 47: Resistivity plot in dependence of the sample temperature of the Au/PBT/Au device.

The resistivity of this PBT sample, in its reduced state, is ca. $\rho = 14 \text{ M}\Omega\text{cm}$ at room temperature (23°C), and it decreases to ca. $55'000 \text{ }\Omega\text{cm}$ at 82° C. In the literature [1], a resistivity of ca. $6000 \text{ M}\Omega\text{cm}$ is found for undoped poly(3-octylthiophene). In fig. 47, a semiconductor behavior is observed, as the resistivity decreases with increasing temperature. From the Arrhenius plot in fig. 48, made by reporting the natural logarithm of the conductivity σ ($=1/\rho$) vs. the inverse absolute temperature, it is possible to calculate the apparent activation energy E_a .

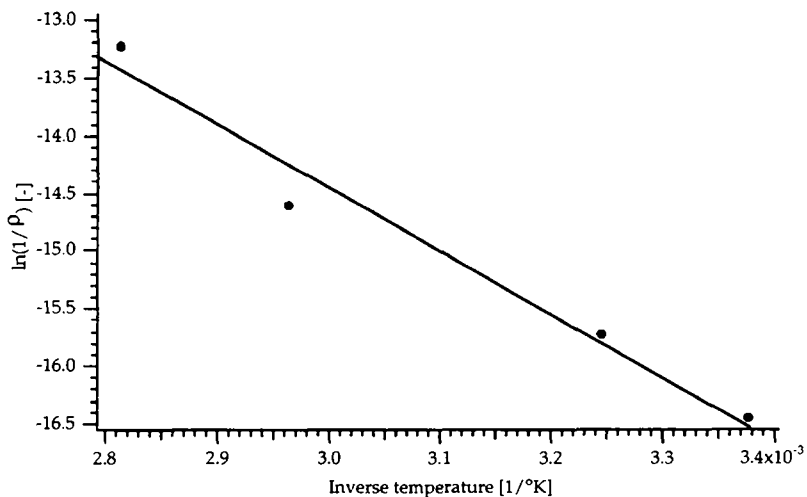


Figure 48: Arrhenius plot of the resistivity against temperature for the Au/PBT/Au device.

The linear interpolation of the $\ln(1/\rho)$ against $1/T$ plot in fig. 48 allows to estimate an activation energy of $E_a = 0.46$ eV for the conductivity dependence as a function of the temperature. That compares to the activation energy value found in the literature [14], where $E_a = 0.53$ eV for undoped poly(3-hexylthiophene) prepared by chemical oxidation of the monomer with FeCl_3 .

5.3. Gold/p-poly(bithiophene)/aluminium Schottky diode

A Au/p-PBT(reduced)/Al sandwich structure was made in order to investigate its electrical and photovoltaic properties.

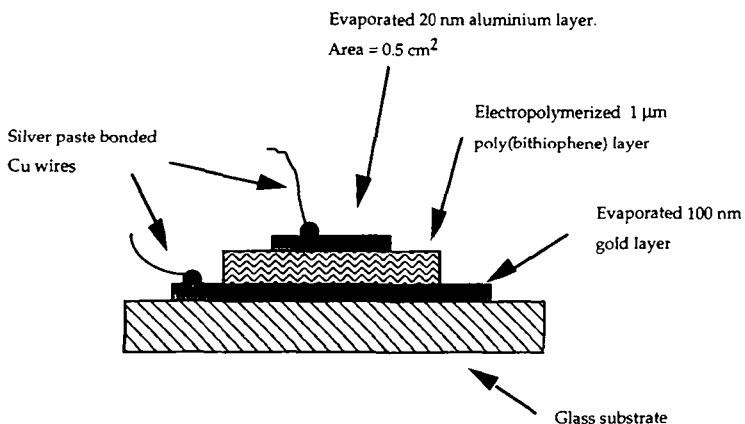


Figure 49: Schematic build-up of the Au/PBT/Al device to study the Al/PBT contact.

A 100 nm thick gold layer, physical vapor deposited (PVD) on glass at a pressure of 5×10^{-6} mbar, was used as the working electrode, on which the poly(bithiophene) grew electrochemically. The galvanostatically (0.2 mA/cm^2 for 600 s) deposited PBT was electrochemically reduced by applying a voltage of -0.4 V vs. Ag/AgCl for 200 s. The so reduced polymer looked orange-red. The electrodeposited PBT film had an average thickness of ca. $1.7 \mu\text{m}$, but its surface was rather irregular, as the thickness of the polymeric layer range from 0.5 to $3 \mu\text{m}$ when measured with a Tencor stylus thickness profilometer. On top of the polymer layer, a 20 nm thick aluminium layer, acting as the negative terminal, was deposited by PVD at a pressure of ca. 10^{-5} mbar. The gold electrode acted as the positive terminal of the device.

Fig. 50 shows the J-V characteristics of the Au/PBT/Al device when biased in the range between ± 5 V. The measure was performed at room temperature (23°C).

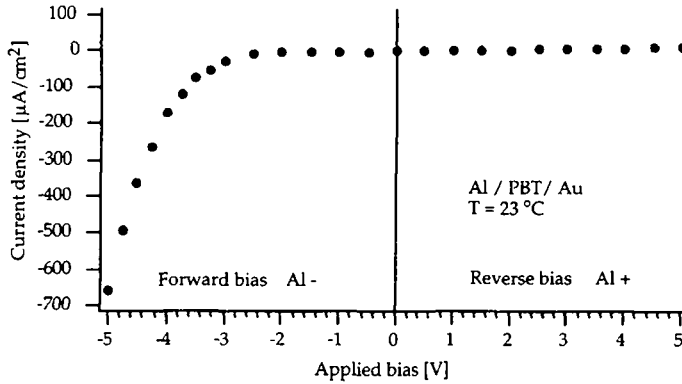


Figure 50: Current density-voltage characteristics of the Au/PBT/Al sandwich device, the voltage scanning rate was 50 mV/s.

The current flow was non-linear and depended on the polarization direction of the junction. A rectifying behavior of the Al/p-PBT (reduced)/Au device is readily apparent in fig. 50. At +/- 5 V bias, the rectifying ratio was ca. 1:47.

According to the theory of the Schottky barrier [15 p. 250-262], the work function of the metal must be smaller than that of the p-type semiconductor, and a rectifying barrier would be formed at the interface. If the work functions are in reverse order, an ohmic contact would exist rather than the rectifying behavior. Since an ohmic behavior does exist in the Au/p-PBT/Au device (fig. 45) and a rectifying contact is found in the Al/p-PBT/Au device (fig. 50), the PBT behaves as a p-type semiconductor with a work function in between those of Al (4.1 eV) and Au (5.1 eV).

The electrical properties of this metal-semiconductor junction, which is a Schottky diode, can be described by the diode equation linking the junction current density J to the applied bias V .

$$J = J_s \left[\exp \left(- \frac{qV}{nkT} \right) - 1 \right] \quad (24)$$

which can be reduced to the simpler expression

$$J = J_s \exp \left(- \frac{qV}{nkT} \right) \quad (25)$$

in the case when the applied bias V is much higher than the thermal energy kT/q which equals 25 mV at 20 °C. J_s is the saturation current density and is given by the Richardson equation [13, 15 p. 256].

$$J_s = A_R T^2 \exp\left(\frac{-q\phi_b}{kT}\right) \quad (15)$$

where n is the diode ideality factor (also called diode quality factor), A_R is the effective Richardson constant ($120 \text{ A/K}^2 \text{ cm}^2$ for free electrons), q is the electrical charge and ϕ_b is the barrier height. By plotting the natural logarithm of the current density vs. the applied bias, as showed in fig. 51, the saturation current density J_s , the diode quality factor n , and by using eq. 15, the barrier height ϕ_b can be estimated.

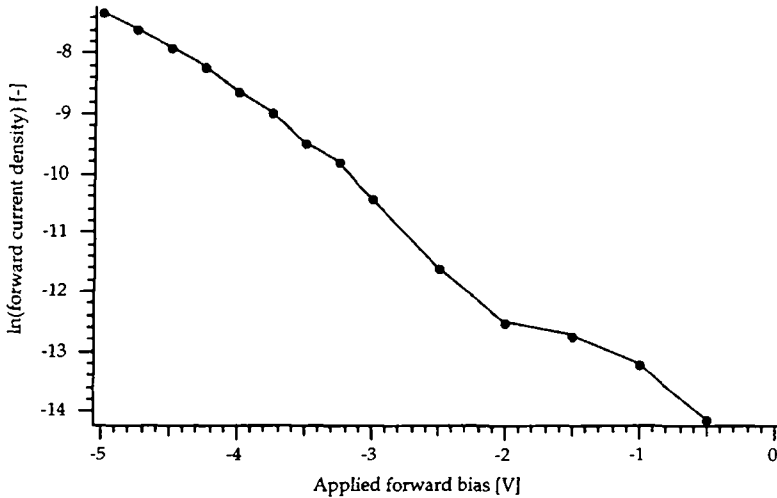


Figure 51: Plot of the natural logarithm of the current density against the applied forward bias of the Au/PBT/Al diode.

The slope (-1.59) and the intercept (-15.14) of the $\ln(I)$ -V plot (fig.51), allows to estimate a saturation current density $J_s = 0.26 \mu\text{A/cm}^2$ and a barrier height of $\phi_b = 0.8 \text{ eV}$. This barrier height value is consistent with literature data [8] since aluminum has a work function of $\phi_{Al} = 4.1. \text{ eV}$ [15 p.251] which is close to that of TiO_2 ($\phi_{\text{TiO}_2} = 4.3 \text{ eV}$).

The photovoltaic response was investigated by irradiating the Au/PBT/Al diode from the aluminium electrode side with an intensity of $800 \mu\text{W/cm}^2$ at a wavelength of 470 nm. This wavelength was chosen after a wavelength scan showed the peak photocurrent to be at 470 nm. Most of the incident light is absorbed in the 20 nm thick aluminum top layer which transmits only ca. 16 % at 470 nm as measured with a spectrophotometer (Ultraspec 2000, Pharmacia, Uppsala Sweden). Fig. 52 shows the J-V characteristics.

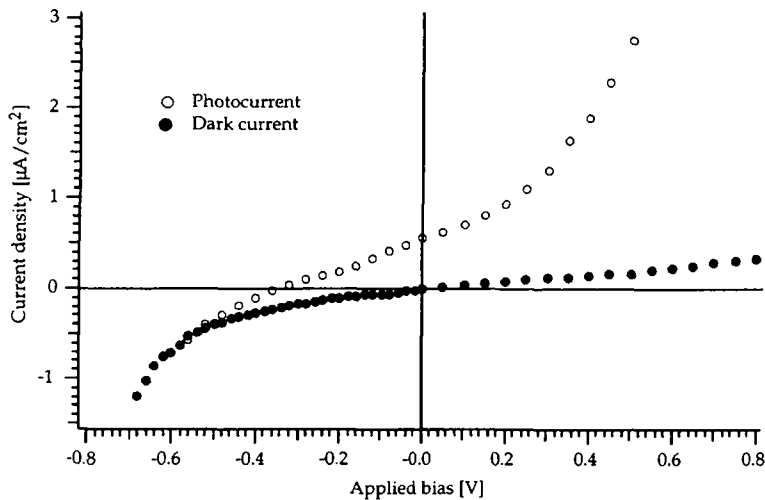


Figure 52: Current density-voltage plots of the Au/PBT/Al diode in the dark (black dots) and under $800 \mu\text{W}/\text{cm}^2$ monochromatic irradiation at 470 nm through the Al window (open circles).

From the forward bias characteristics (the Al electrode was the negative electrode), an open-circuit voltage V_{oc} of ca. 360 mV and a short-circuit current density J_{sc} of $0.55 \mu\text{A}/\text{cm}^2$ was observed. The dark current plot in fig. 52, shows that there is a parallel shunt resistance of ca. $5.2 \text{ M}\Omega$ due to a current leakage from the negative to the positive terminal, probably due to a small pinhole in the polymer film. The parallel shunt resistance value was estimated from the slope around 0 V in the J-V diagram and knowing that the electrode surface is 0.5 cm^2 . Interesting to see from the reverse bias plot (i.e. Al was positive) in fig. 52 is that the photocurrent rapidly increases at reverse polarization of the junction. This photocurrent increase is probably due to a photoconductance effect, where the photogenerated charges are increasing the overall electrical conductivity of the polymer.

5.4. Flat $\text{TiO}_2/\text{p-poly}(\text{bithiophene})$ heterojunction

In order to investigate the photovoltaic properties of a flat p-PBT/ TiO_2 junction, the following device was made: On a piece of ITO (Indium Tin Oxide) covered glass (Flachglas), a 50 mM solution of titanium tetrabutoxide in isopropanol was spread out with a glass rod gliding on a $50 \mu\text{m}$ spacer made from a 3M Scotch Magic tape lanes on each side of the glass electrode. After drying in ambient (= hydrolysis in ambient humidity of the Ti alkoxyde), this deposition process was repeated once more. A transparent layer formed having a faint pink to green interference color which was observed when looking perpendicularly at the layer.

After baking at 400 °C for 60 min., a green interference color was observed when looking at the reflection of the film. The so deposited titanium oxide layer is ca. 50 nm thick as measured with a Tencor stylus profilometer. It is called "compact-TiO₂" in contrast with the fractal or colloidal TiO₂ layers used.

The conducting rim of the so treated ITO-glass was sealed with hot-melt, and the poly(bithiophene) was deposited chronoamperometrically from a 50 mM solution of bithiophene in propylene carbonate with 0.1 M LiClO₄ as supporting salt. The deposition time was 900 s at a current of 0.23 mA/cm². The reference electrode used was a Ag/AgCl electrode and the counter-electrode was a Pt foil of 0.7 cm². A dark blue layer of oxidized poly(bithiophene) (p-PBT) formed on the whole surface of the electrode. This polymer film has been potentiostatically reduced at -0.4 V vs. Ag/AgCl for 200 s using the same solution as for the deposition. The p-PBT layer turned into a orange-brownish material. The top positive electrode consisted of a 40 nm thick gold pad of 0.5 cm² deposited by PVD onto the reduced p-PBT. The device was stored in the dark at ambient conditions. Fig. 53 shows the flat junction device assembly:

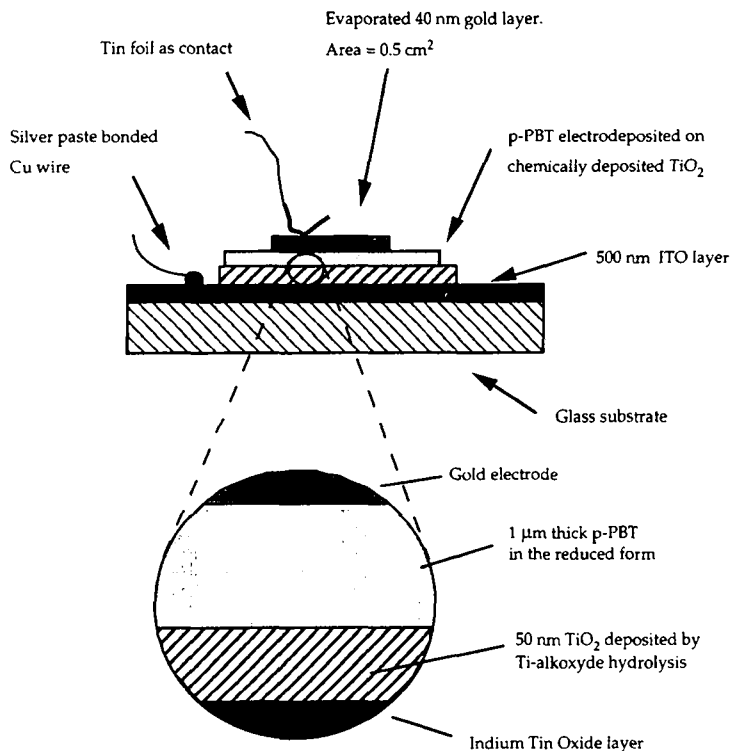


Figure 53: Schematic build-up of the Au/PBT/compact-TiO₂/ITO device for the study of the photoelectrical behavior of the PBT/TiO₂ contact.

The diode characteristics of this flat junction were investigated with the J-V measurement at different polarizations and with the Mott-Schottky technique. The dark J-V plot of the Au/PBT/compact-TiO₂ junction is given in fig. 54

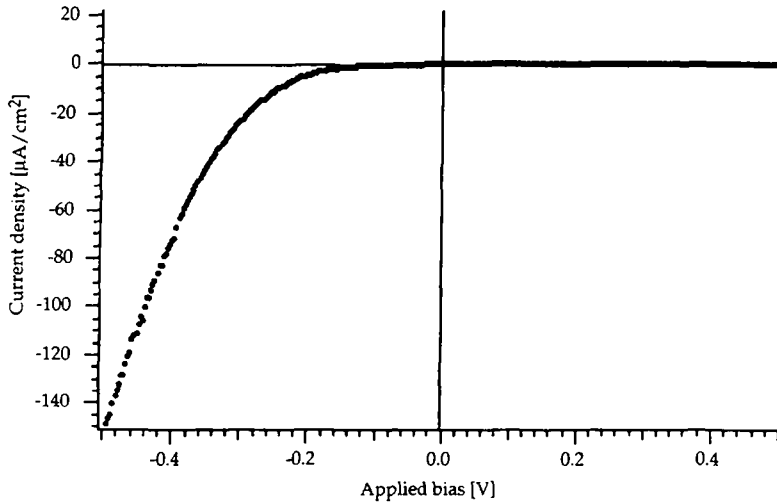


Figure 54: Dark current density plot as a function of the applied bias, measured with the Au/PBT/compact-TiO₂/ITO sandwich device.

The dark current plot shows that the current is non-linear with the voltage and is depending on the polarization direction of the junction. Hence, the flat TiO₂/PBT interface behaves as a n-p heterojunction, where the n-side is the TiO₂ and the p-side the reduced PBT showing a current rectifying behavior. The ln(I)-V plot obtained with this heterojunction is in fig. 55.

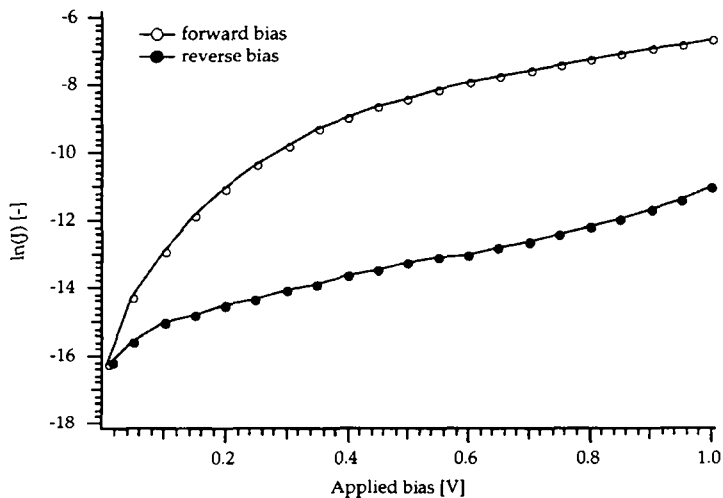


Figure 55: Plot of the natural logarithm of the current density in function of the forward bias (open circles) and the reverse bias (black dots) of the Au/PBT/compact-TiO₂ junction. Forward bias means that the Au contact pad deposited on the TiO₂ goes negative in potential with respect to the ITO glass electrode bearing the PBT.

From fig 55, the best rectifying ratio of ca 1: 200 can be estimated and was attained at a bias of +/- 600 mV. The reverse bias leakage current is around 2 $\mu\text{A}/\text{cm}^2$ at 600 mV. The barrier height ϕ_b and the diode ideality factor n of the TiO₂/p-PBT junction was estimated by using the ideal diode equation (eq. 25) and the Richardson expression (eq. 15) in the forward bias range between 400 and 1000 mV of the $\ln(J)$ vs. V plot in fig 55. A diode ideality factor of $n = 2$ and a barrier height of $\phi_b = 0.9$ eV was found. This barrier value is comparable to the data found by Torsi et al., where $\phi_b = 0.8 \pm 0.1$ eV for a TiO₂/PBT junction made on anodically grown TiO₂ [8]. The diode ideality factor is relevant since the open circuit voltage V_{oc} can be deduced from the solar cell equation describing the current density J vs. the applied bias V , as

$$V_{oc} = \frac{nkT}{q} \ln \left(\frac{J_L}{J_s} \right) \quad (12)$$

with J_L is the short-circuit current density and J_s the saturation current density. This relation shows that the open-circuit voltage V_{oc} decreases, at $T = 298$ °K, by n times $kT/q = 59$ mV if the incident light intensity decreases by a decade.

The device showed a photovoltage of $V_{oc} = 480$ mV and a short circuit current density of $j_{sc} = 130$ $\mu\text{A}/\text{cm}^2$ when irradiated at one sun (simulated), i.e. 100

mW/cm^2 . Even at a light level of only 1000 lux ($1/100^{\text{th}}$ of a sun), an open circuit voltage of ca. 300 mV was observed. This high sensitivity is a sign that the junction is working well in this device, which is in accordance with the estimated diode ideality factor of $n = 2$. The photovoltaic characteristics in very strong light is shown in fig 56, where the light intensity was $1.2 \text{ W}/\text{cm}^2$ from a Xe-lamp filtered with a Schott 113 filter cutting below 380 nm.

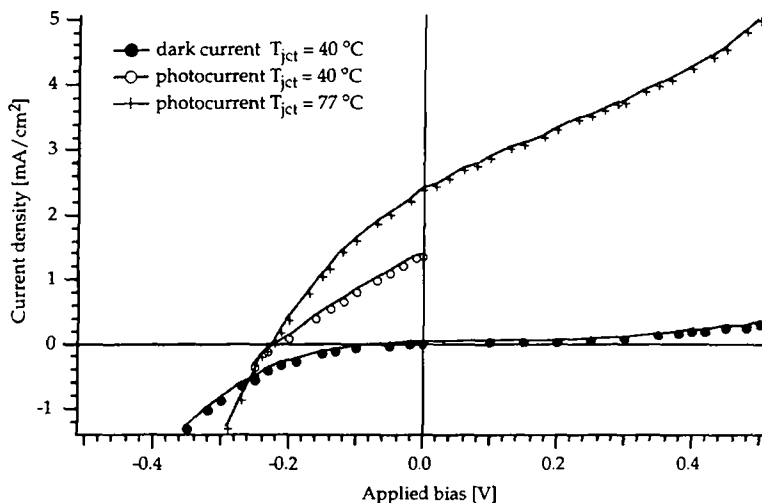


Figure 56: J-V plot of the Au/PBT/compact-TiO₂ device, performed at a light intensity of $1.2 \text{ W}/\text{cm}^2$ with a UV filtered Xe-lamp. The temperature was $40 \text{ }^\circ\text{C}$ for the dark current plot (black dots) and for the photocurrent plot (open circles), and the photocurrent plot was also measured at $77 \text{ }^\circ\text{C}$ (crosses). The forward bias direction is the left hand side from the zero bias point.

From the photocurrent plots in the forward direction, we see that the open-circuit voltage is only 230 mV at $40 \text{ }^\circ\text{C}$ and 215 mV at $77 \text{ }^\circ\text{C}$ junction temperature. This low open-circuit voltages are due to the increased conductivity of the PBT at high temperatures, thus offering a parallel resistance that degrades the open-circuit voltage of the PBT/TiO₂ junction. When comparing the photocurrents plots in fig. 56 at 40 and $77 \text{ }^\circ\text{C}$, a strong dependence of the short-circuit current density on temperature is observed, as the current density rises from $J_{\text{sc}} = 1.28 \text{ mA}/\text{cm}^2$ at $40 \text{ }^\circ\text{C}$ to $J_{\text{sc}} = 2.28 \text{ mA}/\text{cm}^2$ at $77 \text{ }^\circ\text{C}$ junction temperature. This increase of J_{sc} is probably due to a higher charge carrier mobility in the PBT (holes) and the TiO₂ (electrons) films.

In an other experiment, natural sunlight (ca. $50 \text{ mW}/\text{cm}^2$) was focused with a 2.7 cm diameter magnifying glass (spot diameter 1.2 mm) onto the front side (conducting glass side) of the device. A short-circuit current density of ca. $16 \text{ mA}/\text{cm}^2$ was obtained that way, in a concentrated irradiation of ca 500 times the

sun. During this experiment, the device heated to about 150 °C for a few seconds without showing any signs of destruction.

Some of the J-V plots were made two years after device assembly, showing that the electrical and optical properties of the reduced PBT are not changing after very long exposure to the ambient environment.

The Mott-Schottky plots of the flat TiO₂/PBT junction were measured in order to estimate the doping profile and the built-in voltage [15 p. 74]. It is assumed that the n-TiO₂/p-PBT heterojunction can be assimilated to an abrupt junction where the concentration of the donor impurities in the n-TiO₂ changes abruptly at the junction interface to the acceptor impurities in the p-PBT. For a compact electrode, the capacitance is given by [15 p. 79]

$$C = \sqrt{\frac{q\epsilon N}{2}} (V_{bi} \pm V - 2kT/q)^{-1/2} \quad (26)$$

where C is the junction capacitance in As/Vcm², V the applied bias in V, q the electron charge, ε the dielectric constant, and N the doping density in cm⁻³, which may vary with the distance from the p-n junction interface. The junction capacitance C, which is the capacity per area, can be measured with the alternating current (AC) impedance technique, where a small sine-shaped AC signal of a few mV of amplitude is applied to the sample and the phase and amplitude of the current, which is the output signal, is recorded. The phase and the amplitude of the current gives the real and imaginary part of the impedance. This technique is used in impedance spectroscopy where the real (Z') and imaginary parts (Z'') of the impedance Z is measured at different frequencies. The capacitance C can be calculated by

$$C = \frac{1}{2 \pi Z'' \nu} [As/Vcm^2] \quad (27)$$

where ν is the frequency in Hz and Z'' the real part of the impedance in Ω for a known junction area.

From the capacitance expression (eq. 26), the doping density N(W) for a p-n junction is given by [15 p. 81]

$$\frac{d(C^{-2})}{dV} = \frac{2}{q\epsilon N(W)} \quad (28)$$

So, by plotting the inverse square of the capacitance (1/C²) against the applied bias V, the doping density profile N(W) can be found by taking the slope of the 1/C² vs. V plot. The 1/C² vs. V plot is also called the Mott-Schottky plot. The intercept of the Mott-Schottky plot with the bias axis gives the built-in voltage V_{bi} of the junction. The Mott-Schottky plots of the flat heterojunction Au/p-PBT/n-

TiO₂/ITO was measured at 45 KHz (fig. 57), 887 Hz (fig. 58) and 98 Hz (fig. 59) with a sine-shaped AC voltage ripple of 10 mV:

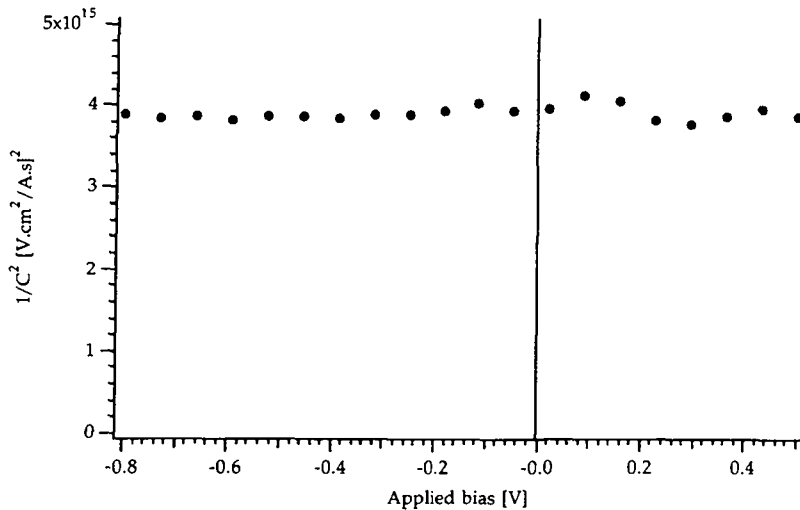


Figure 57: Mott-Schottky plot of the flat TiO₂/PBT junction made at an AC frequency of 45 KHz.

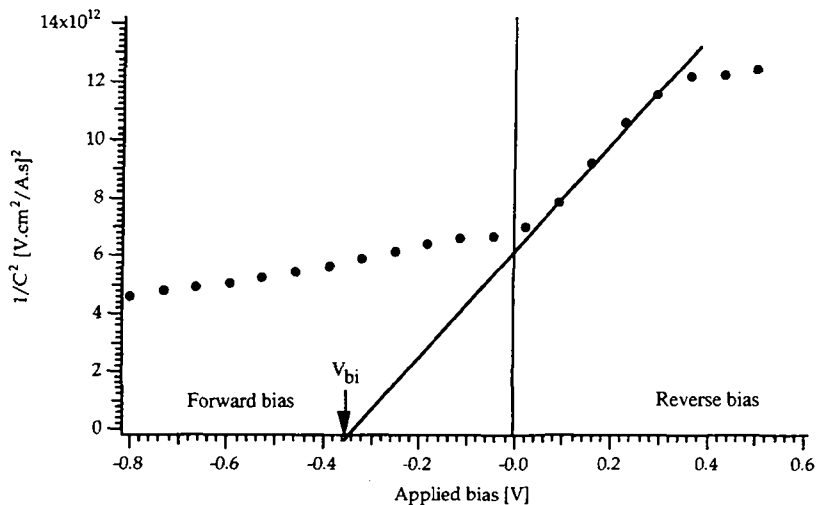


Figure 58: Mott-Schottky plot of the flat TiO₂/PBT junction made at an AC frequency of 887 Hz.

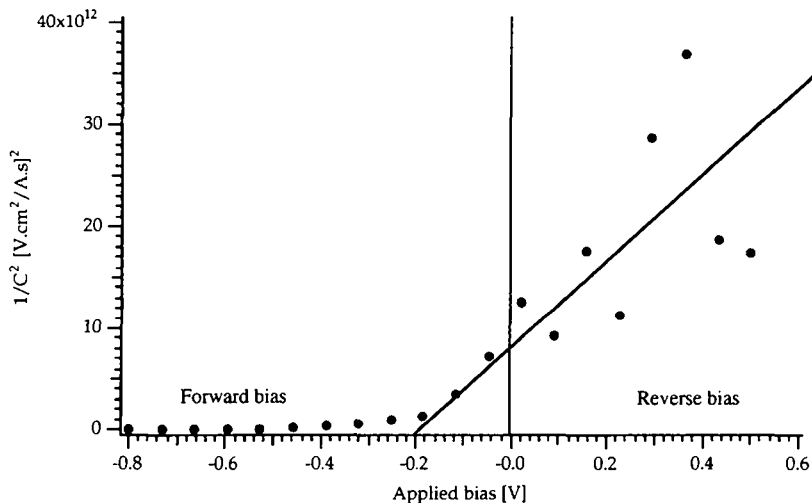


Figure 59: Mott-Schottky plot of the flat TiO₂/PBT junction made at an AC frequency of 98 Hz.

In the high frequency plot at 45 KHz, the inverse square capacitance with a value of ca. $4 \times 10^{15} [(Vcm^2/As)^2]$ is independent of the applied bias. From this value, a capacitance of ca. 16 nF/cm² can be calculated (F (Farad) = As/V). At high frequency, the Au/PBT/TiO₂/ITO device behaves as a plane plate capacitor with a capacity of ca. 16 nF/cm².

In the medium and low frequency domain, a potential dependent capacitance develops, similar to what Fang et al. [1. p. 383] found with their Al/P3OT/ITO structure scanned at 300 Hz, as the low frequency allows to detect the true junction capacitance.

Hence, at 887 Hz (fig. 58) a doping density of $N_A = 2(\text{slope})/q\epsilon = 7 \times 10^{16} \text{ cm}^{-3}$ can be estimated from the positive slope ($= 1.6 \times 10^{12}$) of the Mott-Schottky plot in fig. 58, assuming a dielectric constant ϵ of ca. $3.54 \times 10^{-13} \text{ As/Vcm}$ for the PBT [11, p. C725]. A positive slope indicates a p-type doping of the PBT, which is expected from these kinds of materials.

The intercept of the straight line with the bias axis indicates an apparent built-in voltage of 0.4 V. Doing the same calculation as above with the positive slope ($= 3.7 \times 10^{13}$) found in the plot made at 98 Hz (fig. 59), gives a donor density of $N_A = 8 \times 10^{17} \text{ cm}^{-3}$ and the built-in voltage seems to be around 0.2 V. In § 5.2., a doping density of $N_A = 1.7 \times 10^{16} \text{ cm}^{-3}$ was deduced from the resistivity of the PBT measured with a symmetric Au/PBT/Au ohmic contact structure. This doping

value is in the same order of magnitude as the one found with the Mott-Schottky plot at 887 Hz.

A large frequency variation of the junction capacitance is observed with this Au/PBT/TiO₂/ITO system, indicating that more or less deep traps are acting in the charge storage within the junction as the AC frequency is changed. A low frequency signal would charge and discharge deeper traps than a high frequency signal, as a charge carrier needs more time to be detrapped from a deep trap (for a constant temperature).

Such a phenomenon is observed in our case, where the "doping" concentration, which is in fact a trap concentration, changes nearly by a order of magnitude when going from 887 Hz to 98 Hz.

Finally a word of caution to the interpretation of the Mott-Schottky plot results must be said. It has to be reminded that the Mott-Schottky plots are only valid for an abrupt junction with a frank change of dopants concentration across the p-n interface, which is probably not the case with a flat layer of n-type TiO₂ covered with electrochemically grown p-type PBT, forming spherically shaped nodules (see fig. 41). Moreover, the ohmic junction formed between the gold pad and the PBT, and the one formed between the TiO₂ and the ITO are probably also contributing to the frequency dependence of the capacitance of the ITO/TiO₂/PBT/Au device, as these interfaces also have most probably interface states acting as traps.

5.5. Nanostructured TiO₂/p-poly(bithiophene) heterojunction

A Au/p-PBT/nc-TiO₂ structure was made in order to study its electrical and photovoltaic behavior. Again, the PBT was in the reduced form and the titanium oxide used was in the "fractal" type nanocrystalline form, with pores and cracks in the nm range, as shown in the SEM photograph in fig. 17 (chapter 4). The nanocrystalline TiO₂/PBT device assembly is shown in fig. 60.

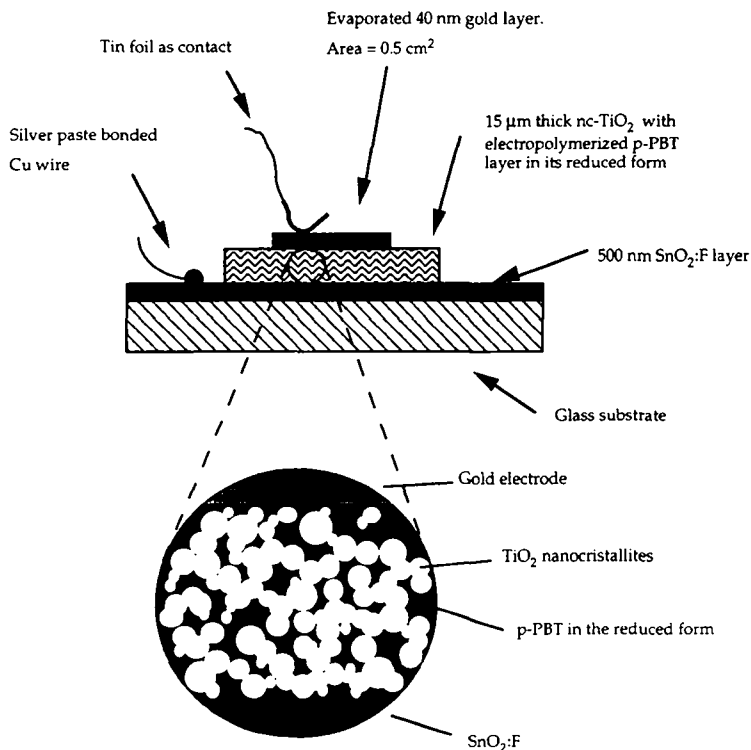


Figure 60: Schematic build-up of the Au/PBT/fractal-TiO₂/SnO₂ device to study the photoelectrical behavior of the PBT/TiO₂ contact. The inset shows schematically the PBT filling the pores, or cracks, of the fractal TiO₂ "sponge" and thus contacting the Au top contact (positive terminal) and the SnO₂ layer which is the negative contact.

The nc-TiO₂ used for this experiment was a "fractal" type of TiO₂ layer made by deposition of an aqueous TiCl₄ solution onto the SnO₂:F conducting glass (Asahi, 10 Ω/sq.) followed by a hydrolysis in controlled humidity atmosphere and a baking at 450 °C. This deposition and baking process was repeated 9 times to achieve a fractal TiO₂ thickness of ca. 15 μm [16, 17]. The rim of the conducting glass electrode was insulated with hot-melt prior to the PBT deposition in order to avoid preferential polymer electrodeposition at the highly conducting blank SnO₂:F rim of the electrode. The PBT was electrodeposited at a current of ca. 0.2 mA/cm² into the cracks of the TiO₂ film until filaments of PBT were growing outside the TiO₂ film. A total charge of 820 mC/cm² had passed at a voltage of 1.2 - 1.3 V vs. Ag/AgCl. The PBT filaments were removed by gently wiping them off the electrode, and the PBT film was electrochemically reduced by applying a potential of -0.4 V vs. Ag/AgCl for 300 s. Upon reduction, the polymer turns dark orange-red in color. A layer of 40 nm of gold for the positive contact was

deposited by PVD onto the reduced p-PBT layer. Preliminary device testing showed an apparent electrical resistance of ca. $5 \text{ M}\Omega$ in the dark, and a open-circuit voltage of 350 mV when lit by a halogen spot. As shown in fig. 60, the PBT grew from the conductive $\text{SnO}_2\text{:F}$ layer that was not covered by the insulating fractal TiO_2 particles. So the pores of the fractal TiO_2 were filled with PBT. Obviously such a situation allows some short-circuit possibilities between the gold electrode and the $\text{SnO}_2\text{:F}$ layer. Effectively, at room temperature, where the reduced PBT is a rather poor conductor, the device shows fairly good rectifying properties as shown in fig 61. But when the junction temperature is high, the device behaves as a parallel shunted diode. This is due to the increased conductivity of the PBT allowing a short-circuit between the gold electrode and the conductive glass. Fig. 61 shows the temperature effects on the photovoltaic behavior, using a monochromatic light source at 540 nm with a light intensity of ca. 1.8 mW/cm^2 . All J-V plots were made with the light entering the SnO_2 side of the device.

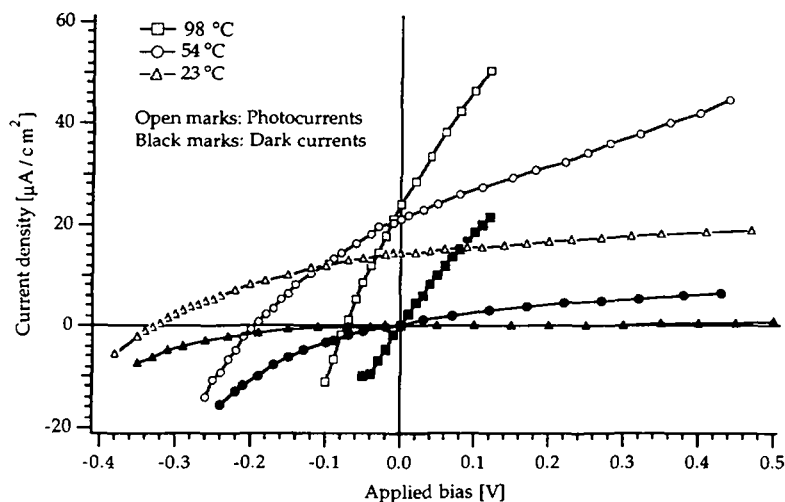


Figure 61: J-V plots of the PBT/nc-TiO₂ device, made at 23°C (triangles), 54°C (circles) and at 98°C (squares). The black marks are for the dark currents, and the open marks for the photocurrents, measured with a 1.8 mW/cm^2 intense monochromatic light at 540 nm.

The device exhibits the J-V characteristics of a pn-junction at room temperature, but as the temperature increases, a parallel shunt resistance was created by the increasingly better conducting PBT. The PBT started to short-circuit the device, since direct contact is allowed between the conducting glass electrode (negative terminal) and the top gold electrode (positive terminal). The J-V curve measured at 23 °C shows that the photocurrent is only slowly increasing in the reverse bias condition. This indicates that the charge separation is already effective in the built-in electrical field. The strength of the electrical field necessary for the

photogenerated charges separation is given by ratio of the open circuit voltage ($V_{oc} = 0.33$ V) and the depletion layer width $W=15$ μm . Assuming that the depletion layer is stretching throughout the whole nanocrystalline titanium oxide layer, the built-in electric field is ca. $E_{bi} = 22'000$ V/m. Fig. 62 shows the J-V characteristics at a light intensity of 60 mW/cm^2 , measured at room temperature (25 $^{\circ}\text{C}$) and at elevated temperature (90 $^{\circ}\text{C}$).

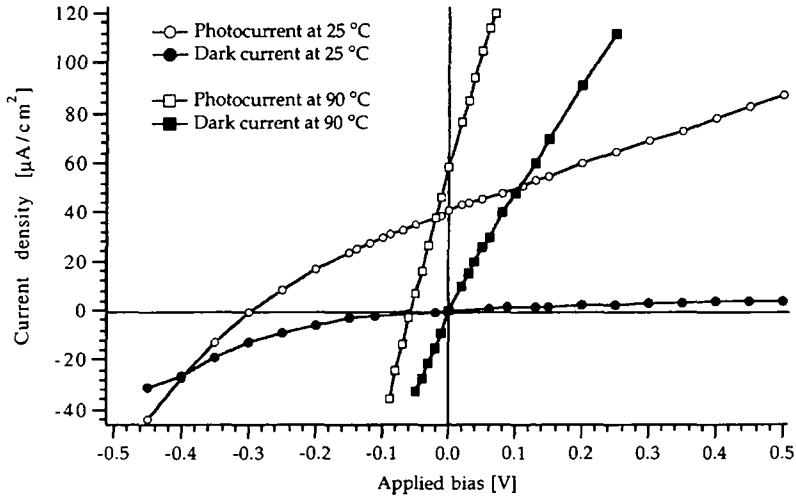


Figure 62: J-V plots of the PBT/nc-TiO₂ device, made at 25°C (circles) and at 90°C (squares). The black marks are for the dark currents and the open marks for the photocurrents, made with a 60 mW/cm^2 light from a UV-filtered Xe-lamp.

The effect of the temperature increase from 25°C to 90°C is double: on the one hand, the parallel shunt resistance in the polymer is decreasing from ca. 150 $\text{K}\Omega$ to 2.2 $\text{K}\Omega$, creating a short-circuit that is in competition with the photocurrent, and on the other hand, the photocurrent is increased as it is limited by the poor carrier transport characteristics of the PBT at room temperature. The figures show the photovoltaic behavior of the device in strong irradiation: fig. 63 at 330 mW/cm^2 and fig. 64 at 1200 mW/cm^2 (= ca. 12 suns).

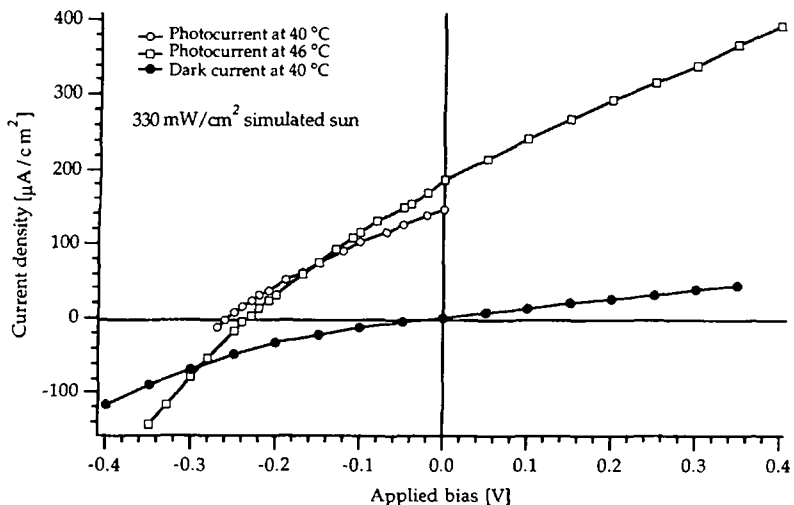


Figure 63: J-V plots of the PBT/nc-TiO₂ device, made at 40°C (circles) and at 46°C (squares). The black dots are for the dark current and the open marks for the photocurrents, done with a 330 mW/cm^2 light from a UV-filtered Xe-lamp.

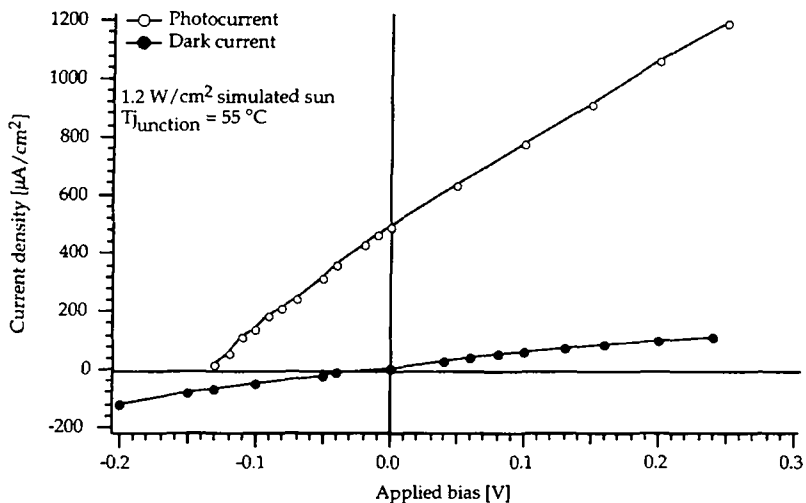


Figure 64: J-V plots of the PBT/nc-TiO₂ device, made at 55°C, the dark current is represented with the black dots and the open circles are for the photocurrent, performed at 1.2 W/cm^2 light intensity from a UV-filtered Xe-lamp.

Again, the temperature dependence of the photovoltaic behavior in strong irradiation is similar to that at low light levels. The open circuit voltage drops from $V_{oc} = 0.26$ V to $V_{oc} = 0.23$ V, when the junction temperature rises from 40°C to 46°C, and with the same temperature increase, the short-circuit current rises by ca. 25 %. This is a sign that the carrier collection is somehow impeded by the ohmic resistance, i.e. the low mobility of the polymeric semiconductor.

The action spectrum in fig. 65 is done by plotting the short-circuit photocurrent in function of the incident wavelength. The light source was a Xe-lamp equipped with a Schott N° 113 filter to remove the UV radiation below 380 nm and the IR peaks of the Xe-lamp. An Oriel monochromator was used as wavelength selector from 350 to 820 nm. The intensity at 540 nm was ca. 1.8 mW/cm².

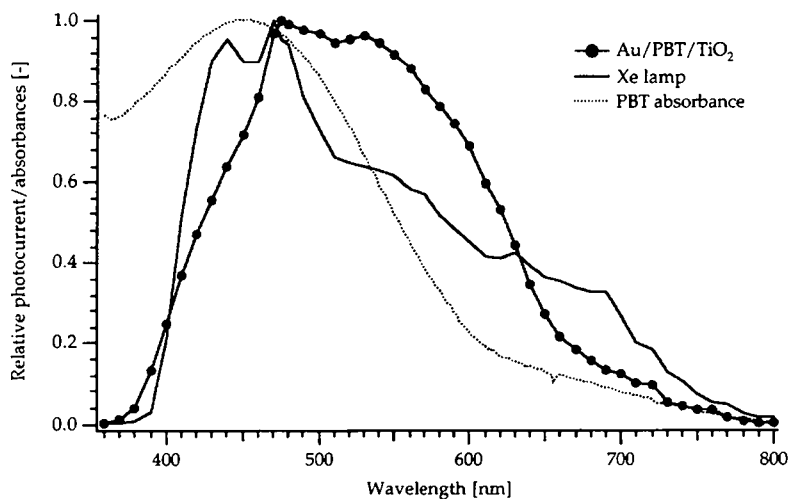


Figure 65: Photocurrent action spectrum (black dots) of the PBT/nc-TiO₂ device, absorption spectrum of the PBT (dotted line) and action spectrum of the Xe-lamp (solid line).

The action spectrum shows a steep onset of the photocurrent at ca. 660 nm (1.9 eV), which is consistent with the band gap of the p-PBT in its reduced form ($E_g \approx 2$ eV), although the photocurrent signal is tailing out up to 800 nm. This low energy photocurrents are may be due to the presence of interface or bulk states in the TiO₂/PBT junction.

5.6 Conclusion

The observed photovoltaic responses in visible light proved that the electrochemically reduced form of PBT can act as sensitizer for flat and nanocrystalline TiO₂ electrodes. Photocurrent densities of 60 $\mu\text{A}/\text{cm}^2$ and open-circuit voltages of ca. 350 mV were observed with a nanocrystalline TiO₂/PBT device at 60 mW/cm^2 simulated sunlight. Under a strong irradiation of 1.2 W/cm^2 , a photocurrent of up to 0.5 mA/cm^2 was measured with the same nanocrystalline TiO₂/PBT device and a flat TiO₂/PBT junction showed even photocurrents of up to 2.5 mA/cm^2 .

But all the devices showed a strong dependance of their photovoltaic characteristics upon change of temperature: At room temperature, the reduced form of the PBT behaved practically as an insulator, allowing high photovoltages, up to 350 mV to develop across the lit TiO₂/PBT junctions. But when the junction is heated, e.g. when lit by strong irradiation, the open-circuit voltage dropped from 350 mV at room temperature to only 100 mV at 77°C, and the J-V characteristics indicated a parallel shunting across the hot TiO₂/PBT junction. This shunting was created by the increased electrical conductivity of the reduced PBT at elevated temperature. Through unwanted pinholes in the TiO₂ layer, the PBT was contacting both junction terminals creating a short-circuit, or shunt, between the ITO coating of the conductive glass and the gold pad evaporated onto the TiO₂ electrode. This undesirable junction shunting can be avoided by using either a pinhole free TiO₂ layer or a compact TiO₂ underlayer preventing the direct contact of the PBT with the ITO coating.

From the observed short-circuit currents in strong irradiation, it seems that the nanocrystalline junction didn't perform better than the flat TiO₂ /PBT devices. The good performances of the flat TiO₂ /PBT diodes are probably due to the very thin layers of TiO₂ (50 nm) and PBT (1 μm) used, allowing a high electrical field in the device and minimized electrical conduction paths in the poorly conducting TiO₂ and reduced PBT. In contrast, in the case of the nanocrystalline TiO₂/PBT junction, the porous fractal type TiO₂ layer filled with PBT, was ca. 15 μm thick, and the ohmic gold contact pad was only contacting the top layer of the TiO₂ electrode, thus the photoelectrically created holes had to travel over several microns in the poorly conducting PBT, with the high chance to recombine with conduction band electrons of the TiO₂.

The action spectrum of the nanocrystalline TiO₂/PBT junction shows a visible response peak at ca. 500-600 nm, with a tail up to 800 nm. This is a clear indication that the electrochemically deposited and electrochemically reduced PBT, having a band gap of ca. 2 eV, is able to inject photogenerated electrons into the conduction band of TiO₂.

So, PBT is not only a promising hole conducting layer but also a sensitizer of TiO₂. This opens the possibility to build a photovoltaic devices based on flat or nanocrystalline TiO₂ layer and a carefully chosen conductive polymer, like a substituted polythiophene, acting as a hole conductor and as a sensitizer for the visible light.

References for chapter 5.

1. Y. Fang and S.-A. Chen, *Materials Chemistry and Physics*, 32 (1992) 380.
2. C. Kuo, F. Wakim, S. Sengupta and S. Tripathy, *Journal of Applied Physics*, 74 (1993) 2957.
3. G. Rikken, E. Staring and R. Demandt, *Applied Physics Letters*, 65 (1994) 219.
4. H. Antoniadis, B. Hsieh, M. Abkowitz, S. Jenekhe and M. Stolka, *Synthetic Metals*, 62 (1994) 265.
5. I. Youm, M. Cadene and D. Laplaze, *Journal de Chimie Physique*, 89 (1992) 1111.
6. D. Braun, G. Gustafsson, D. McBranch and A.J. Heeger, *Journal of Applied Physics*, 72 (1992) 564.
7. H. Nguyen Cong, C. Sene and P. Chartier, *Journal de Chimie Physique*, 89 (1992) 1073.
8. L. Torsi, C. Malitesta, F. Palmisano, L. Sabbatini and P. Zambonin; G. Scamarcio and M. Lugara, *Surface Science Letters*, 273 (1992) L409-L413.
9. T. Meyer, "Etude sur le Poly(benzo[c]thiophène Utilisé comme Contre-Electrode dans une Cellule Photovoltaïque Electrochimique" diploma thesis work (1992), Institut de Chimie Physique II, EPFL.
10. G. Horowitz, H. von Berdeleben and A. Yassar, *Synthetic Metals*, 62 (1994) 245.
11. D. Fichou, G. Horowitz, Y. Nishikitani and F. Garnier, *Synthetic Metals*, 28 (1989) C725.
12. M.A. Lampert and P. Mark in "Current Injection in Solids", Academic Press, New-York, 1970.
13. H. Tomozawa, D. Braun, S. Phillips, A.-J. Heeger and H. Kroemer, *Synthetic Metals*, 22 (1987) 63.
14. R. Sugimoto, S. Takeda, H.B. Gu and K. Yoshino, *Chemistry Express*, 11 (1986) 638.
15. S.M. Sze "Physics of Semiconductor Devices", 2nd Edition, John Wiley & Sons, New-York, 1981.
16. P. Liska, "Praktische Aspekte der Licht-Energieumwandlung am Beispiel einer TiO₂-Farbstoffzelle" Ph.D thesis work N° 1269 (1994) EPFL.

17. N. Vlachopoulos, P.Liska, J. Augustynski and M. Graetzel, *Journal of the American Chemical Society*, 110 (1988) 1216.

6. Inorganic junctions: CuI/nanocrystalline-TiO₂ cells

In several studies, sensitized p-type wide bandgap semiconductors were investigated as a photoelectrode. Care must be taken that the dye used as a sensitizer efficiently injects the holes into the valence band of the p-type material. This process is also called "cathodic sensitization". The studies of S. Poznyak et al. [1] described the sensitization of highly porous bismuth oxyhalide photoelectrodes with rhodamine and other dyes. A peak quantum efficiency (IPCE) of ca. 7 % was achieved with BiOCl as p-type semiconductor (bandgap 2.9 eV). Already in 1984, a light-to-electricity conversion efficiency of ca. 2.8 % was achieved by K. Tennakone et al. [2], sensitizing an anodically deposited copper thiocyanate (CuSCN) electrode with a monomolecular layer of "thiocyanated" methyl violet as sensitizer. The open-circuit voltage was ca. 840 mV and the short-circuit current density around 400 $\mu\text{A}/\text{cm}^2$ at a light intensity of 4 mW/cm^2 . This system seemed to be efficient, as the CuSCN p-type semiconductor (bandgap 3.2 eV) electrode readily absorbs the "thiocyanated" dyes which have a SCN⁻ counterion acting as an attaching group made by exchanging the usual Cl⁻ counterion in a boiling ethanolic KSCN solution. The importance of having the SCN⁻ as an attaching counterion was also reported in an other work of Tennakone [3] and Fernando [4]. A very high quantum efficiency above 50 % was reported by O'Regan and Schwartz [5] with a cyanine dye sensitized CuSCN electrode used in a photoelectrochemical cell having I⁻/I₃⁻ as redox couple. The use of porous copper iodide (CuI) as a photoelectrode was investigated by Tennakone et al. [6], where a chlorophyll sensitized electrode gave ca. 180 $\mu\text{A}/\text{cm}^2$.

Copper iodide is a wide bandgap p-type semiconductor with a direct bandgap of $E_g = 2.95$ eV at 300°K. At room temperature, CuI is in the γ phase with a zincblende type crystalline structure [7]. In nature, CuI occurs as the mineral *marshite* [8]. Copper iodide is a white crystalline powder obtained either by direct combination of the elements or by reacting CuSO₄ and KI in aqueous solution [9]. The schematic energetic diagram of such a device is shown in fig. 66:

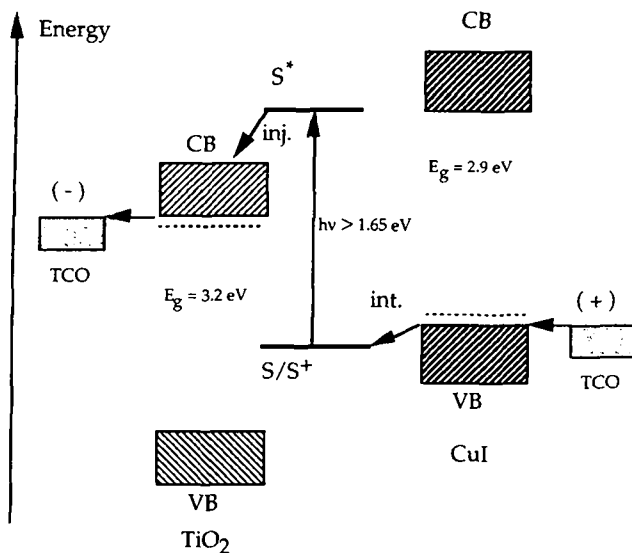


Figure 66: Schematic energy band diagram of the TiO_2 and CuI showing the relative position of the valence band (VB) edges and the conduction band (CB) edges of the TiO_2 and the CuI with respect to the energy diagram of the sensitizer $\text{RuL}_2(\text{NCS})_2$ depicted as the ground state level S/S^+ and the excited state level S^* .

Tennakone et al. [10] claimed to achieve nanostructured *solid state* junctions using nanocrystalline titanium oxide and solution cast CuI electrodes, made from a solution of 0.6 g CuI in 50 ml acetonitrile, showing photocurrents in the milliampère range when sensitized with a cyanidine dye and illuminated with 80 mW/cm^2 of sunlight. Open circuit voltages in the range of 580 mV were observed. The CuI used by Tennakone had a surface resistance of ca. $50\text{-}60 \text{ }\Omega/\text{sq}$. at a layer thickness of ca. $3 \text{ }\mu\text{m}$ [10 p. 1691], so the specific resistivity of the CuI is around $0.015 \text{ }\Omega\text{cm}$.

The idea was to deposit the optically transparent p-type semiconductor CuI into the highly porous structure of the nanocrystalline n-type TiO_2 layer, in order to form an intimate p-n junction between the two materials, this without harm to the sensitizer adsorbed on the nc- TiO_2 layer. The difficulty is to avoid the clogging of the nanometer-sized pores of the TiO_2 while depositing the CuI . Finally, the deposition process should not use either chemicals or conditions that could damage the adsorbed sensitizer (Ru-dye) molecules on the TiO_2 crystallites. This excludes deposition processes using alkaline water that desorbs the dye or temperatures above $200 \text{ }^\circ\text{C}$ that destroys the dye molecules.

6.1. Electrode preparation

In order to achieve a good rectifying TiO_2/CuI junction, it is essential to avoid the direct contact between the conductive $\text{SnO}_2:\text{F}$ layer of the glass substrate and the solution cast CuI semiconductor, since the contact between the tin oxide and CuI is ohmic. Hence, a barrier layer of compact TiO_2 must be deposited prior deposition of the highly porous nanostructured titanium oxide layer. A good way to achieve such a compact titanium oxide layer is to grow it out of an organic precursor suspended in an organic solvent: Ca. 200 μl of a 20 mM tetrabutyl orthotitanate (Fluka) solution in dry propanol (Fluka) are spread out with a glass rod on a 25 cm^2 sized and 1 mm thick $\text{SnO}_2:\text{F}$ coated conductive glass (Nippon Sheet Glass) having a surface resistance of 10 Ω/sq . After drying, the electrode is baked at 400 $^\circ\text{C}$ for 5 min. (heating and cooling rates: 100 $^\circ\text{C}/\text{min}$.) A transparent layer of titanium oxide of ca. 100 nm thickness is formed, as measured with a Tencor stylus profilometer. Then, the above described deposition and baking process is repeated 10 times till the electrical conductivity is above 20 $\text{M}\Omega$ (measured with a digital volt-ohmmeter using the 2 point method). The nanocrystalline titanium oxide aqueous solution (TM6CW, Solaronix SA, Aubonne) is deposited using the doctor blade process: on each side of the electrode, two lanes of adhesive tapes (3M Scotch Magic, ca 50 μm thick) are forming the spacer giving the thickness of the wet film of titanium oxide solution. After drying the electrode with a hair dryer, the electrode was fired at 450 $^\circ\text{C}$ for 20 min. The thickness of the fired nanocrystalline titanium oxide is ca. 10 μm as measured with a the stylus profilometer (probe tip force 11 mg). A saturated CuI (Fluka, used as received) is made by dissolving ca. 0.2 g CuI in 20 ml acetonitrile (Fluka, used as received) and stirred overnight. A slightly yellowish solution is formed, the yellow color coming from free iodine residues (CuI is photosensitive). The specific conductivity of the solution cast CuI was estimated by using the arrangement shown in fig. 67.

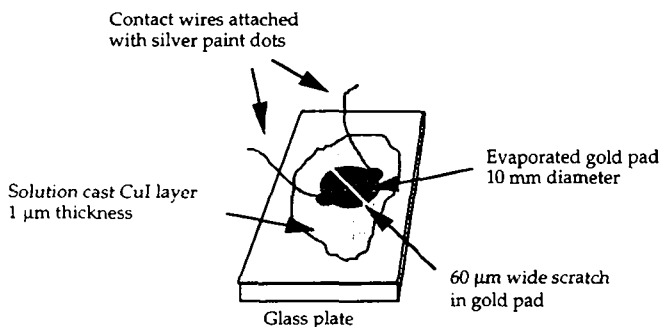


Figure 67: Schematic display of the setup used to estimate the specific resistance of the solution cast CuI layers.

Gold was chosen as contact since it was known to be an ohmic contact to the CuI [10]. Hence, by measuring the resistance of a 1 μm thick CuI film deposited by

solution casting on glass, a value for the specific conductivity of $\rho = 0.3 \Omega\text{cm}$ was found, assuming a homogenous layer thickness.

6.2. Flat compact TiO_2/CuI heterojunction

Preliminary experiments showed that a Ni coated tip was working well as ohmic contact to the CuI, too. The junction was contacted with a Ni-tip as ohmic contact on the positive, i.e. the p-CuI side. The junction area was ca. 0.7 cm^2 , but the effective junction area may be smaller since only the tip was making the electrical contact. In fig. 68, the J-V characteristics of the flat compact- TiO_2/CuI heterojunction are shown.

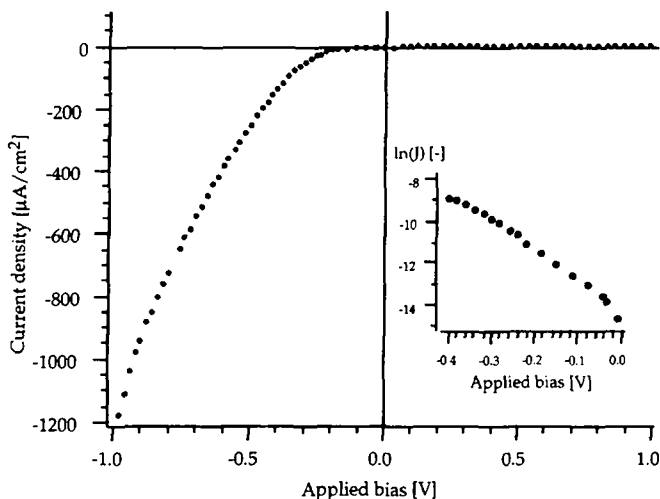


Figure 68: J-V characteristics measured in the dark of the compact- TiO_2/CuI device. The inset shows the voltage dependence of the natural logarithm of the current density in the forward bias direction, i.e. when the TiO_2 goes negative with respect to the CuI electrode.

The J-V characteristics are non-linear and asymmetric, with the current increasing rapidly when the n- $\text{TiO}_2/\text{p-CuI}$ junction is forward polarized, i.e. when the TiO_2 side goes negative with respect to the CuI side. The current density ratio at $\pm 1 \text{ V}$ is ca. 1:200. This behavior indicates that the compact- TiO_2/CuI interface acts as a current rectifier. According to the Schottky theory describing rectifying junctions [11, p. 250], the saturation current density J_s , the barrier height Φ_b , and the diode quality factor n can be estimated by linearly fitting $\ln(J)$ vs. the applied bias plot (see inset of fig. 68), where J is the current density observed in the dark when forward biasing the junction. The $\ln(J)$ -V plot was taken in the bias range between 0 and -0.4 V, where the voltage drop due to

the ohmic resistance in the junction is neglectable. In the high bias range above -0.6 V, the J-V curve is essentially an ohmic line, where the resistance is ca. 3500 Ω . The estimated saturation current density is ca. $J_s = 0.6 \mu\text{A}/\text{cm}^2$, and by using the Richardson equation [11, p. 262], the barrier height of the junction can be estimated to be $\phi_b = 0.77 \text{ V}$. The ideality factor of this diode is ca. $n = 2.7$, indicating that recombination at the junction interface is contributing to current losses. The J-V plot in chopped light is shown in fig. 69.

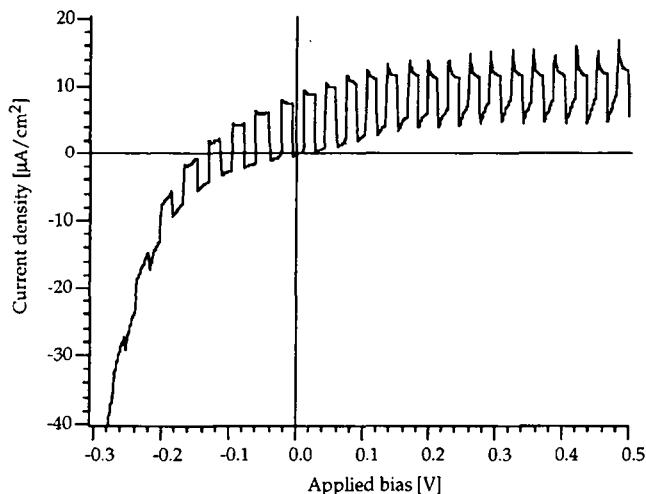


Figure 69: J-V plot of the compact-TiO₂/CuI device, done in chopped light. The voltage scan rate was 25 mV/s. The unfiltered Xe-lamp intensity was 110 mW/cm².

Clearly, a current modulation is visible throughout the whole bias range where the current is always increased when the light is on, indicating some photovoltaic effects of the junction. An open-circuit voltage of ca. $V_{oc} = 150 \text{ mV}$ and a short-circuit current density of ca. $J_{sc} = 8 \mu\text{A}/\text{cm}^2$ is observed. At potential conditions above the open-circuit voltage, i.e. at biases going from -0.15 to + 1.0 V, always a transient in current is observed when the light is cut-off, indicating a slow charge conduction occurring in the TiO₂/CuI flat junction. The observed photocurrent are due to the intrinsic UV absorption of the TiO₂ ($E_g = 3.2 \text{ eV}$) and the CuI ($E_g = 2.95 \text{ eV}$), thus generating electron-hole pairs that are separated by the built-in electrical field.

The Mott-Schottky plots of the flat, compact n-TiO₂/p-CuI hetero-junction were measured with an AC signal at frequency of 1051 Hz (fig. 70) and at 9462 Hz (fig. 71). Both plots were obtained with a sine-shaped AC ripple of 10 mV.

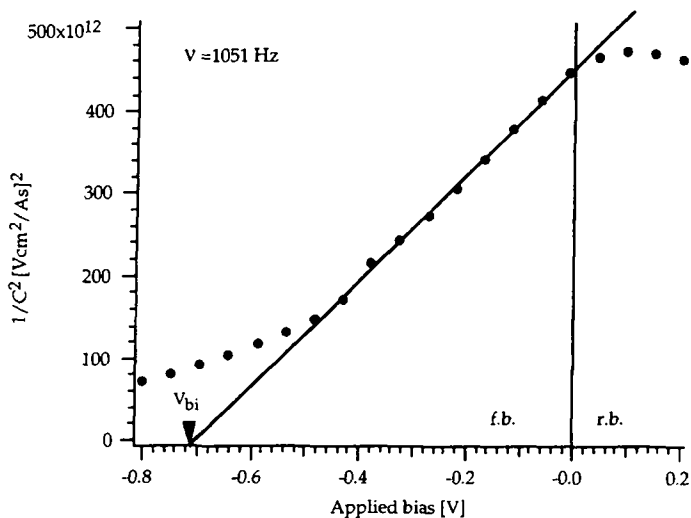


Figure 70: Mott-Schottky plot of the compact-TiO₂/CuI diode, measured at an AC signal frequency of 1051 Hz; f.b. stands for forward bias, i.e. the n-TiO₂ was negative in voltage and r.b. is for the reverse bias where the n-TiO₂ was positive with respect to the p-CuI side.

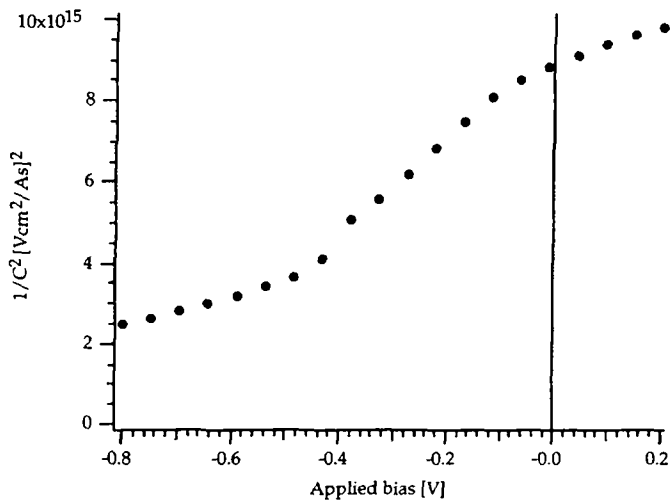


Figure 71: Mott-Schottky plot of the compact-TiO₂/CuI diode, obtained at an AC signal frequency of 9462 Hz.

From the Mott-Schottky plots in fig. 70 and fig. 71, apparently a potential dependent capacitance develops at the AC signal frequency of 1051 Hz and 9462 Hz respectively. This indicates a space charge layer that is formed at the interface of the p-CuI in contact with the n-TiO₂ (see chapter 1). A doping density of $N_A = 2(\text{slope})/q\epsilon = 3.5 \times 10^{19} \text{ cm}^{-3}$ can be estimated from the positive slope ($= 6.4 \times 10^{14}$) of the Mott-Schottky plot made at 1051 Hz (fig. 70), assuming a dielectric constant of ca. $\epsilon = 4.3 \times 10^{-13} \text{ As/Vcm}$ for CuI [7, p. 253]. The intercept of the straight line with the bias axis, indicates an apparent built-in voltage of $V_{bi} = 0.7 \text{ V}$. The same calculation as above with the positive slope ($= 1 \times 10^{16}$) found in the plot made at 9462 Hz (fig. 71), gives a donor density of $N_A = 5 \times 10^{20} \text{ cm}^{-3}$ and the built-in voltage is 0.8 V. These doping levels in the $10^{19} - 10^{20} \text{ cm}^{-3}$ range have to be compared with the atom concentration in the CuI, which can be calculated knowing that CuI crystallizes in the zincblende structure with 8 atoms per cell, a lattice parameter of 0.604 nm, hence a total atom density of $1.76 \times 10^{21} \text{ cm}^{-3}$ is found. This yields doping levels between 1 and 10 % in the CuI according to the Mott-Schottky plots. A large frequency variation of the junction capacitance was observed with the SnO₂/TiO₂/CuI/Ni system, indicating that more or less deep traps are acting in the charge storage in the junction, as the AC frequency is changed. A low frequency signal would charge and discharge deeper traps than a high frequency signal, as a charge carrier needs more time to be detrapped from a deep trap.

Again, a word of caution to the interpretation of the Mott-Schottky plot results must be said, as the junctions formed between the nickel tip and the CuI and the one formed between the TiO₂ and the ITO are probably also contributing to the frequency dependence of the overall capacitance of the ITO/TiO₂/CuI/Ni device.

6.3. Nanocrystalline sensitized TiO₂/CuI junction

The current density-voltage characteristics of the non-sensitized colloidal nc-TiO₂/CuI junction was obtained by scanning the potential from -4 V to +4V at 20 mV/s scan rate and recording the current in the dark. Voltages going negative is the forward bias direction, i.e. where the TiO₂ goes negative with respect to the CuI electrode. The device had a compact TiO₂ layer, deposited by solution casting tetrabutyl orthotitanate dissolved in propanol, as blocking layer to avoid short-circuits through the porous TiO₂ film, between CuI and the SnO₂ coated support glass. The positive contact was a Ni tip acting as contact to the CuI layer. During the build-up of the device, the rim around the device was scratched away to remove all excess CuI contacting the SnO₂ glass. The sensitizer used was RuL₂(NCS)₂, which was adsorbed onto the nc-TiO₂ electrode from a $3 \times 10^{-4} \text{ M}$ ethanolic solution during 24 hours, prior being impregnated with the solution cast CuI.

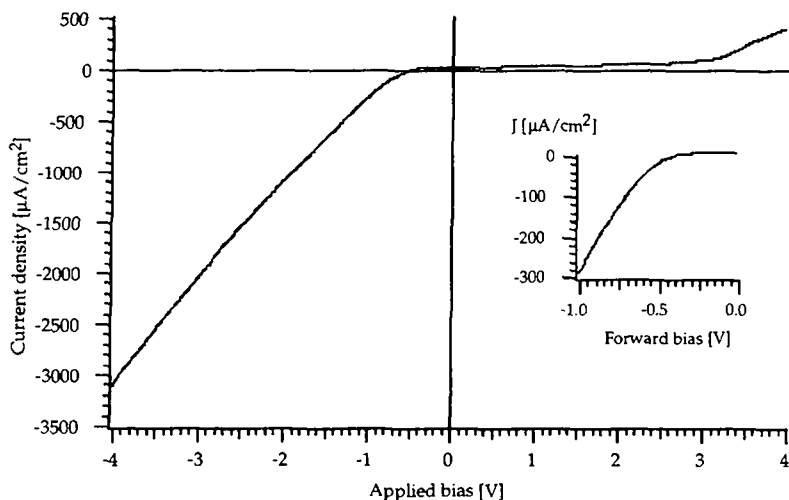


Figure 72: J-V plot of the sensitized nc-TiO₂/CuI junction made in the dark; the inset shows the forward bias behavior in the voltage range between 0 and -1 V, where the J-V plot is behaving exponentially.

From the slope of the J-V plot for biases above -1V, an apparent device serial resistance can be estimated to be ca. 1000 Ω, when taking the voltage-current ratio between -3 and -4 V. The electrical properties of the nc-TiO₂/CuI junction can be described by the diode equation, linking the junction current density J to the applied bias V , assuming that this junction behaves as a Schottky junction with the CuI as rectifying "metal" contact. This can be assumed as CuI is highly doped, as calculated from the Mott-Schottky plots and since its resistivity is around 0.3 Ωcm. Similar to the calculations made above, the saturation current density J_s , the diode quality factor n , and the barrier height ϕ_b can be deduced from the forward bias branch of the $\ln(J)$ -V plot of the nc-TiO₂/CuI diode. The $\ln(J)$ vs. V plot in fig. 73 was taken in the forward polarization region between -100 and -700 mV where the plot is approximately linear.

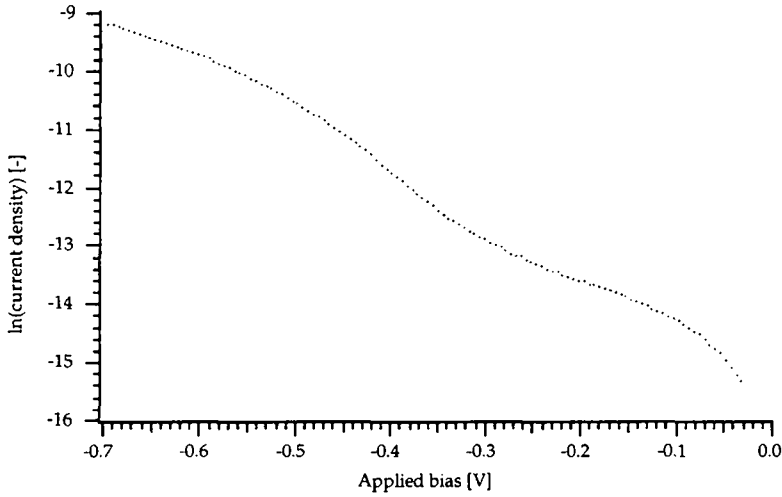


Figure 73: Forward bias branch of the $\ln(J)$ -V plot of the nc-TiO₂/CuI junction.

From the slope (-9.29) and the intercept (-15.42) of the $\ln(J)$ -V plot in fig. 73, a saturation current density $J_S = 0.2 \mu\text{A}/\text{cm}^2$ and a diode quality factor of $n = 4.2$ was estimated. The high diode quality factor is due to junction imperfections acting as recombination centers either at the nc-TiO₂/CuI interface or in the bulk of the semiconductors.

Using the Richardson equation [11 p. 256]

$$J_S = A_R T^2 \exp\left(\frac{-q\phi_b}{kT}\right) \quad (15)$$

where A_R is the effective Richardson constant ($120 \text{ A}/\text{K}^2 \text{ cm}^2$ for free electrons), q is the electrical charge and ϕ_b is the barrier height, the saturation current density J_S was calculated. Using $J_S = 2 \times 10^{-7} \text{ A}/\text{cm}^2$, and $T = 295 \text{ °K}$, the barrier height can be calculated, and $\phi_b = 0.81 \text{ eV}$ was found. This barrier height value is consistent with the estimated built-in voltage values of 0.7 - 0.8 V deduced from the Mott-Schottky plots (see fig. 70 and fig. 71).

The I-V characteristics in fig. 74 were measured at a light intensity of 93 mW/cm² ($\approx 1 \text{ sun}$). The irradiation is always made on the front side, i.e. the side of the titanium oxide layer (negative electrode).

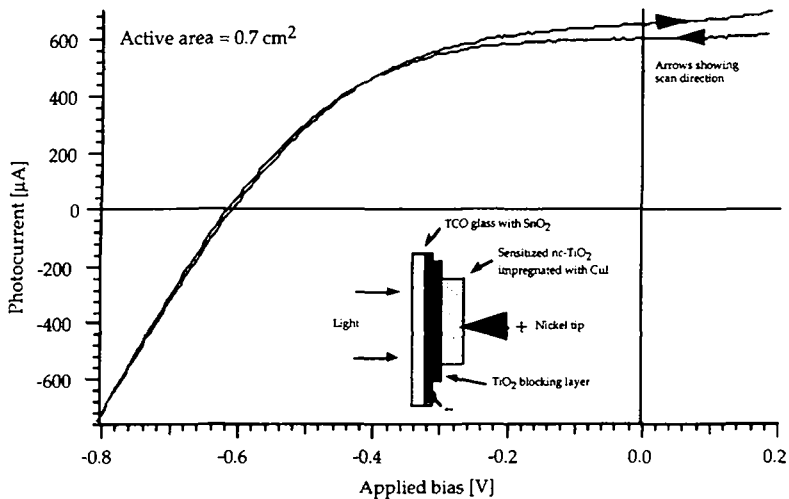


Figure 74: I-V plot of the sensitized nc-TiO₂/CuI diode at an irradiation of 93 mW/cm² from a UV-filtered Xe-lamp. The junction area was 0.7 cm². The inset shows the schema of the device used, the arrow on the I-V plot indicate the voltage scanning directions.

The I-V plot in fig. 74. shows a short circuit current of $I_{sc} = 650 \mu\text{A}$ for a surface of 0.7 cm², i.e. a short-circuit current density of $J_{sc} = 930 \mu\text{A}/\text{cm}^2$, an open-circuit voltage of $V_{oc} = 600 \text{ mV}$, and a fill-factor of ca. $\text{FF} = 0.5$. The maximal light-to-electricity conversion efficiency was ca. $\eta = 0.3 \%$. The I-V characteristics in fig. 75, were measured at 9.3 W/cm² using the same lamp and a 1:10 attenuation filter made of thin metal mesh. A short-circuit current of $I_{sc} = 75 \mu\text{A}$, giving a short-circuit density of $J_s = 107 \mu\text{A}/\text{cm}^2$ and an open-circuit voltage of $V_{oc} = 510 \text{ mV}$ was observed.

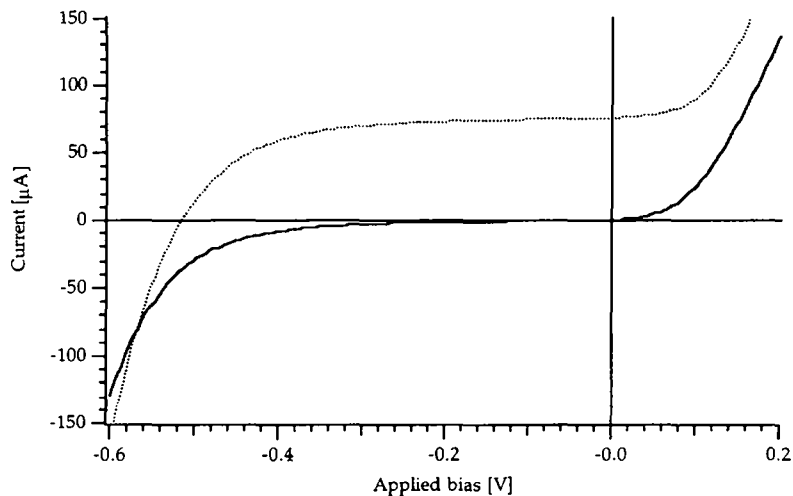


Figure 75: I-V plot of a sensitized nc-TiO₂/CuI diode, measured in the dark (solid line) and in 9.3 mW/cm² of simulated sun (dotted line). The active area of the device was 0.7 cm².

The dark current in fig. 75 shows a high reverse bias current. It seems that the nanocrystalline CuI/TiO₂ junction has a soft reverse breakdown, in contrast with the flat compact-TiO₂/CuI junction showing no signs of reverse breakdown at reverse biases up to 1 V, as depicted in the dark current plot in fig. 68. The photocurrent plot made at only 9.3 mW/cm² light intensity in fig. 75 shows a better fill factor of FF = 0.66 than that made at full light of 93 mW/cm² shown in fig. 74 where FF = 0.5. The same holds for the overall light-to-electricity conversion efficiency, which is $\eta = 0.4\%$ at 9.3 mW/cm² compared with $\eta = 0.3\%$ at 93 mW/cm² light intensity. These better low-light performances are due to the junction resistance which is introducing ohmic losses diminishing the photocurrent at full light.

The $\ln(J)$ -V plot in fig. 76 was taken in the forward polarization region between 100 and 600 mV where the plot is linear, and it allowed to estimate the saturation current density J_s , the diode quality factor n , and the barrier height ϕ_b , using the Schottky and Richardson equation already mentioned above.

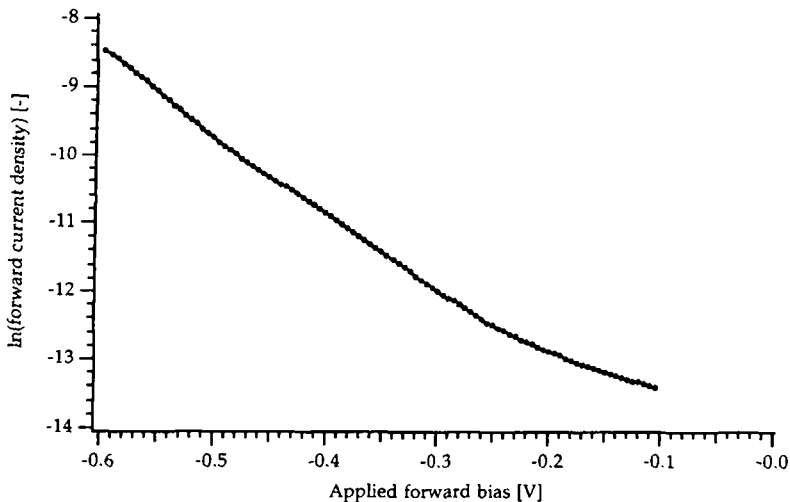


Figure 76: $\ln(J)$ - V plot obtained with a sensitized nc-TiO₂/CuI device in the forward bias branch.

From the slope (-10.33 and the intercept (-14.92) of the $\ln(J)$ - V plot in fig. 76, a saturation current density $J_s = 0.33 \mu\text{A}/\text{cm}^2$, and a diode quality factor of $n = 3.8$ was estimated. Using the Richardson expression (eq. 15, chapter 1) and using $J_s = 3.3 \times 10^{-7} \text{ A}/\text{cm}^2$ and $T = 295^\circ\text{K}$, the barrier height can be calculated, and $\phi_b = 0.78 \text{ eV}$ was found. This value is similar to the one found above.

The design of the used cell is not optimal, since the positive electrode was a nickel plated tip directly contacting the CuI crystallites on top of the nanocrystalline titanium oxide electrode. In this arrangement, the photogenerated holes have to travel up to ca. 4 μm in the nanocrystalline TiO₂/CuI material, until they are picked-up by the nickel contact. Although the device is a majority carrier device, i.e. the p-CuI will only carry holes generated by the light absorption occurring in the sensitizing Ru-dye, recombination with conduction band electrons from the titanium oxide cannot be excluded, as both materials should be in intimate contact making up the "nanocrystalline" nature of the junction.

The action spectrum was obtained by plotting the short-circuit photocurrent at different wavelengths going from 300 to 800 nm in 10 nm steps. The Oriel monochromator used had 2 mm wide entry and exit slits. For all wavelengths above 600 nm, a 435 nm cut-off filter was placed in the exit beam to avoid the superposition of the second-order diffracted light from the monochromator. The relative light intensity loss due to the 435 nm filter was compensated by increasing the lamp intensity so that the photo currents (at 600 nm) with and without filter were the same. Fig. 77 shows the IPCE action spectrum of the sensitized nc-TiO₂/CuI junction.

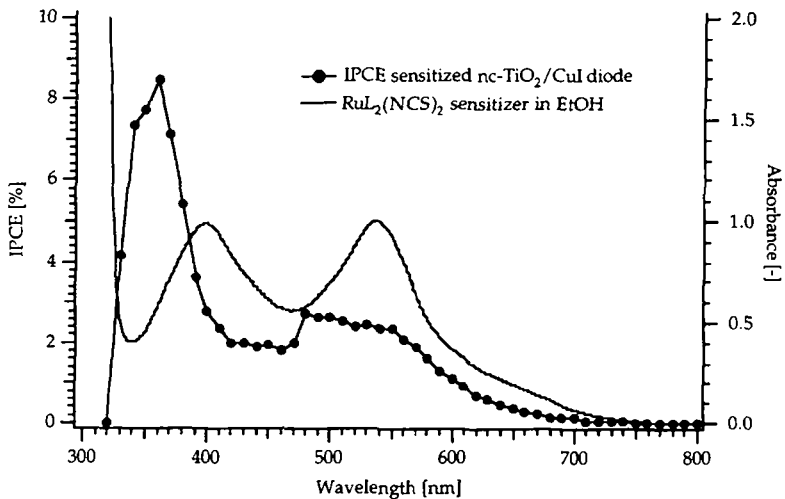


Figure 77: IPCE action spectrum of the sensitized nc-TiO₂/CuI junction (black dots) and the absorbance spectrum of RuL₂(NCS)₂ in ethanolic solution.

The IPCE action spectrum of the sensitized nc-TiO₂/CuI junction shows a domain where IPCE > 4 % in the wavelength range from 330 to 400 nm, and a low efficiency domain for all wavelengths above 400 nm. The peak efficiency is reached at 370 nm, given by the optimum between the combined bandgap excitation of the anatase ($E_g = 3.2$ eV, indirect) together with the excitation of the CuI ($E_g = 2.9$ eV, direct), and the absorption of the SnO₂ coated glass, which blocks the incoming light under 350 nm. Hence, in the domain from 330 to 400 nm, the photocurrent is produced by the intrinsic light absorption of the semiconducting junction materials. An IPCE in the 8 % range shows that the contact between the TiO₂ nanocrystals and the crystalline CuI is far from perfect, as only one tenth of the electrons generated from the absorbed UV-photons are collected. The photocurrent onset is following the absorption tail of the sensitizer situated at ca. 750 nm. The < 4 % IPCE domain is overlapping with the visible light domain, where the sensitizer absorbs and produces most of the current. The fact that the IPCE is lower in this region than in the UV part shows that there is a loss mechanism in the electron flow of the device, as the hole is not properly carried away by CuI from the oxidized dye molecule. This is not surprising, since the used sensitizer RuL₂(NCS)₂ has no attaching groups helping for the hole injection into the valence band of CuI. The low IPCE values achieved over the whole spectrum are reflected in the low short-circuit currents of ca. 1 mA/cm² obtained at full sun (see fig. 74) with this TiO₂/CuI heterojunction. This is to compare with the 15-18 mA/cm² obtained with the liquid electrolyte based dye solar cells having an efficiency of ca. 8-9 % in full sun and an IPCE close to 100 % [13].

The photocurrent transient experiments were performed by mechanically chopping the 93 mW/cm^2 intense Xe-lamp light and monitoring the short-circuit current. The shutter took ca. 10 ms to switch on and off the light, hence the time resolution of these experiments was in the 10 ms range. Figure 78 shows the on and off transient made with the same nc-TiO₂/CuI device as used above.

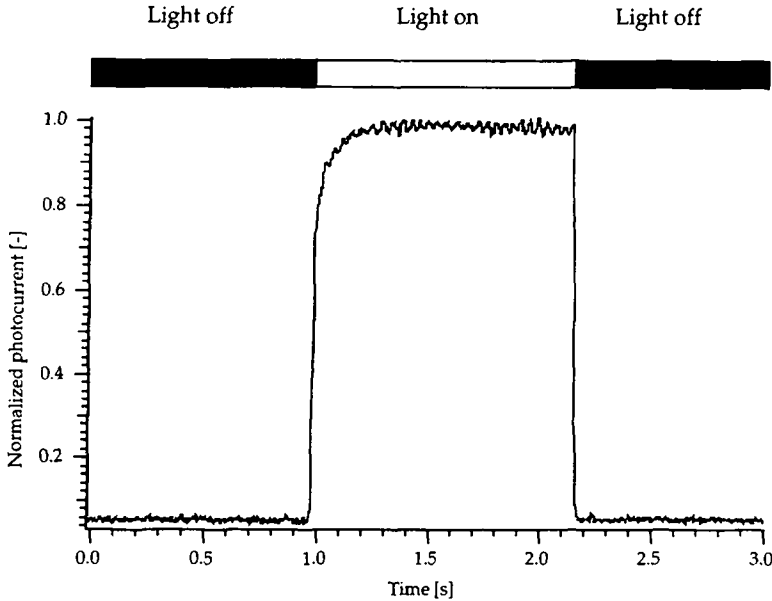


Figure 78: Photocurrent transients of a sensitized nc-TiO₂/CuI junction, measured by chopping the filtered Xe-light having an intensity of 93 mW/cm^2 .

The current transient plot shows an initial steep rise of the photocurrent. Then, it takes ca. 300 ms to reach the maximal value when the light is switched on. The initial photocurrent drop is rather quick (not resolved in this time scale). Such a transient behavior was reported by F. Willig et al. [12], using a liquid/nc-TiO₂ junction. This slow response was explained by the trapping of the majority carriers (electrons for n-TiO₂, holes for p-CuI) in the bulk of the semiconductors which led to a slow current response.

The effect on the transient behavior of the collector tip position was investigated by recording the transients with the contact tip centered in the middle of the irradiation zone and with the tip completely out of the irradiated zone, having a spot diameter of 5 mm. In the former case, the holes have to travel at a distance of up to 2-3 mm, and in the latter case, the travel distance increased up to 10-14 mm. In both cases, the photogenerated electrons travel only over the maximal distance given by the thickness of the nc-TiO₂ electrode, i.e. not more than 10 μm . In fig. 79 the schemes of the two contact tip arrangements are shown.

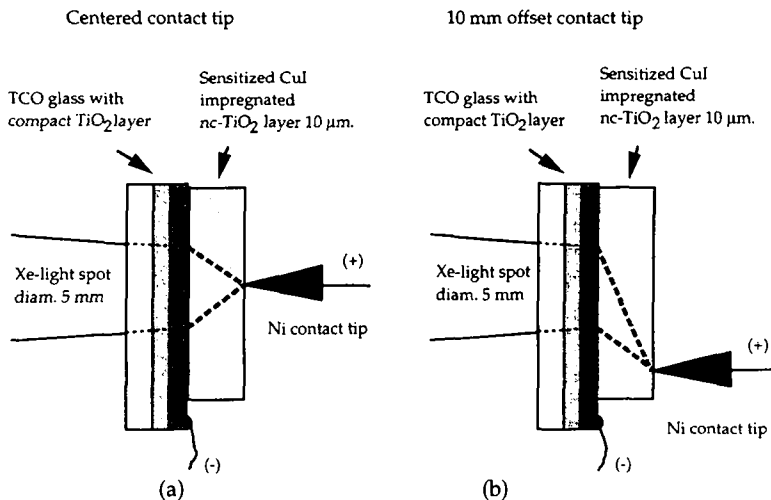


Figure 79: Schematic nc-TiO₂/CuI device setup showing the nickel coated tip position in the centered (a) and offset (b) fashion. The offset is ca. 10 mm, and the lit spot is 5 mm in diameter. The light intensity was ca. 40 mW/cm². The thick dotted lines indicate for both contact tip positions the maximal travel distance of the holes in the CuI impregnated nanoporous TiO₂ electrode.

The registered photo current transients for both contact tip positions are given in fig. 80.

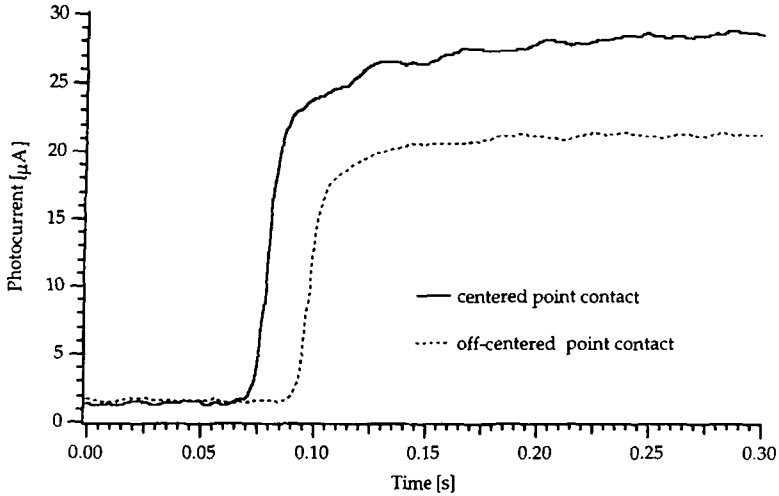


Figure 80: Photocurrent transients of a sensitized nc-TiO₂/CuI junction made by chopping the filtered Xe-light having an intensity of 93 mW/cm².

The wavelike fluctuations in the transient responses are due to minor variations of the unregulated Xe-lamp. Both transient curves show a similar behavior in time response, but the short-circuit photocurrent is ca. 25 % lower in the case where the Ni contact tip is off-center by about 10 mm, respective to the light spot having a diameter of 5 mm. The lower short-circuit current is probably due to the additional ohmic loss in the longer current path in the TiO₂/CuI layer.

The stability of the sensitized nc-TiO₂/CuI junction was checked by irradiating the device with a Xe-lamp equipped with a Schott 113 filter. The light intensity was ca. 97 mW/cm², and the sample temperature rose to ca 30 °C during irradiation. Fig. 81 shows the short-circuit current density during 3000 s of irradiation. The device was exposed to ambient air.

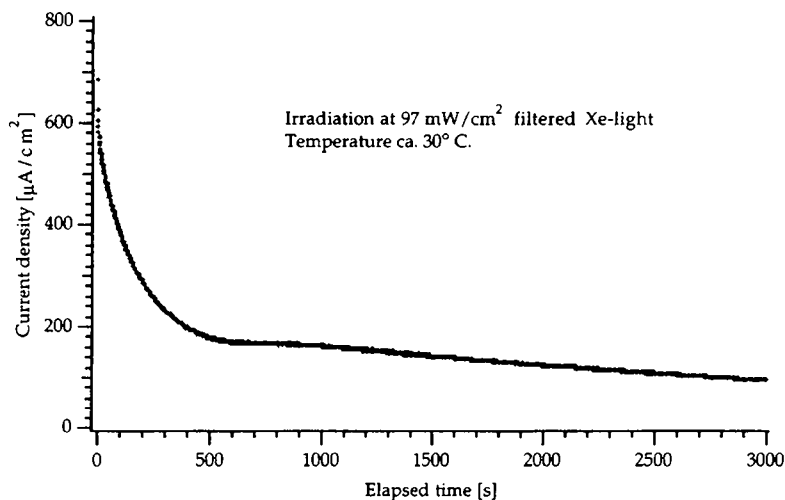


Figure 81: Short-term stability of the short-circuit current of the sensitized nc-TiO₂/CuI device under 97 mW/cm^2 irradiation from a filtered Xe-lamp; the sample temperature was ca. 30°C .

There is sharp exponentially-looking decrease in current, starting at ca. $700 \mu\text{A/cm}^2$, followed by a plateau at around $180 \mu\text{A/cm}^2$, followed by a slower and regular current diminution. Apparently, most of the degradation happens in the first few minutes of light exposure. The test continued at the same light intensity for a total of 2 hours. After that, a J-V plot of the device in the "degraded" state was taken, as shown in fig. 82.

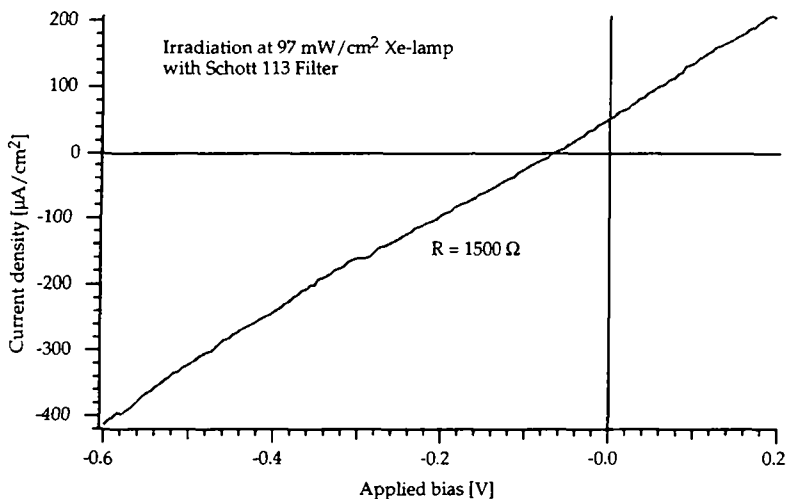


Figure 82: J-V plot of the same nc-TiO₂/CuI device as used for the J-V plot in fig. 81, after a total of 3 hours irradiation at 97 mW/cm² of filtered Xe-light.

Obviously, some major changes in the J-V characteristics have occurred during the 2 hours of intense irradiation. First, the open circuit voltage dropped to 60 mV, and the short-circuit current was reduced to a value of ca. 40 µA/cm². The fill-factor dropped from 0.5 in fig. 74 to ca. 0.2. The device showed an overall resistance of ca. 1500 Ω as given by the slope of the J-V curve of the fig. 82. It seems that something degraded in the device while forming a electrical conductor that shunts the junction with a resistance of only 1500 Ω. This shunt seriously degraded the electrical performances. A possible explanation of the phenomenon is the partial photodissociation of CuI, leading to a higher doping level, hence increase in conductivity. CuI is known to be photosensitive [8]. This is a sign that maybe CuI is not ideal as a stable p-type transparent semiconductor to be used as hole conductor replacing the electrolyte in the dye solar cell.

6.4 Conclusion

The use of a transparent mineral wide bandgap p-type semiconductor, copper iodide (CuI), acting as hole conducting layer, was demonstrated in a flat TiO₂/CuI device and in a Ru-complex sensitized nanocrystalline junction made of highly porous TiO₂ impregnated with solution-cast CuI. The flat TiO₂/CuI junction showed a rectification ration of 1:200 at a bias of +/- 1 V, indicating that this junction is a true diode. A photocurrent of ca. 10 µA/cm² and a open-circuit voltage of 150 mV was observed when such a flat optically transparent TiO₂/CuI junction was illuminated with UV light. A nanocrystalline Ru-complex sensitized TiO₂/CuI junction showed a short-circuit current of 1 mA/cm², a

open-circuit voltage of 600 mV and a light-to-power conversion efficiency of 0.3 % at 100 mW/cm² of simulated sun light with a UV filter cutting below 365 nm. The stability of the Ru-complex sensitized devices in ambient atmosphere and room temperature was rather poor, as the photocurrent sharply dropped to a 1/4 of the initial value after only 10 minutes of irradiation.

These values are below the ones obtained by Tennakone *et. al.* [10] where photocurrents of ca. 2-3 mA/cm² at 80 mW/cm² irradiation and a stability over several hours, although under inert atmosphere, are reported using a cyanidine sensitized nanocrystalline TiO₂/CuI photocell.

The action spectrum of the Ru-complex sensitized nanocrystalline TiO₂/CuI device showed a peak quantum efficiency of 8 % in the UV, and 3 % in the visible light, this indicates that the nanocrystalline junction is not working efficiently.

There are three reasons for the improper working of the Ru-complex sensitized nanocrystalline TiO₂/CuI junctions: First a point-contact geometry of the ohmic nickel contact was chosen for practical reasons, but this way of contacting the active junction materials uses only a fraction of the totally available junction area. Second, the contact between the TiO₂ nanocrystallites and the CuI crystals is far from perfect as there is no lattice matching between the two junction materials. Moreover, the CuI is solution-cast, thus pores and cracks are created by the evaporating solvent, these defects are reducing the active contact area of the two materials in the device. Finally, the Ru-sensitizer, *cis*-bis(isothiocyanato)bis(2,2'-bipyridyl-4,4'-dicarboxylato)-ruthenium(II), was not tuned to inject holes into the valence band of CuI, meaning that there is no strong coupling of the Ru-complex (in its oxidized form) and the orbitals forming the valence band of CuI, in contrast to the good electronic coupling between the Ru-dye and the orbitals forming the conduction band of the TiO₂. This optimal interplay between the sensitizer and the TiO₂ electrode is rendered possible by the specially designed attaching carboxy moieties of the Ru-dye and it allows quantitative photoelectron injection. A similar attaching group, which is electronically linking the sensitizer with the hole conductor, must be made available, unless the quantum efficiency, and the electrical performances of the sensitized TiO₂/CuI photocell will be still poor, even if the other two sources of losses mentioned are reduced to the minimum. Probably the cyanidine dye used by Tennakone *et. al.* has a better electronic coupling with the CuI than the Ru-complexes used in this work, this could explain the better performances obtained with their sensitized nanocrystalline TiO₂/CuI junctions.

References for chapter 6.

1. S. Poznyak and A. Kulak, *Electrochimica Acta*, 35 (1990) 1941.
2. K. Tennakone, M. Kahanda, C. Kasige and P. Abeysooriya; R. Wijayanayaka and P. Kaviratna, *Journal of the Electrochemical Society*, 131 (1984) 1574.
3. K. Tennakone, C. Fernando, and M. Dewasurendra, *Journal of Photochemistry*, 38 (1987) 75.
4. C. Fernando, A. Kitagawa, M. Suzuki, K. Takahashi and T. Komura, *Solar Energy Materials and Solar Cells*, 33 (1994) 301.
5. B. O'Regan and D. Schwartz, *Chemistry Materials*, 7 (1995) 1349.
6. K. Tennakone, A. Kumarasinghe, P. Sirimanne and G. Kumara, *Journal of Photochemistry and Photobiology A: Chemistry*, 91 (1995) 59.
7. O. Magdelung, *Landolt-Börnstein*, New Series III/22a "Cuprous iodide (g-CuI)", Springer-Verlag, Berlin, 1987, pp. 250.
8. The Merck Index, 9th Edition, Merck & Sons, Rahway New-Jersey USA, (1982), pp 2658.
9. R.J. Meyer, *Gmelin*, Kupfer, Teil B, Lieferung 1, "Kupfer und Jod" (60), 8th Edition, Verlag Chemie GmbH, Weinheim/Bergstrasse, Germany, 1958, pp. 389.
10. K. Tennakone, G. Kumara, A. Kumarasinghe, K. Wijyantha and P. Sirimanne, *Semiconductor Science and Technology*, 10 (1995) 1689.
11. S.M. Sze in "Physics of Semiconductor Devices", 2nd Edition, John Wiley & Sons, New-York, 1981.
12. F. Willig, R. Kietzmann and K. Schwarzburg, *Proceedings of the Ninth International Conference on Photochemical Conversion and Storage of Solar Energy*; IPS-9, August 23-28, 1992 Beijing China; International Academic Publishers: Beijing China, 1992; pp. 129-139.
13. M.K. Nazeeruddin, A. Kay, I. Rodicio, R. Humphry-Baker, E. Müller, P.Liska, N. Vlachopoulos and M. Graetzel, *Journal of the American Chemical Society*, 115 (1993) 6382.

7. Conclusion and outlook

This work showed that a solid state sensitized TiO₂ based photovoltaic cell is possible, either by using a high work-function metal like silver or gold, which are forming a rectifying contact with the TiO₂, or a electrochemically deposited conductive polymer, poly(bithiophene), in its reduced semiconducting form,, which was acting as a hole conducting layer and as a visible light sensitizer for flat and nanocrystalline TiO₂, or with a mineral wide band-gap p-type semiconductor like copper iodide, CuI, acting as a hole conducting layer.

The silver or gold contacted nanocrystalline TiO₂ photoelectrodes, which were sensitized with different dyes showed photocurrents in the 70-80 $\mu\text{A}/\text{cm}^2$ range and photovoltages of 500 mV, when irradiated with 100 mW/cm² of simulated sunlight with a UV filter cutting below 380 nm, thus avoiding the direct TiO₂ excitation adding about 50 to 100 $\mu\text{A}/\text{cm}^2$ of short-circuit current as experimentally shown with non-sensitized TiO₂/Ag diodes.

With reduced polybithiophene as sensitizer and hole conductor, short-circuit currents densities of up to 2.5 mA/cm² and open-circuit voltages of ca. 350 mV were achieved using a flat TiO₂/PBT/Au device.

Photocurrent densities of 1 mA/cm² and a overall light to current efficiency of 0.3 % were achieved in full sun irradiation with a Ru-complex sensitized nanocrystalline TiO₂ electrode impregnated with CuI.

There is a major problem when the liquid electrolyte is replaced by a solid: The liquid-solid interface is practically perfect as every atom or molecule on the surface of the solid is in intimate contact with the surrounding liquid.

Even if the solid has a fractal or highly porous surface, the liquid will enter in every pore as the capillary forces are increasing with the pore size reduction. The liquid covering the maximal surface enables an optimal electron transfer between the solid (or molecules adsorbed on the solid) and the liquid phase. This situation is actually encountered in the liquid operated dye solar cell, as the iodide redox species will reduce again the oxidized dye molecules in order to close the electrical circuit (this process is called "interception"). A poor contact between the attached dye molecules and the solvated iodide would lead to a rapid degradation of the cell performance as the dye molecules would be dissociated when allowed to stay too long in the oxidized state.

Now, the solid, replacing the liquid phase, should be deposited in a way that allows the same perfect electrical contact between the n-type semiconductor with its attached sensitizer molecules. Obviously deposition processes like sputtering or vacuum evaporation will rapidly clog the pores, and the material will be

mainly deposited on top of the nanocrystalline "sponge". Hence poor electrical contact with the surfaces underneath. With processes like the chemical bath or chemical vapor deposition, where the precursors enters in all the pores, the problem of pore clogging remains, since there is no real control over the reaction rates at a given area. Maybe, a chemical or electrochemical deposition process where the reaction rate is controlled by e.g. the pore size or surface curvature could solve some of the pore clogging.

The ideal case would be the use of an ordered "nanocrystalline" (n-type) semiconductor, where all the surface atoms can be "seen" when looked-at from the top:

Most pores are hidden

All surface is accessible



(a)



(b)

Figure 83: Schematic cross-section of a highly porous electrode, case (a) shows the situation with hidden pores, whereas in case (b) all the internal surface is accessible without any "bottlenecks".

In the case shown in fig. 83 (a) most of the surface is inaccessible and the pores could be easily clogged when a solid grows out of a solution or a vapor phase. But in the situation of fig. 83 (b), the solid would grow by matching on all the surface exposed to the deposition media. Such a ordered "nanocrystalline" p-n junction based device would look as depicted in fig. 84.

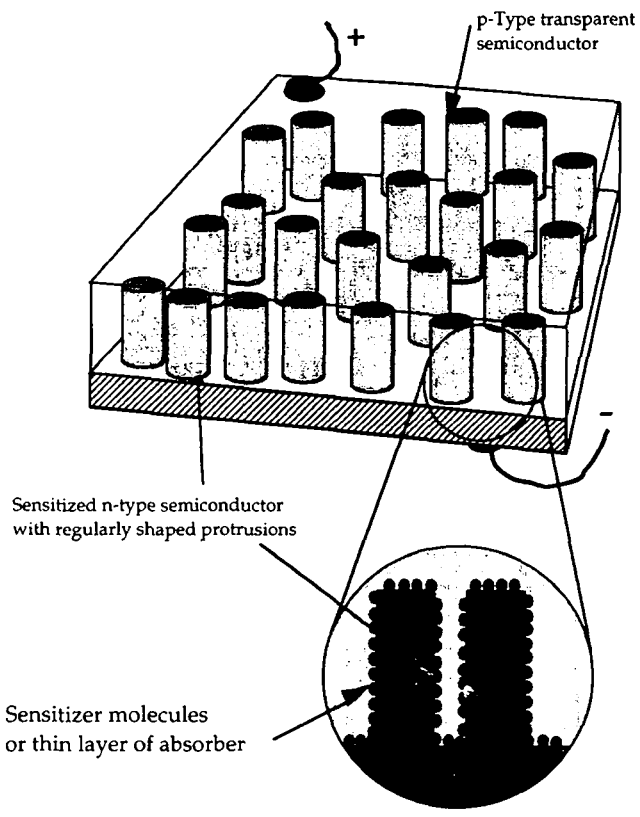


Figure 84: Schematic view of a “nano-ordered” highly and “selectively” porous semiconductor electrode. The inset shows the sensitizer molecules or absorber clusters (represented as black dots) being attached to the surface.

Such a nano-ordered semiconductor electrode could be made by using template techniques [1-3]. A high-temperature resistant polymer disk, rendered porous by nuclear fission products bombardment [1], will act as a template in which, for example, the TiO_2 is deposited using the solution-cast technique (see chapter 6). This technique allows the filling of the 10-50 nm wide and 2 to 10 μm deep pores made in the polymer template. Firing the polymer- TiO_2 compound at 450 $^\circ\text{C}$ will sinter the titanium oxide, and with an appropriate etching process, or thermal decomposition, the pure nano-ordered TiO_2 would be released from the template. A similar procedure can be made by using anodically grown Al_2O_3 as a template which also has very narrowly distributed pores like the porous filter membranes made by Alltech Associates, Inc. [2].

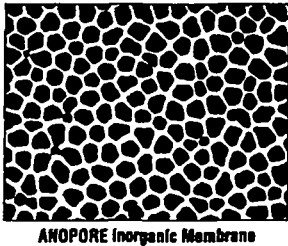


Figure 85: SEM micrograph of a controlled capillary pore inorganic membrane surface (taken from [2]).

In this case, the etching process must be chosen so that only the aluminium oxide will be removed without destroying the probably very fragile nano-ordered TiO_2 semiconductor electrode.

Such a nano-ordered electrodes' inner surface is much easier to completely contact, e.g. with a solution-cast hole transporting agent replacing the electrolyte used in the dye solar cell. This would allow to make a "nanocrystalline" junction where the interface between the two junction materials is controlled and neat. Only a exact mastering of the p-n interface within the "nanocrystalline" device will lead to reproducible and performant devices, similar to the liquid based dye solar cells.

References for chapter 7.

1. R. Fleischer, P. Price, R. Walker in "Nuclear Tracks in Solids", Univ. of California Press, Berkeley, CA, 1975.
2. "ANOTEC® Inorganic Membrane Technology", Bulletin N° 171, Alltech Associates, Inc., Deerfield, IL, 1989.
3. C. R. Martin, *Science*, 266 (1994) 1961.

List of symbols

Symbol	Description	Unit
a	Absorption	%
$\alpha(\lambda)$	Absorption coefficient	cm^{-1}
AC	Alternating current	
AM1.5	Normalized solar spectral irradiation: 84.4	mW/cm^2
A_R	Effective Richardson constant: 120	$\text{Acm}^{-2}/\text{K}^{-2}$
bipy	2,2'-bipyridine	
BOS	Balance of system	
c	Charge concentration	cm^{-3}
χ	Semiconductor electron affinity	eV
C.E.	Counter-electrode	
CB	Conductance band	-
D	Diffusion coefficient	cm^2/s
DC	Direct current	
D_n	Electron diffusion coefficient	cm^2/s
D_p	Hole diffusion coefficient	cm^2/s
DSC	Dye solar cell, also sometimes called "Graetzel" solar cell	
E	Electrical field	V/m
E	Energy	eV
ϵ	Extinction coefficient	$\text{M}^{-1} \text{cm}^{-2}$
ϵ	Dielectric constant of the material ($=\epsilon_0\epsilon$)	As/Vcm

E_a	Activation energy	eV
E_c	Conduction band lower edge energy	eV
E_f	Fermi-level energy	eV
E_g	Bandgap energy	eV
ϵ_0	Dielectric constant in vacuum: 8.854×10^{-14}	As/Vcm
E_v	Valence band upper edge energy	eV
ϕ_B	Barrier height	eV
FF	Fill-factor	-
ϕ_p	Potential energy barrier	eV
ϕ_{phot}	photon flux	$\text{cm}^{-2} \text{s}^{-1}$
η	Light-to-power conversion efficiency	%
h	Plank's constant: 6.626×10^{-34}	Js
η_A	Absorption efficiency	-
HCL	Hole conducting layer	
η_{coll}	Collection efficiency	-
η_{inj}	Quantum yield of charge injection	-
η_{sep}	Charge separation efficiency	-
I	Current	μA , mA
IPCE	Incident photon to current conversion efficiency	%
IR	Wavelengths above 800 nm	
I_{sc}	Short-circuit current	mA
ITO	Indium tin oxide (90% In_2O_3 10% SnO_2)	
J	Current density	mA/cm^2
J_L	Photocurrent density	mA/cm^2

J_p	Hole flux	cm^{-2}
J_s	Diode saturation current density	mA/cm^2
J_{sc}	Short-circuit photocurrent density	mA/cm^2
k	Boltzmann's constant: 1.38×10^{-23}	J/K
k	Reciprocal lattice space	nm^{-1}
kT	Thermal energy	eV
KW_p	Peak output power of a PV installation	KW
L	Charge carrier diffusion length	μm
L	Layer thickness	μm
LHE	Light harvesting efficiency	%
m^*	Effective mass of carrier	Kg
n	Diode quality factor or ideality factor	-
ν	Frequency	Hz
n	Refraction index	-
n^+	strong n doping	-
N_A	Doping atoms concentration in the p-type side	cm^{-3}
N_C	Effective density of states in conduction band	cm^{-3}
n_c	Nanocrystalline	
N_D	Doping atoms concentration in the n-type side	cm^{-3}
NHE	Normal Hydrogen Electrode	
$NREL$	National Renewable Energy Laboratory, Golden, CO, USA	
N_{sc}	Surface trapping center density	cm^{-2}
N_T	Recombination center density	cm^{-3}
N_V	Effective density of states in valence band	cm^{-3}

ϕ_M	Work function of the material M	eV
p^+	strong p doping	-
P3MT	Poly(3-methylthiophene)	
P3OT	Poly(3-octylthiophene)	
PBT	Poly(bithiophene)	
PITN	Poly(isothianaphene)	
P_{max}	Maximal electrical output power	W
PTh	Polythiophene	
PV	Photovoltaic	
PVD	Physical vapor deposited	
q	Elementary charge: 1.602×10^{-19}	As
q_n	Charge density of the fixed n-type dopant ions	As/cm ³
q_v	Charge density of the fixed p-type dopant ions	As/cm ³
R	Electrical resistance	Ω
ρ	Specific resistivity	Ωcm
S	Surface recombination velocity	cm ⁻¹
σ	Absorption cross section	cm ⁻¹ /mol
σ	Specific conductivity	$\Omega^{-1}\text{cm}^{-1}$
S, S ⁺	Sensitiser, oxidized sensitizer energy level	V
SCE	Standard Calomel Electrode	
SEM	Scanning electron microscope	
σ_{sc}	Surface trap capture cross-section	cm ⁻²
σ_t	Capture cross-section of the trap	cm ⁻³
τ	Minority carrier lifetime	s

TCO	Transparent Conducting Oxide	
TPATBF	Tetrapropylammonium tetrafluoroborate	
UV	Ultraviolet (< 400 nm)	
V	Applied bias	V
VB	Valence band	-
V_{bi}	Junction build-in voltage	V
VIS	Visible spectral range (400-800 nm)	
V_{oc}	Open-circuit voltage	V
V_{th}	Thermal velocity of the minority carriers	cm/s
W	Depletion layer thickness	μm
W.E.	Working electrode	
x	Distance	cm
ψ	Electrostatic potential	V
Z	Impedance	Ω
Z'	Imaginary part of the impedance	Ω
Z''	Real part of the impedance	Ω
μ_n	Electron mobility	cm^2/Vs
μ_p	Hole mobility	cm^2/Vs
ΔE	Energy difference	eV
Δk	Reciprocal lattice space difference	nm^{-1}

Acknowledgments

First of all, I would like to thank my adviser Professor Michael Graetzel for having given me the opportunity to work on the dye solar cell. In particular, I appreciated the great liberty he allowed me in pursuing my ideas.

I am grateful to all the members of the ICP2 (Institut de Chimie Physique) for the comfortable working atmosphere in the institute, and for their help and availability at different stages of this work, especially to Dr. Nick Vlachopoulos and Udo Bach for the delicate Xe-lamp calibrations.

I am indebted to Stefan Ruile for the manuscript corrections he suggested to me with a good sense of humor.

I acknowledge gratefully Prof. H. Vogel of ICP4 for the permission to use his vacuum evaporation apparatus.

Special thanks to Dr. Valery Shklover of the Crystallography Institute at ETH Zürich for the SEM photographs he made for me.

A great thank to my family for the support they provided to me.

The financial support of the Office Fédéral de l'Energie is gratefully acknowledged and the financial contribution of Solaronix SA made this work possible.

Curriculum vitae

Tobias Balthasar Meyer, born on August 12, 1966 in Basel, Switzerland.

- 1982-1986 Gymnasium Champittet in Pully, final exam: "Maturité Fédérale type C".
- 1987-1991 Student in chemical engineering at the Swiss Federal Institute of Technology Lausanne, "Diplôme d'ingénieur chimiste".
- 1991-1992 Diploma thesis under the direction of Dr. A. McEvoy at the Institute of Physical Chemistry on the "Etude sur le Poly(benzo[c]thiophène Utilisé comme Contre-Electrode dans une Cellule Photovoltaïque Electrochimique".
- 1992-1996 Ph.D. student under the direction of Prof. M. Graetzel at the Institute of Physical Chemistry, Swiss Federal Institute of Technology Lausanne.

Professional activities

- 1993 Together with Andreas, my twin brother, I own Solaronix SA, Aubonne, a swiss corporation.
- 1993-1996 Build-up of this corporation, active in the field of electro-optic devices based on nanocrystalline materials. A novel design of the dye solar cell is developed, and it allows large-scale production of photovoltaic energy sources, first intended to power electronic appliances, then, later on for the energy market.